Programa de Doctorado en Biociencias Moleculares

Doctoral thesis

Development of lentiviral-based strategies to modulate angiogenesis during post-infarction heart remodeling

Magdalena Maria Żak

Madrid, 2018

Departamento de Bioquímica

Facultad de Medicina

Universidad Autónoma de Madrid

Doctoral thesis

Development of lentiviral-based strategies to modulate angiogenesis during post-infarction heart remodeling

Magdalena Maria Żak

PhD thesis director

Alicia García Arroyo MD PhD

Centro Nacional de Investigaciones Cardiovasculares Carlos III (CNIC)

Madrid, 2018

The research leading to these results has received funding from the People Programme (Marie Curie Actions) of the European Union´s Seventh Framework Programme (FP7/2007-2013) under REA grant agreement nº 608027 (¨CardioNext¨ Initial Training Networks project)

Acknowledgments

There have been many people during the last four years without whose professional and, equally important, personal support, it would not have been possible to finish this work. I would like to express my gratitude toward them here.

To begin with, I would like to thank Dr. Alicia García Arroyo for giving me the opportunity to perform this research in her lab at CNIC, and for providing guidance throughout this challenging project.

I would like to thank Prof. Michele de Palma and Dr. Mario Squadrito for the opportunity to work with them at EPFL in Lausanne and for showing me their way of doing science. Thanks also to Dr. Gisèle Deblandre for introducing me to the business side of science and for providing positive feedback at a time when it was particularly needed.

Without the help of CNIC's specialized units, this work would have been much more difficult if not impossible to complete. Specifically, I would like to thank the excellent Microscopy Unit, especially Veronica and Antonio for all the help they provided over the years; the Animal Facility, especially Ruben, Frank and Lorena for performing mouse surgeries; the Advanced Imaging Unit, in particular Lorena and Ana Vanessa for performing and analyzing echocardiographies, and also Dr. Borreguero and Dr. Maria Villalba for their expertise in interpreting the results; the Cellomics Unit, especially Jose and Raquel for their technical support and expertise; the Proteomics Unit, especially Alessia and, last but not least, the Histology Unit.

Thanks to Lilit for her friendship and for helping me navigate Spanish bureaucracy on multiple occasions.

I would like to thank the people from my lab, especially Susana for helping me take my first steps there, and Xenia for her help with image analysis; and, more broadly, the people from 1st North for the time and fun we shared over the years.

I would like to thank my CNIC friends: Teresa, for saving me countless times in my battles with everyday life in Spain and for all the parties, gin, and Spanish wine we shared;

Briane (Mózg), for all the fun we had together, and especially for English proofreading of this thesis; Patri for the support and laughs we shared; Riju for his crazy stories, and Giulio for all the coffee and Italian crackers I stole from him. Special thanks to CNIC's Polacos, Magda, Olka and Jarek, for making me feel like a part of home is here, not to mention the fun we had introducing Spanish people to polish alcohols☺. To Magda, special thanks for the scientific discussions, which were very helpful to me.

To my parents; my siblings, Kuba, Asiunia and Mateusz; my niece Jagoda; my grandparents; Tomek, and the rest of my big crazy Polish family (including Śruba), who made me who I am today. Without your love and support, I would not have been able to get where I am now.

Dziękuję moim Rodziciom; rodzeństwu, Kubie, Asiuni i Mateuszowi; Jagódce; moim Dziadkom; Tomkowi i reszcie mojej wielkiej zwiariowanej polskiej rodziny (włączając Śrubę), którzy ukształtowali mnie taką jaką dziś jestem. Bez Waszego wsparcia i miłości nigdy nie dotarłabym tam gdzie jestem.

I would like to thank my Polish friends, Nat, Hachulska, Duczmal, Aśka, Niunia, Iro, Ela, Karol, Tomek and Jacek, for believing in me, giving me a shoulder to cry on, and pushing me when it was needed. Most of you have been in my life for more than twenty great years. It is crazy how old we got in the meantime!

To Ian, for everything we shared, not to mention English proofreading of this thesis.

Summary

Despite remarkable improvement since the implementation of angioplasty in acute treatment of myocardial infarction, long-term consequences of myocardial infarction, including heart failure, remain a challenge for modern medicine. Over the past decades, a need for an effective therapy to improve or rather to prevent adverse remodeling, and as a consequence prevent heart failure after myocardial infarction, remains unmet. To date, tested therapies have been aimed at various goals, including the prevention of cardiomyocyte death, reprograming cardiac fibroblasts into cardiomyocytes or cardiac progenitors, tuning immune responses, and modulating angiogenesis. Here we implemented a novel gene-cell therapy, combining the actions of two proangiogenic factors: VEGF-A and S1P delivered by *ex-vivo* lentivirus-infected bone marrow cells. Selection of the factors was based on their efficiency in inducing sprouting in an aortic ring assay. In the ischemia reperfusion model of myocardial infarction, bone marrow cells overexpressing hVEGF or hSphK1 were sequentially injected into mice at days 4 and 7 after myocardial infarction.

Analysis of control and treated mice at 28 days post-ischemia reperfusion showed mild improvement in stroke volume, with no impact on ejection fraction in VEGF/S1P-treated mice. Adverse heart remodeling was decreased in treated animals, represented as a mild improvement in left ventricle systolic and diastolic volumes, prevention of cardiomyocyte hypertrophy, and better preservation of the ellipsoid heart shape. Moreover, sequential VEGF/S1P gene-cell therapy mitigated extension of the fibrotic scar. Analysis of immune response patterns in treated and control mice revealed distinct chemokine-receptor profile of circulating monocytes in the treated mice, suggesting their shift into a more reparative phenotype. Additionally, cardiac macrophages were less abundant in the remote zone of the mice injected with BM^{VEGF}/BM^{SphK1}. Finally, as primarily aimed, sequential delivery of VEGF and S1P resulted in increased capillary density, ameliorated adverse angioadaptation, and improved tissue oxygenation. Furthermore, the fibrotic index indicating myofibroblast abundance decreased in the infarct zone of hearts from treated mice.

Our results identify a new strategy for sequential cell delivery of angiogenic factors to improve cardiac performance after myocardial infarction.

Resumen

A pesar de la mejora notable por la implementación de la angioplastia en el tratamiento agudo del infarto de miocardio, las consecuencias a largo plazo del infarto de miocardio, incluida la insuficiencia cardíaca, siguen siendo un desafío para la medicina moderna. En las últimas décadas, la necesidad de una terapia eficaz para mejorar o, mejor dicho, evitar una remodelación adversa y, como consecuencia, la insuficiencia cardíaca después de un infarto de miocardio, sigue sin cumplirse. Hasta la fecha, las terapias probadas se han dirigido hacia diversos objetivos, incluida la prevención de la muerte de los cardiomiocitos, la reprogramación de fibroblastos cardíacos en cardiomiocitos o progenitores cardíacos, el ajuste de las respuestas inmune y la modulación de la angiogénesis. Aquí, implementamos una nueva terapia de génica-celular, que combina las acciones de dos factores proangiogénicos VEGF-A y S1P administrados por células de médula ósea infectadas con lentivirus *ex vivo*. La selección de los factores se basó en su eficacia para inducir angiogénesis en un ensayo de anillo aórtico. En el modelo de isquemia-reperfusión de infarto de miocardio, las células de médula ósea que sobreexpresan hVEGF o hSphK1 se inyectaron secuencialmente en los ratones los días 4 y 7 después del infarto de miocardio.

El análisis de los ratones control y los tratados 28 días después de la isquemia-reperfusión mostró una mejoría leve en el volumen del latido sin impacto en la fracción de eyección en ratones tratados con VEGF/S1P. La remodelación adversa del corazón disminuyó en los animales tratados, representada como una mejoría leve en los volúmenes sistólico y diastólico finales del ventrículo izquierdo, la prevención de la hipertrofia de los cardiomiocitos y la mejor preservación de la forma elipsoide del corazón. Además, la terapia secuencial gen-célula VEGF/S1P mitigó la extensión de la cicatriz fibrótica. El análisis de los patrones de la respuesta inmune en ratones tratados y control reveló un perfil distinto de receptores de quimioquinas en los monocitos circulantes de los ratones tratados, lo que sugiere su cambio hacia un fenotipo más reparador. Además, los macrófagos cardíacos fueron menos abundantes en la zona remota de los ratones inyectados con BM^{VEGF}/BM^{SphK1}. Finalmente, y conforme al objetivo primario, la administración secuencial de VEGF y S1P dio como resultado un aumento de la densidad capilar, un menor angioadaptación adversa y

una oxigenación tisular mejorada. Además, el índice fibrótico que indica la abundancia de miofibroblastos disminuyó en la zona de infarto de los corazones de los ratones tratados.

Nuestros resultados identifican una nueva estrategia basada en el suministro secuencial de células productoras de factores angiogénicos para mejorar función cardíaca después de un infarto de miocardio.

Table of Contents

Abbreviations

AAV	Adeno Associated Virus
Ad	Adenovirus
Ang1	Angiopoietin 1
BMMNC	Bone Marrow-Delivered Mononuclear Cells
CHD	Coronary Heart Disease
CVD	Cardiovascular Disease
Dll4	Delta-like Notch receptor ligand 4
EC	Endothelial Cell
ECM	Extracellular Matrix
EPC	Endothelial Progenitor Cells
HF	Heart Failure
HIF	Hypoxia Inducible Factors
HSC	Hematopoietic Stem Cells
I/R	Ischemia/Reperfusion
IB4	Isolectin B4
LAD	Left Anterior Descending
LV	Lentivirus
LVEDP	Left Ventricle End Diastolic Pressure
LVEDV	Left Ventricle End Diastolic Volume
LVEF	Left Ventricle Ejection Fraction
LVESV	Left Ventricle End Systolic Volume
MI	Myocardial Infarction
msBM	Mouse Bone Marrow Cells
MSC	Mesenchymal Stem Cells
PCI	Percutaneous Coronary Intervention
PDGF	Platelet-Delivered Growth Factor
PDGFRβ	Platelet-Derived Growth Factor Receptor beta
PlGF	Placental Growth Factor
S1P	Sphingosine 1-Phosphate
S1P1	Sphingosine 1-Phosphate Receptor 1
SMA	Smooth Muscle Actin
SMC	Smooth Muscle Cell
SphK1	Sphingosine Kinase 1
STEMI	ST-Elevation Myocardial Infarction

SV	Stroke Volume
TNF	Tumor Necrosis Factor
VEGF	Vascular Endothelial Growth Factor
VEGFR	Vascular Endothelial Growth Factor Receptor

INTRODUCTION

1. Myocardial infarction and heart failure

Cardiovascular disease (CVD) has been the leading cause of death in the US since the beginning of 20th century. In the US in 2014, 28.7% of male deaths and 22.3% of female deaths were caused by CVD. Almost half of these deaths were caused by coronary heart disease (CHD).

Heart failure (HF) is the most common long-term consequence of CHD. Despite the fact that heart failure prevalence has increased from 5.7 million (2009 to 2012) to 6.5 million (2011 to 2014), the total number of deaths caused directly by CHD decreased by 19.2% between 2004 and 2014, in part due to an improvement in diagnosis and acute treatment of CVD[1].

One of the clinical manifestations of CHD is myocardial infarction (MI), defined as the sudden death of myocardial tissue from ischemia provoked by a blockage of a coronary artery, usually from an atherosclerotic plaque rupture[2]. After the onset of MI, a cascade of events occurs, including cardiomyocyte death, acute inflammation, angiogenesis and scar formation (Figure 1)[3]. Inflammatory and angiogenic responses in myocardial infarction will be further elaborated in this work (see subsections 1.1 and 1.2).

Due to the limited ability of the adult mammalian heart to regenerate, the main healing mechanism after MI is through the formation of fibrotic scar[2]. Fibrosis causes abnormalities in both relaxation and contractility of the heart muscle. After myocardial infarction, accumulation of these pathological processes (e.g. cardiomyocyte loss, fibrosis and prolonged inflammation) leads to cardiac remodeling over time.

Ventricular remodeling is either an adaptive or maladaptive mechanism of heart adaptation to adverse stimuli such as reduced contractility or/and increased wall stress caused among others by MI. The adaptive heart remodeling includes changes in the heart structure arising to sustain cardiac function, whereas maladaptive remodeling occurs during sustained stress and leads to irreversible changes in the geometry of the heart, resulting in abnormalities in its function[4]. Cardiac remodeling includes left ventricle wall thinning, ventricle dilation, and changes in the heart's shape from ellipsoid to more spherical (Figure 2).

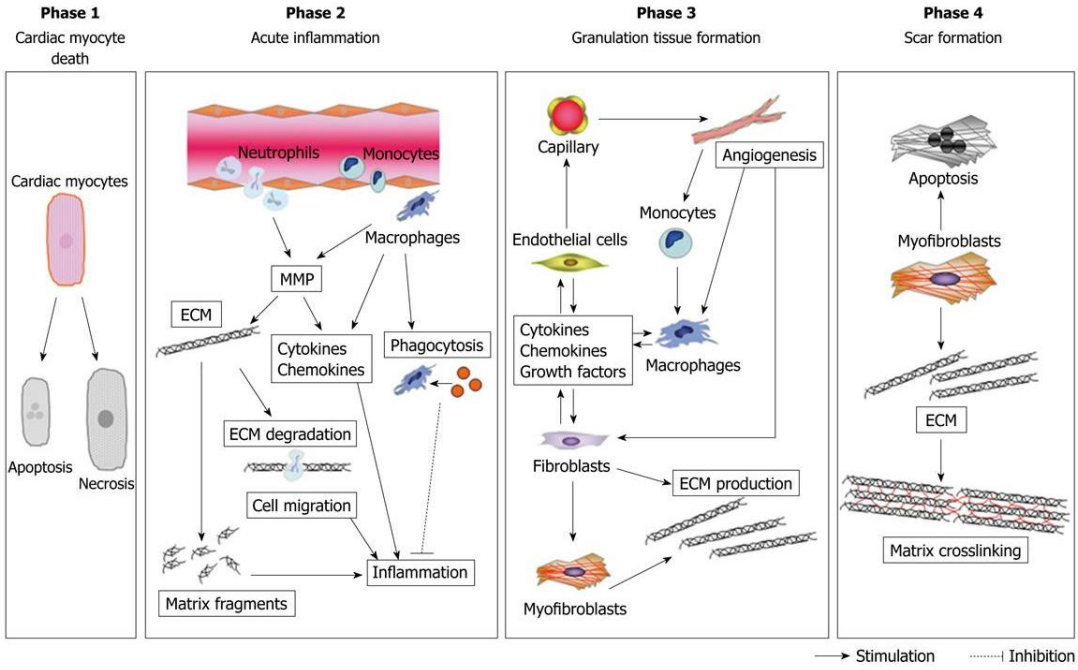

Figure 1. Phases of healing after myocardial infarction. Cardiomyocyte death, caused by ischemia, is followed by an acute inflammation phase. Signals are sent by dying cardiomyocytes mobilize monocytes and neutrophils to extravasate into injury site. Extracellular matrix is fragmented to facilitate cell migration and monocyte-derived macrophages ingest dead cells. Next step is formation of granulated tissue when process of angiogenesis occurs. Last phase is formation of scar tissue in to preserve ventricular integrity. Adapted from [3].

On the cellular level, cardiomyocytes in the viable myocardium undergo hypertrophy triggered by increased load, which further leads to the abovementioned dilation of the left ventricle. These malformations create increasing wall stress on the beating heart, which causes further dilation, increase in the left ventricle end-systolic and end-diastolic volumes, higher myocardial oxygen demand, and could cause further increase of the area at risk for ischemia[5].

Heart failure is a clinical syndrome in which heart muscle is not able to maintain cardiac output (the amount of blood pumped by the heart over time) and, as a consequence, venous return. Ischemia caused by myocardial infarction is one of the main causes of HF together with hypertension and diabetes[7]. Pathological heart remodeling caused by MI and the secondary hypoxia, leads to HF over time[8].

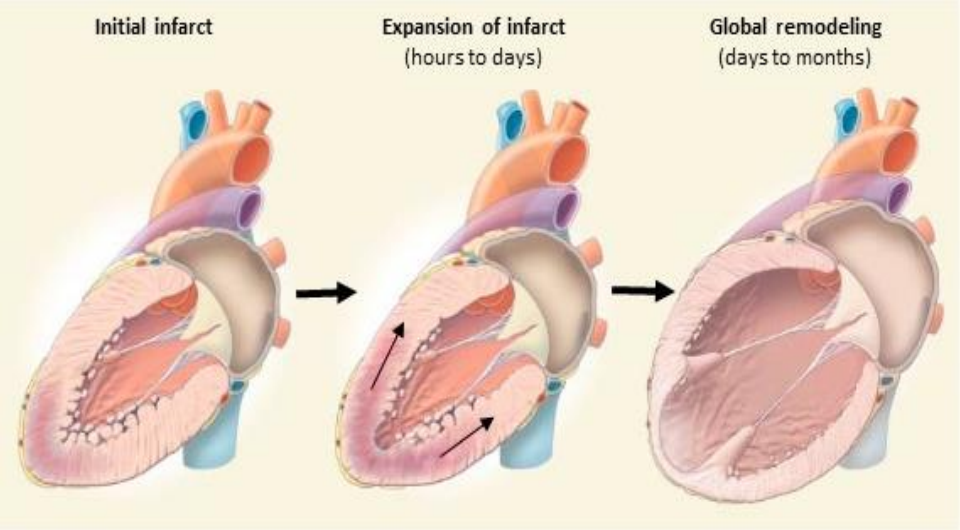

Figure 2. Ventricular remodeling after acute myocardial infarction. Healthy myocardium has a ellipsoidal shape, although over time after myocardial infarction it become more round, losing its contractile properties. This remodeling is a consequence of scar formation and maladaptation to overcome pressure load. When part of the ventricle contain scar tissue, which doesn't contract, is not capable to pump blood properly. As a result, changes in geometry of the heart occur which finally result in further abnormalities in its function. Adapted from[6].

There are two types of heart failure: with preserved and decreased left ventricle ejection fraction (LVEF). Diastolic dysfunction occurs when LVEF is higher than 40% and systolic dysfunction when it is lower than 40%. Symptoms of diastolic and systolic HF are the same and include diminished cardiac output, which leads to global hypoperfusion and an increased amount of blood in the ventricle, which in turn increases end-systolic and end-diastolic volumes. These pathological changes lead to an increase in the LVEDP (left ventricle end diastolic pressure) and left atrial pressure as well as an increase in blood pressure in capillaries in the lungs, which causes pulmonary edema, the major clinical symptom of HF[7].

Depending on the patient's age and comorbidities, the onset of HF may appear immediately after MI or be delayed. HF has become the main cause of death of patients older than 65 years within 6 years after myocardial infarction[9]. For that reason, prevention and ameliorating the effects of HF seem to be of great importance.

1.1. Inflammatory response to myocardial infarction

The immune system exists to defend the host organism against external pathogens, but also to promote tissue repair after so called 'sterile inflammation' like myocardial infarction. In healthy heart tissue, similarly to other organs, there are resident immune cells, mostly macrophages, usually situated near endothelial cells (ECs) or in the interstitial space[10]. There are also mast cells, which have an important role in the activation of early immune response, especially in the context of reperfusion during myocardial infarction[11].

Following the first phase of MI, which comprises cardiomyocyte death, a phase of acute inflammatory response begins. Necrotic and/or apoptotic cardiomyocytes release their cytosolic content (composed of damage-associated molecular patterns) into the extracellular matrix (ECM), which is sensed by the cardiac resident immune cells as well as non-immune cells[12]. The inflammatory response starts when activated cells start secreting cytokines and chemokines essential for recruiting leukocytes from the blood stream into the injury site[13]. Additionally, in the context of ischemia reperfusion injury, resident mast cells and complement proteins play an important role. Restoration of the blood flow after myocardial infarction by PCI (percutaneous coronary intervention/angioplasty) has become a common practice in the acute treatment of myocardial infarction. Even though blood flow restoration is crucial for rescuing still viable myocardium, it also causes amplification of the immune response. Complement proteins from restored blood flow enter the myocardium through the injured EC layer and trigger a proinflammatory response of the resident mast cells, which secrete mediators of inflammation like histamine and tumor necrosis factor (TNF)[11]. Furthermore, activated complement proteins attract neutrophils and facilitate their extravasation into the injured tissue.

Neutrophils are the first innate immune cell subset recruited into the myocardium. Damaged cells release mitochondrial DNA and formylated peptides, which are structurally similar to bacterial components and therefore are sensed by neutrophils and promote their migration into the injury site. Furthermore, TNF and histamine secreted by mast cells activate endothelium and increase its permeability facilitating neutrophil infiltration into damaged tissue. Although neutrophils are crucial in the context of a pathogen-driven innate immune response, their protective role in sterile inflammation remains elusive; in fact,

proteases produced by neutrophils may aggravate the injury. Advantageously, neutrophil accumulation peaks at 24 hours after injury when they are phagocytized by monocytes/macrophages[10].

From the first day after MI, monocytes and their successors, macrophages, dominate in the cellular infiltrate of the ischemic heart. To describe recruitment of these cells, a biphasic model of monocyte/macrophage infiltration into the infarcted myocardium was proposed[14] (Figure 3).

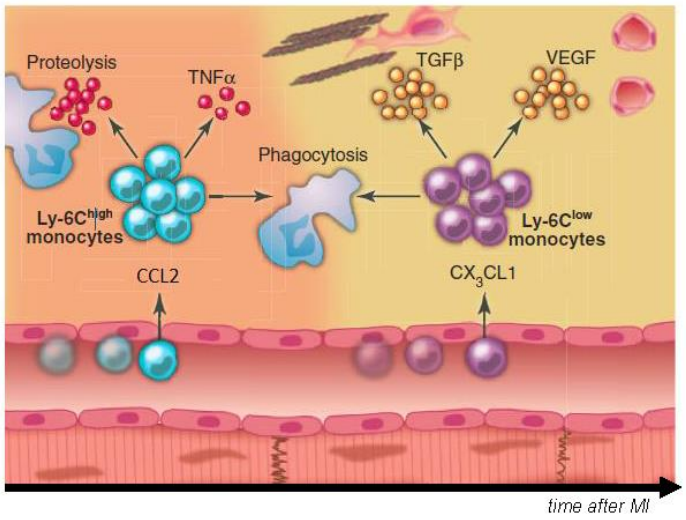

Figure 3. Monocyte recruitment to infarcted myocardium. First monocyte subset recruited to infarcted myocardium are Ly6C^{hi} monocytes, sensing CCL2 released by damaged tissue. Ly6C^{hi} monocytes take part in acute inflammatory response by removing debris, phagocytize neutrophils, and secrete proteases. During resolution of inflammation, second monocyte subset, Ly6C^{low} is recruited in response to CX_3CL1. They secrete anti-inflammatory cytokines and take part in angiogenesis by secreting VEGF. Adapted from[15].

At first, in response to CCL2 released by the damaged tissue, a population of Ly6C^{hi} inflammatory monocytes is attracted into the injury site. After a few days, the wounded heart switches to CX_3CL1-dependent recruitment of Ly6C^{low} reparative monocytes; however, the mechanism of that switch remains unknown[15]. Although both monocyte subsets show the phagocytic phenotype, their role in the ischemic myocardium is distinct. As mentioned above, Ly6C^{hi} dominate in the first 4 days post-MI and are rich in proinflammatory mediators. Their role in a recently injured heart is to digest infarcted tissue, remove debris, phagocytize neutrophils, and secrete proteases and matrix metalloproteinases. During resolution of the inflammation, the second phase, the Ly6C^{low} monocyte population takes over. Reparative Ly6C^{low} monocytes promote resolution of the inflammation by secreting anti-inflammatory cytokines: IL-10 and TGFβ. They also promote angiogenesis by secreting

vascular endothelial growth factor A (VEGF-A), stimulating collagen synthesis and deposition. Monocytes in the infarcted myocardium can play both protective and destructive roles, therefore coordinated cell recruitment seems to be crucial for proper healing[14-16].

Monocytes are also recruited to the remote myocardium, although to a much lower extent. Here, similarly to the infarct zone, they may be beneficial by promoting angiogenesis, but also harmful by promoting proteolysis of the collagen matrix. Excessive ECM proteolysis may facilitate left ventricle dilation by promoting interstitial fibrosis and/or secreting proinflammatory factors by activated fibroblasts[15].

In the long term, there are almost no monocytes in the infarcted heart. Instead, we can observe macrophages which, by being strictly linked with monocytes, may be either harmful or protective in the post-ischemic myocardium. As mentioned above, in a healthy heart there is a population of resident macrophages which help to maintain organ homeostasis. The population of macrophages present in the remote zone of an infarcted heart comes from both local proliferation and the recruitment of monocytes, which then differentiate into macrophages. It is well established that prolonged inflammation after myocardial infarction may aggravate the disease. In fact, it has been shown that activated macrophages of the remote zone take part in pathological left ventricle remodeling and development of heart failure. Mechanical strain which comes from the overloaded viable part of the myocardium may cause proinflammatory activation, as well as proliferation of the remote zone macrophages[16,17].

Monocytes/macrophages recruited to the ischemic heart are of both bone marrow and splenic origin. A large number of the initially recruited monocytes comes from the splenic reservoir. Subsequently, to meet the demand of the infarcted heart, cell production increases in the bone marrow and spleen triggered by the sympathetic nervous system and the release of noradrenaline in response to anxiety and pain at the time of MI event[15]. About half of total monocytes/macrophages recruited into infarcted heart come from the spleen origin. The link between them and heart failure was demonstrated using a mouse model of permanent LAD (left anterior descending) artery ligation where splenectomy reduced chronic HF events[18]. Thus, modulation of the inflammatory response after myocardial infarction is one of the therapeutic targets for HF treatment.

1.2. Angiogenesis in myocardial infarction

During the third phase of MI, endothelial cells and fibroblasts proliferate and form a granulation tissue. During this process, there is an increased load on the viable myocardium, which might cause left ventricle free wall rupture and death. As a result of the healing process, a scar will be form in the place of granulation tissue and most of the ECs and fibroblasts will undergo apoptosis. Angiogenesis takes place in both infarcted and viable myocardium, and although most of the newly formed vessels in the granulation tissue will be lost during scar formation, neovascularization of the myocardium surrounding infarcted tissue might be a crucial factor to allow tissue salvage and to prevent heart remodeling which in turns leads to heart failure[19].

Sprouting angiogenesis is a process of the formation of new vessels from pre-existing ones in response to hypoxia, growth factors, nitric oxide and lipid mediators[2] (Figure 4). When ECs are not supplied with oxygen (e.g. after MI), signaling through hypoxia inducible factors (HIF) upregulates many angiogenic genes, principally VEGF-A[21]. VEGF-A is the most important regulator of blood vessel formation and a member of a large family of angiogenic regulators, including PlGF, VEGF-B, VEGF-C and VEGF-D[22].

By binding to vascular endothelial factor receptor 2 (VEGFR2), VEGF-A promotes EC proliferation, as well as chemotaxis and differentiation of EC precursors. Adherent and tight junctions of quiescent ECs become dissolved and some of the cells within the capillary acquire a tip cell phenotype and start to lead a growing sprout (Figure 4). Tip cell phenotype is activated by expression of Dll4 (Notch receptor ligand) and activation of Notch signaling in surrounding (stalk) cells which prevents them from sprouting[22]. Extracellular matrix reorganization allows progression of the sprouts as well as prevents newly formed vessels from collapsing. Changes in the ECM composition provoke smooth muscle cell (SMC) migration and provide support to EC guiding them to their targets[21].

Formation of the lumen and the onset of blood flow helps to stabilize new vascular connections by improving oxygenation. Subsequently, hypoxia and VEGF-A related signaling become hindered, causing blockage of EC proliferation[22].

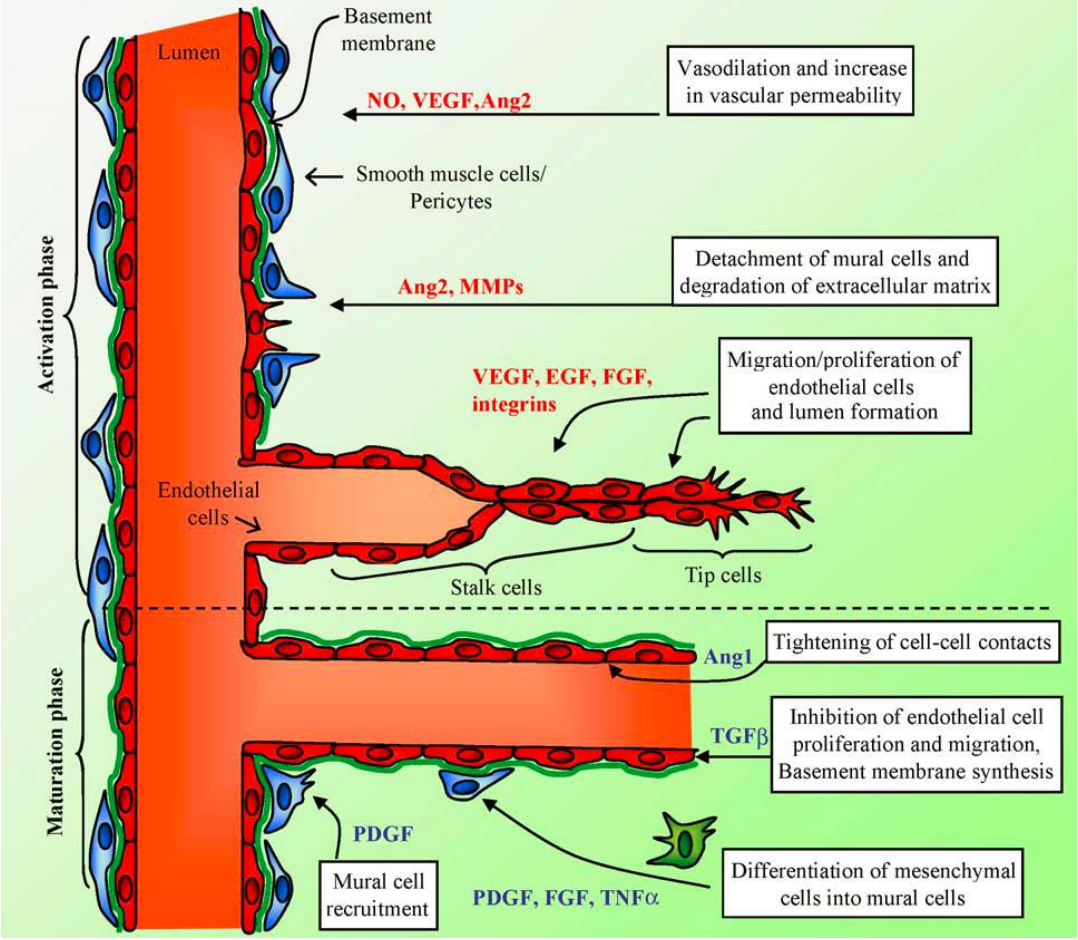

Figure 4. Scheme of activation and maturation phases of angiogenesis process. Sprouting angiogenesis is a strictly controlled and chronologically organized process where new vessels are formed from existing ones. During activation phase, in response to VEGF and other signals, tight junctions between quiescent endothelial cells become loose and they start to proliferate. Sprout progresses following the tip cell, while extracellular matrix reorganization prevents it from collapsing. During maturation phase, onset of the blood flow helps to stabilize newly formed vessels and blocks hypoxia-related VEGF signaling. Therefore, proliferation of endothelial cells is stops. ECM deposition causes migration of smooth muscle cells and pericytes, which help to form a stable vasculature. Many factors take place in maturation phase, including Ang1, PDGF and S1P. Adapted from[20].

To establish a functional vessel network, transformation of the newly formed vessels into more mature ones is essential. ECM deposition and recruitment of the mural cells (SMC and pericytes) and their interaction with the newly formed vessels regulates EC survival, vessel branching, blood flow and permeability. There are many factors participating in vessel stabilization, including platelet-delivered growth factor (PDGF), angiopoietins and lipid mediators like sphingosine 1-phosphate (S1P)[23]. PDGF is involved in vessel stabilization by recruiting PDGFRβ^{+} mesenchymal progenitors.

Angiopoietin 1 (Ang1) is a secreted glycoprotein and a member of angiopoietin growth factors family including Ang2, 3 and 4[24]. Ang1 is a ligand of the Tie2 receptor, which is expressed on vascular endothelial cells as well as the proangiogenic monocyte subset identified by De Palma et al.[25,26]. Ang1 deficient mice die at an early embryonic stage due to disorganized and dilated vasculature networks[27]. During the maturation phase of angiogenesis, Ang1 activates the Tie2 receptor and promotes EC-mural cell interactions and the recruitment of pericytes[21].

Sphingosine 1- phosphate (S1P) is an important lipid mediator of cell growth, proliferation and migration *in vitro*. It also regulates angiogenesis, immune cell trafficking *in vivo*[28] and is involved in cardiomyocyte protection in response to ischemia[29]. In angiogenesis, S1P plays a dual role: it promotes EC migration and, most importantly, takes part in the stabilization of newly formed vessels. Endothelial cell migration is mediated by the signaling from sphingosine 1-phosphate receptors 1 and 3 (S1P1 and S1P3). It was demonstrated in *in vitro* studies of 3D matrix cultures of endothelial cells, that S1P promotes lumen formation and EC branching morphogenesis[30]. On the other hand, S1P signaling through S1P1 is an important player in vessel stabilization; S1P1 gene ablation in mice impaired mural cell accumulation to the vessels during the maturation stage of angiogenesis[31]. After this discovery, it was shown that S1P mediates formation of N-cadherin based junctions, which facilitate EC interaction between cells expressing this molecule, including other ECs and SMC, which is important for vessel stabilization[32].

Interestingly, the VEGF and S1P pathways seem to crosstalk in regulating angiogenesis and the vasculature. It was shown that VEGF treatment of bovine aortic EC induced overexpression of the S1P1 receptor on mRNA and protein levels. Furthermore, preincubation with VEGF increased subsequent S1P-dependent eNOS activation and phosphorylation in these cells as well as phosphorylation of Akt kinase, which is one of the kinases involved in the RISK pathway. The same study showed that VEGF pretreatment markedly induced S1P-mediated eNOS phosphorylation and vasorelaxation in isolated rat arteries. Therefore it was suggested that VEGF sensitizes vascular endothelium to lipid mediators via promoting overexpression of S1P1, which implies potential cross-talk in eNOS signaling pathways in the vasculature[33].

2. Cell and gene therapies in myocardial infarction treatment

The main treatment for myocardial infarction is acute coronary angioplasty ideally within 90 minutes door to balloon time in developed countries. This procedure involves inserting a catheter through the femoral or radial artery and, when the occlusion site is reached, inflating a balloon to restore blood flow and/or remove a thrombus. In some cases, implantation of a stent is necessary to prevent a vessel wall from collapsing[34]. Reperfusion of the coronary artery restores blood flow in the cardiac muscle and prevents further damage. Higher availability of this method correlates with lower morbidity of patients with STEMI (ST-elevation myocardial infarction) in which one of the main arteries is blocked[35]. Depending on the time between the first sign of MI to intervention, damage of the heart muscle may eventually lead to developing heart failure. For that reason, there is a need to develop therapies aimed at reducing the area at risk or to ameliorate the pathological effects of MI (Figure 5).

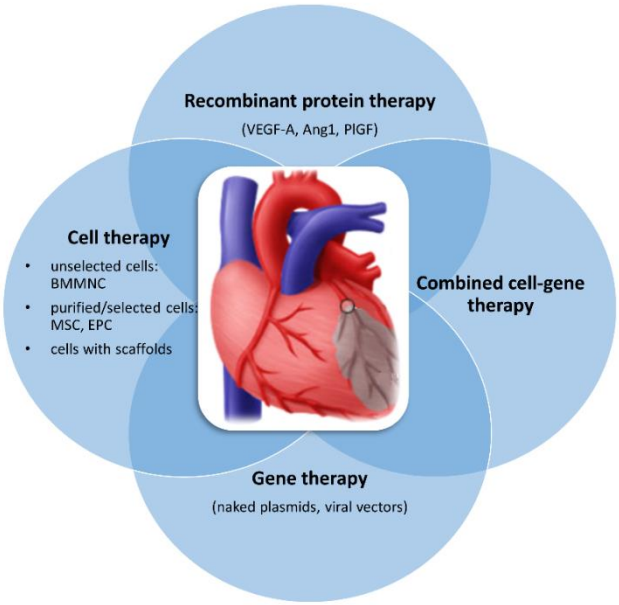

Figure 5. Strategies in treatment of myocardial infarction by promoting angiogenesis. Despite improvement in acute treatment of myocardial infarction, long term consequences remain severe and lead to heart failure. Over past decades, many strategies were developed to ameliorate effects of myocardial ischemia including recombinant protein therapies, gene therapies, cell therapies and combined gene cell therapies. All these approaches focus on a few main goals of post myocardial infarction therapies: improving angiogenesis, activation of adult cardiomyocyte proliferation, attenuating innate and adaptive immune response, and preventing cardiac cell apoptosis and necrosis.

One of the main strategies is to promote angiogenesis which, as mentioned above, takes part in endogenous healing of infarcted myocardium. Many different approaches were developed over time, including delivery of proangiogenic proteins directly or using various carriers, gene delivery using naked or encapsulated plasmids, as well as viral vectors. Another concept is to use various cell types, including unselected bone marrow-delivered mononuclear cells (BMMNC), as well as various purified cell populations like mesenchymal stem cells (MSC), endothelial progenitors (EPC) and many others. For the purpose of this work, only gene and cell therapy approaches will be further elaborated.

2.1. Cell-based therapies in treatment of myocardial infarction

Cell therapies have primarily been based on the idea that stem cells present in the bone marrow are capable of differentiating into cardiomyocytes and replacing damaged ones. One of the first trials in a mouse model of myocardial infarction (by Orlic et al), showed improved myocardial contractility and the formation of new myocardium in the infarcted zone of the heart transplanted with Lin^- $c\text{-}kit^+$ cells[36]. Since then, many preclinical and clinical trials have been launched using heterogeneous cell populations as well as purified ones and the focus has turned towards the paracrine effect of these cells on infarcted myocardium.

Therapies using bone marrow-derived mononuclear cells (BMMNC) have been tested in various clinical trials. Accessible harvest and processing methods, as well as high yields, make them feasible for acute treatment of acute MI patients.

The largest randomized clinical trial, REPAIR-AMI with intracoronary injection of BMMNC to the patients who underwent a PCI procedure, showed overall improvement in LVEF but there were no changes in end-diastolic volumes 4 months after intervention[37]. Additionally, there was decreased mortality in two years' follow-up[38]. Another randomized clinical trial, BOOST, also showed short-term improvement in EF 18-months post-MI, but it was not confirmed in a 5-year follow-up[39,40]. Moreover, the ASTAMI second phase clinical trial showed no beneficial effect on global EF, left ventricle dimensions or infarct size at 4-6 months follow-up[41]. Meta analyses of 50 randomized and cohort trials on a total of almost 3000 patients performed to unravel these mixed results showed a mild but positive

effect on the improvement of EF, decreased left ventricle-dimensions, and smaller infarct size[42].

Purified cell populations were also tested in various clinical trials, among them mesenchymal stem cells (MSC) of bone marrow and adipose tissue origin, cardiac stem cells, hematopoietic stem cells (HSC), as well as endothelial progenitor cells (EPC)[43,44].

Endothelial progenitor cells is a population of circulating cells of bone marrow, hematopoietic or adipose tissue origin, capable of proliferating, self-renewing and to repairing endothelial tissue. The exact definition of these cells remains controversial especially taking into account 'early' and 'late' subpopulations, although there are certain cell surface markers used to describe their phenotype including: CD34, VEGFR1, Tie2, vWF and CD113[45,46].

The more broad population of $CD34^+$ stem cells which includes both hematopoietic and endothelial cell progenitors have been used in various animal and clinical trials to induce angiogenesis in ischemic diseases including myocardial infarction[47]. Autologous injection of $CD34^+$ cells improved exercise time and decreased chest pain frequency in patients with refractory angina and no option for standard revascularization procedure, enrolled in RENEW clinical trial[48]. On the other hand, in the REGENT trial, patients with acute myocardial infarction followed by PCI, who received autologous injection of $CD34^+CXCR4^+$ cells, showed no improvement in EF 6 months after intervention[49].

In parallel to cell therapy trials, gene-based approaches are also being investigated.

2.2. Proangiogenic gene-based therapies to treat myocardial infarction

There are a few possible routes for gene delivery in cardiovascular therapies. From the most straightforward, using naked or encapsulated plasmids encoding desired genes, to more complicated with the use of adeno or lentiviruses (LV) (Figure 6).

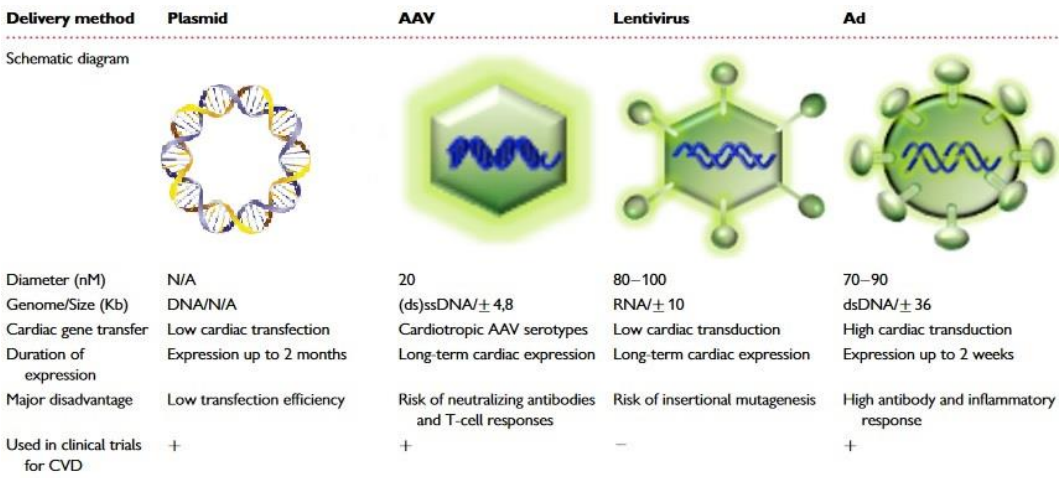

Delivery method	Plasmid	AAV	Lentivirus	Ad
Schematic diagram				
Diameter (nM)	N/A	20	80–100	70–90
Genome/Size (Kb)	DNA/N/A	(ds)ssDNA/± 4,8	RNA/± 10	dsDNA/± 36
Cardiac gene transfer	Low cardiac transfection	Cardiotropic AAV serotypes	Low cardiac transduction	High cardiac transduction
Duration of expression	Expression up to 2 months	Long-term cardiac expression	Long-term cardiac expression	Expression up to 2 weeks
Major disadvantage	Low transfection efficiency	Risk of neutralizing antibodies and T-cell responses	Risk of insertional mutagenesis	High antibody and inflammatory response
Used in clinical trials for CVD	+	+	−	+

Figure 6. Tools used in gene therapies. To deliver therapeutic genes into host cells, many approaches are used, starting from most straightforward plasmid to more sophisticated viruses. Pros and cons of each method are presented. Adapted from[50].

Because of their simplicity, plasmid-based approaches were used in many animal, and also clinical trials[50,51]. Intramyocardial injections of plasmids expressing VEGF in a sheep model of coronary artery ligation reduced scar size and improved perfusion but had no effect on global left ventricle function[52]. A plasmid approach using a proangiogenic VEGF gene was also used in clinical trials. There was no improvement in myocardial perfusion in patients with coronary artery disease after intramyocardial injection of plasmid VEGF during NORTHERN or EuroinjectOne trials[53,54]. A disadvantage in using plasmid vectors comes from the fact that they are cleared out of the circulation by nucleases. To overcome this obstacle, various encapsulation materials are used, including liposomes and polymers.

Seeking a more efficient method for gene delivery, attention was focused on viral vectors, which in general have a higher translation efficiency than plasmid-based approaches.

In the Kuopio Angiogenesis Trial (KAT) clinical trial, patients with coronary heart disease received intracoronary delivery of Ad VEGF or plasmid liposome VEGF. A six-month follow-up showed improvement in myocardial perfusion in the adenovirus-treated group, but no difference in exercise time between groups[55]. Adenoviruses (Ad) are capable of transiently transducing dividing and non-dividing cells within heart tissue, therefore they attracted attention for proangiogenic gene therapy where short term gene expression might

be beneficial. Especially serotype Ad49 seemed to be especially interesting, considering its increased transduction efficiency in EC and SMC[56]. On the other hand, these non-integrating, non-enveloped vectors induce a strong inflammatory response which might influence transduction capability and utility in clinical setting because of safety reasons[50].

On the contrary, adeno associated viruses (AAV) cause much lower inflammatory response. Additionally, they provide sustained gene expression in the heart[57]. Similarly to Ad vectors, they provide episomal, nonintegrated expression of transgene. There are many serotypes of adenoviruses, also specifically cardiotropic after systemic delivery, like AAV1, AAV6, AAV8 and AAV9[58,59]. In a porcine model of LAD ligation, intracardiac coinjection of two proangiogenic genes VEGF and Ang1 delivered using AAVs improved cardiac function (EF and LVESV) as well as myocardial perfusion at 8 but not 2 weeks after intervention[60]. The disadvantage of using AAV vectors comes from the fact that the time length of transgene expression is not controlled; therefore, it might have deleterious effects as shown for prolonged delivery of VEGF[61,62].

The last group of viruses used in research but to a lower extent are lentiviruses. Because of their ability to incorporate into a host genome of dividing and non-dividing cells, they are capable of transducing all cell types with long-term expression; but at the same time, there is a potential risk of insertional oncogenesis, especially when overexpressing proangiogenic genes[63].

2.3. Combined gene-cell therapies in MI treatment

Knowing the advantages and limitations of both cell and gene therapeutic approaches, combined gene-cell therapies received attention. Since cell therapies seem to have only a mild positive effect on damaged myocardium, genetic modification of these cells, for example by overexpression of proangiogenic genes, might improve positive outcomes. At the same time, modifying cells *in vitro* allows for avoiding safety-related issues of direct *in vivo* gene delivery.

There are two strategies for gene-cell therapy. First, to genetically engineer cells in a way that changes their properties, for example, MSC overexpressing Akt to prolong their survival in an ischemic environment[64].

Secondly, to use cells as carriers of genes and allow secretion of a transgene in damaged tissue. In a rat model of ischemic cardiomyopathy, a comparison between the efficiency of direct injection of Ad-VEGF and skeletal muscle cells previously transduced with Ad-VEGF showed that only transduced cells improved heart function measured by fractional shortening. On the other hand, vascularization was enhanced in both groups[65].

OBJECTIVES

In the past decades, many approaches have been developed to improve heart function after ischemic damage. Many of them were focusing on improving angiogenesis, the process of formation of new vessels, which is a part of an endogenous healing process after myocardial infarction. Unfavorably, naturally occurring angiogenesis seems to be inefficient at significantly improving re-vascularization and preventing increased tissue damage, which results in pathological left ventricular remodeling and, over time, heart failure.

In this work, we aimed at developing a combined gene-cell proangiogenic therapy. We hypothesize that sequential delivery of distinct proangiogenic factors would be beneficial to achieve a more functional vasculature. We decided to use a combined gene-cell therapy approach for both safety and efficiency reasons.

To validate this approach we defined the following objectives:

1. To design lentiviral vectors overexpressing proangiogenic or pro-vascular stabilizing factors and to evaluate the best proangiogenic combination of these factors *in vitro*.
2. To establish a combined gene-cell therapy in a mouse model, and characterize its effect on the heart tissue at the functional and cellular level.
3. To gain mechanistic insights into the effects of the combined therapy on the coronary microvasculature, inflammatory response and cardiac function and remodeling.

METHODS

Lentiviral vectors

The human vascular endothelial growth factor (*hVEGF-A*$_{165}$) gene was amplified using the human breast cancer cell line MDA-MB-231 as a template, with the following primers:

- Fwd: 5'-CACTCGAGCCATGAATTTCTGCTGTCTTGG-3',
- Rev: 5'-CAGAATTTTGTCGATGGTGATGGTGT-3'.

The proper band was extracted from the agarose gel using QIAquick Gel Extraction Kit (Qiagen) and cloned into pGEM®-T Easy Vector (Promega), with Quick-Stick Ligase (Bioline). Clones were selected by blue-white screening and after restriction analysis, sequenced and the proper sequence was confirmed with NCBI Nucleotide database.

The human angiopetin 1 (*hAng1*) gene was amplified from a plasmid kindly provided by Prof. Kari Alitalo from the University of Helsinki using the primers

- Fwd: 5'-CATTAATTAAGACCATGACAGTTTTCCT-3',
- Rev: 5'-CAGCGGGCGATGGATGATCCGTTGCTTT-3',

cloned into pGEM®-Easy Vector, selected by blue-white screening and restriction analysis and sequenced.

The human sphingosine kinase 1 (*hSphK1*) gene was amplified from a commercially available plasmid pDONR223 (Changsha Yingrun Biotechnology Co. Ltd) using the primers

- Fwd 5'-CATTAATTAATTGCAACAAATTGATGAGCA-3',
- Rev 5'-CAGCGGCCGCTCATAAGGGCTCTTCTGGCGGT-3',

cloned into pGEM®-T Easy Vector, selected by blue-white screening and restriction analysis, and sequenced.

To clone the desired genes into the lentivirus backbone kindly provided by Dr. Mario Squadrito of the Ecole Polytechnique Federale Lausanne (p1031.8.pCCL.sin.SFFV.*insert*.WPRE). Each gene was amplified with primers containing AgeI and SalI restriction sites as well as START codon and Kozak sequence. Designed primers are summarized in Table 1.

Table 1. Designed primers

Gene	Primer	Sequence
hVEGF-A	Fwd	5'-AAAAAACCGGTGCCGCCATGAACTTTCTGCTGTCTTGG-3'
	Rev	5'-AAAAAGTCGACCTGTCGATGGTGATGGTGT-3'
hAng1	Fwd	5'-AAAAAACCGGTGCCACCATGACAGTTTTCCT-3'
	Rev	5'-AAAAAGTCGACGATGGATGATCCGTTGCTTT-3'
hSphK1	Fwd	5'-AAAAAACCGGTGCCGCCATGTCCGCTCAAGTTCTGG-3'
	Rev	5'-AAAAAGTCGACTCATAAGGGCTCTTCTGGCGGT-3'
GFP	Fwd	5'-AAAGTCGACCAGTTAGCCTCCCCCATCTC-3'
	Rev	5'-AAAACCGGTATCCACGCTGTTTTGACCT-3'

PCR products were purified using the High Pure PCR Product Purification Kit (Roche), digested with AgeI and SalI restriction enzymes, and the right bands were extracted from the agarose gel using the JETQUICK Gel Extraction Spin Kit (GENOMED). Subsequently, desired genes were cloned into the lentiviral backbone under a SFFV promoter using the Quick Ligation Kit (New England Biolabs). Clones were checked by restriction analysis using SalI and EcoRV as well as NcoI restriction enzymes and sequenced using the following primers:

- Fwd 5'-AAGAATAGTAGACATAATAGC-3',
- Rev 5'-AAAGCAGCGTATCCACATAGCG-3'.

To simplify, created vectors were named as follows: LV_hVEGF, LV_hAng1, LV_SphK1 and LV_GFP (**Figure 7**).

The same genes were also cloned into a bidirectional lentiviral backbone provided by Dr. Mario Squadrito with the gene of interest under the PGK promoter and GFP (in case of hVEGF-A) and dNGFR (in case of hAng1 and hSphK1) under the CMV promoter, but they were not further used in this study.

Lentiviral vectors were at first produced in-house using the protocol described in[66]. Briefly, VSV-G pseudotyped 3rd generation vectors were produced using the HEK293T cell line in a DMEM medium containing 10% FBS, penicillin (100U/ml), streptomycin (100U/ml) and glutamine. A plasmid DNA mix was prepared in the presence of $CaCl_2$ 0.25M final concentration, and HEPES buffered saline to form a precipitate. The virus was

concentrated by ultracentrifugation at 22.000 rpm for 2h at 22°C. Lentiviral vectors were resuspended in PBS and stored in aliquots at -80°C.

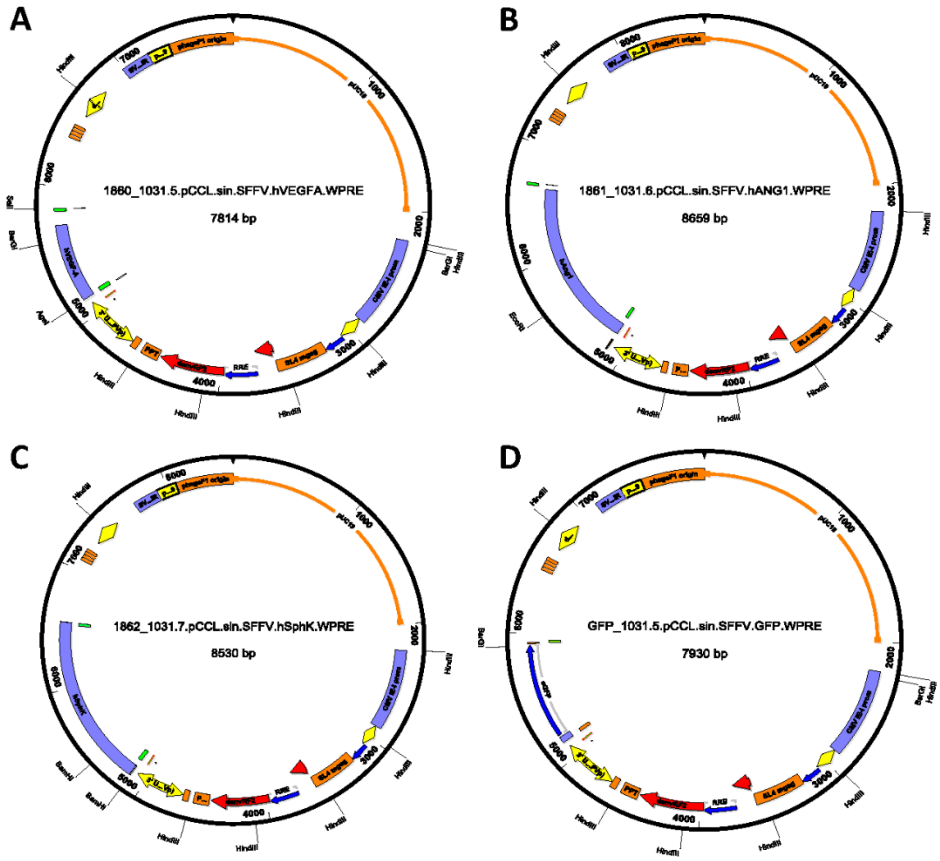

Figure 7. Lentivirus vector maps of A. LV_hVEGF, **B.** LV_hAng1, **C.** LV_SphK1 and **D.** LV_GFP.

Titration was performed by quantitative PCR analysis. Briefly, 200,000 HEK293T cells were seeded per well and infected with once-thawed viral vectors at 10^{-3}, 10^{-4}, 10^{-5}, 10^{-6}, 10^{-7} serial dilutions. After removing the virus, cells were cultured for 7 days. Genomic DNA was isolated using Qiagen KIT.

Once larger amounts were needed, viruses were produced by the Viral Vector Unit at CNIC.

Cell culture and bone marrow harvest

HEK cells were cultured in DMEM medium (Gibco) with addition of 10% FBS (Sigma), 2mM L-glutamine, 100U/ml penicillin and 100U/ml streptomycin (Lonza).

Mouse bone marrow cells were harvested from 9-12 weeks old BL6 mice, or Gt(ROSA)26Sor$^{tm4(ACTB-tdTomato,-EGFP)Luo}$ mice in the case of the cell homing experiment, by flushing femurs and tibias with cold PBS with the addition of 2% FBS. Red blood cell depletion was performed by adding sterile H_2O miliQ on the cell pellet followed immediately with the addition of a large volume of PBS 2% FBS. Cells were cultured in density $2x10^6$ cells per ml on non-adherent plates in 199 medium (Lonza), 10% FBS, 100U/ml penicillin, 100U/ml streptomycin in presence of murine cytokines: 20ng/ml M-CSF and 100ng/ml SCF (Peprotech).

Bone marrow cell MOI experiment

To investigate the best infection condition for bone marrow cells, freshly harvested BM cells were seeded in density $2x10^6$ cells per ml on a 96 well plate in the final volume 300µl. Infection was performed overnight with SFFV_GFP virus MOI 100, 50, 25 and 12.5. The presence of GFP^+ live cells was examined 24h, 3d and 6d after LV infection using FACS Fortessa (B&D).

Real time PCR

HEK cells were infected with a supernatant containing unconcentrated virus and kept in culture for a few passages. Subsequently, the cells were harvested and total RNA isolation was performed using the RNeasy Mini or Micro kit (QIAGEN), depending on the amount of cells. A reverse transcription reaction of 1µg of RNA was performed using the MultiScribe reverse transcriptase (High-Capacity cDNA Reverse Transcription Kit, Applied Biosystems) according to the manufacturer's protocol, with the addition of an RNAse inhibitor (RNasin, Promega). A qPCR reaction was performed in the ABI PRISM® 7900HT FAST Real-Time PCR System using the SYBR®Green dye.

Mouse BM cells were infected with MOI 50 of corresponding LV. After overnight incubation, cells were washed with PBS and put back in the culture. 24h and 72h later, cells and supernatants were collected. Total RNA isolation, RT and qPCR were performed as described above for HEK cells. Experiments were carried out using three housekeeping genes in each approach. In the case of HEK cells, housekeeping genes were hHPRT, hGAPDH, 1433, and, for murine bone marrow cells, m36b4, mGAPDH, mTBP.

All experiments included H_2O sample as a template control, as well as untransduced cells as a negative control. Primers are summarized in Table 2.

Table 2. Primers used for qPCR analysis

Gene	Primer	Sequence
hVEGF-A	Fwd	5'-CTACCTCCACCATGCCAAGT-3'
	Rev	5'-CTCGATTGGATGGCAGTAGC-3'
hAng1[1]	Fwd	5'-TCGTGAGAGTACGACAGACCA-3'
	Rev	5'-TCTCCGACTTCATGTTTTCCAC-3'
hSphK1[2]	Fwd	5'-CATTATGCTGGCTATGAGCAG-3'
	Rev	5'-GTCCACATCAGCAATGAAGC-3'
hGAPDH	Fwd	5'-GGAGCGAGATCCCTCCAAAAT-3'
	Rev	5'-GGCTGTTGTCATACTTCTCATGG-3'
hHPRT	Fwd	5'-CCTGGCGTCGTGATTAGTGAT-3'
	Rev	5'-AGACGTTCAGTCCTGTCCATAA-3'
hYWHAZ	Fwd	5'-CCTGCATGAAGTCTGTAACTGAG-3'
	Rev	5'-GACCTACGGGCTCCTACAACA-3'
mGAPDH	Fwd	5'-AATGCATCCTGCACCACCAA-3'
	Rev	5'-GTGGCAGTGATGGCATGGAC-3'
mTBP	Fwd	5'-GCTCTGGAATTGTACCGCAG-3'
	Rev	5'-CTGGCTCATAGCTCTTGGCTC-3'
m36b4	Fwd	5'-GCGACCTGGAAGTCCAACTA-3'
	Rev	5'-ATCTGCTGCATCTGCTTGG-3'

[1]PrimerBank ID: 21328452c2
[2]sequence described in[67] [61]

ELISA

To detect the presence of hVEGFa and hAng1 in the supernatants of cells previously infected with desired lentiviruses, R&D ELISA kits for these two proteins were used.

Transduced HEK cells, as well as an untransduced control, were seeded on a 24-well plate in 0.5ml of OPTI-MEM medium (Gibco) with 1% FBS, 100U/ml penicillin, 100U/ml streptomycin. After approximately 30h incubation, supernatants were collected and kept in -20°C.

BM cells were incubated overnight with lentiviruses at MOI 50. After washing the virus, cells were seeded in a non-adherent 6-well plate at a density of 2mln/ml and the first collection of supernatant was performed 24h after. Next, cells were seeded back in culture and second supernatants were harvested after 48h and stored at -20°C.

ELISA kits for hVEGFa and hAng1 were performed in proper dilutions according to the manufacturer's instruction. Untransduced cells of both types served as a negative control and medium correction was performed using medium corresponding to each cell types. Optical density was determined using the Benchmark Plus microplate spectrophotometer (BIO-RAD) set at 450nm with wavelength correction at 540nm. Standard curves were created using CurveExpert software[68].

Plasma samples collected at three time points, t_0 (baseline, approximately one week before I/R), t_5 (24h after injection of BM_LV_hVEGF) and t_28 (endpoint), were analyzed for the presence of human VEGF-A protein using the Human VEGF-A Platinum ELISA kit (eBioscience, BMS277/2) according to the manufacturer's instruction. Optical density was measured using the Benchmark Plus microplate spectrophotometer set at 450nm with wavelength correction at 620nm. Standard curves were created using CurveExpert software[68].

Blood and plasma sample collection

Blood samples were collected from the facial vein of the mice (during experiment) or from aorta (at the endpoint) to EDTA coated tubes (Sarstedt Inc). Blood samples were used either for FACS analysis or for plasma collection.

For plasma collection, samples were centrifuged at 2000g for 10 min, followed by a second centrifugation at 2500g for 15min. Subsequently, plasma samples were snap frozen in liquid nitrogen and kept in -80°C for analysis of S1P and hVEGF-A.

Flow cytometry

To analyze peripheral blood monocytes, the flow cytometry technique was used. Blood samples were harvested into EDTA coated tubes and 100µl of each sample was placed into 1ml of 1X RBC Lysis Buffer (eBioscience) for 2-4 min, until the solution became clear. Subsequently, cells were washed with 9ml of 'FACS buffer' (2.5% FBS, 0.5mM EDTA in PBS) and centrifuged for 8min at 1200rpm. Blocking with 100µl of 1:100 Fc block (Mouse BD Fc Block, Purified Rat Anti-Mouse CD16/CD32) in FACS buffer was performed for 20min at 4°C. Cells were washed with 2ml of FACS buffer and centrifuged for 5min in 1200rpm. After that, cells were stained with 1ul/mln CD11b-Alexa fluor-647, 2µl/mln F4/80-PE-Cy7, 1.5µl/mln Ly6C-FITC, 2µl/mln CCR2-PE and 2µl/mln CX_3CR1-Pacific Blue in 100µl of FACS buffer for 15min in RT protected from light. Washing with 2ml of FACS buffer and centrifugation for 5min in 1200rpm was performed. Cells were resuspended in 150µl of FACS buffer with addition of 5µl live/death dye 7-AAD (BD Pharmingen) per sample. Sample acquisition was performed using BD LSRFortessa.

Single cell suspension from splenic tissue was obtained by pressing it through a 100µm cell culture strainer (BD). Subsequently, red blood cell lysis and the rest of the procedure was performed as described above.

Table 3. List of antibodies used for FACS staining

Name	Clone, company
CD11b-Alexa fluor-647	M1/70, BD
F4/80-PE-Cy7	BM8, Biolegend
Ly6C-FITC	AL-21, BD Pharmingen
CCR2-PE	475301, R&D
CX3CR1-Pacific Blue	SA011F11, Biolegend

Aortic rings assay

To assess the angiogenic response for various stimuli *in vitro,* the aortic rings assay described in[69] was used. Briefly, aortas were dissected from 7-10 week old BL6 male mice, cleaned from fat tissue, and cut into approximately 1mm pieces. After overnight starvation in OPTI-MEM (Gibco), 2mM L-glutamine, 100U/ml penicillin, 100U/ml streptomycin

medium, rings were embedded in 1mg/ml rat tail Collagen type I (Merck Millipore) matrix in a 96-well optical plate at longitudinal orientation. OPTI-MEM medium with 2.5%FBS, L-glutamine, penicillin, streptomycin was added in the presence of various combinations of soluble factors (rhVEGF 30ng/ml, rhAng1 70ng/ml, S1P 1µM, Peprotech and Cayman Chemical) or mouse BM cells previously infected with lentivirus (BM_hVEGF, BM_hAng1, BM_SphK1). Ten rings per group were kept in the culture for 8 days and the medium was changed at day 4 and 6. Rings were rinsed with a PBS with ions and fixed with 4% formalin (1.6%PFA) for 30min, RT. Afterwards, permeablization with PBLEC solution (PBS with ions, 0.1mM $MnCl_2$, 1% Tween-20) in two 15min incubations at RT was performed, followed by blocking with DACO buffer (protein block serum free #X0909) 30min at 37°C.

Primary antibodies: IB4 (in the case of experiments with soluble cytokines) or hamster CD31 (in experiments using bone marrow cells) at concentration 1:150 and SMA-Cy3 (1:400) in 50µl of PBLEC buffer per well were incubated overnight at 4°C on a nutator. After 3 x 15min washing with PBS 0.1% Triton-100, incubation with secondary antibodies: streptavidin-488 (1:200) or anti-hamster-647 (1:500) and Hoechst (1:10 000) was performed for 3h at RT. Rings were washed and embedded by adding 1 drop of Fluoromont to each well and kept in 4°C protected from light. Imaging was performed using Nikon A1R confocal system coupled to a Nikon Ti-Eclipse microscope using 10x objective and capturing 400µm in depth with z-stack every 3µm. Analysis of images was performed using a Matlab-based method for 3D-microvasculature developed in our lab, and using Imaris software. Antibodies used are summarized in Table 4 at the end of this chapter.

In vivo experiment protocol

Three days after I/R surgery, echocardiography under inhaled isoflurane anesthesia was performed to confirm myocardial infarction. Four days post I/R, mice were intravenously injected with $5x10^6$ bone marrow previously infected with LV_hVEGF in 100µl of PBS or with PBS as a control group. 24h after first injection, blood samples were collected via facial vein. Seven days post I/R, a second injection was performed, with $5x10^6$ BM cells infected with LV_hSphK1 and blood was collected 24h after injection. At day 28, endpoint

echography was performed and mice were sacrificed using a CO_2 chamber. Blood samples were collected and hearts, lungs and livers were weighed and collected. Heart perfusion was performed through aorta using 5-10ml of cold PBS. Organs were immediately put in 0.4% PFA for overnight incubation at 4°C on a nutator. After washing with PBS, samples were incubated in 20% and 40% sucrose until they sank. For long-term storage, organs were embedded in OCT and kept in -80°C.

Ischemia reperfusion in mice

10-12 week old mice were pre oxygenated with 100% O2 for 5 min and anaesthetized with a combination of 10mg/kg Alfaxalone (Alfaxan®), 1mg/kg Medetomidine (Medeson®) and 2mg/kg Midazolam (Dormicun®). After thoracic fur trimming and application of a gel solution to avoid corneal drying, animals were intubated until they lost the pedal reflex and laid in right lateral recumbency, and chlorhexidine 1% was applied for skin disinfection. Mouse body temperature was maintained using a warmed 38ºC pad, and they were ventilated with 100% O2 (120 breaths per minutes 8ml/kg of tidal volume) using Minivent 680 ventilator (Harvard apparatus). To reach the left ventricle of the heart, a 0.5cm skin incision was made over the projection of the 4th costal space. Without damaging left pectoral muscles, thoracic space was exposed between the 4th and 5th ribs. After a soft pericardiectomy, the left anterior descendent (LAD) coronary artery was visualized and occluded with a small piece of P10 fixed laterally with 7/0 nylon suture (Prolene®). LAD coronary artery reperfusion was allowed after 45 minutes, just releasing the suture and tubing pressure over the vessel. Reperfusion was confirmed after visualization of reddish heart color. Ribs and skin incision were sutured closed by planes with 6/0 silk suture. For recovery, 2mg/kg of atipamezol (Revertor®) was inoculated IP and mice were extubated once they become conscious. To keep postsurgery analgesia, we inoculated SC with 0.1mg/kg of buprenorphine (Buprex®) and 320mg/kg of Paracetamol in drinking water for 3 days.

Lentiviral infection of bone marrow cells

Bone marrow cells were isolated as described above and, after red blood cell depletion, were cultured overnight in 10ml of 199 medium, 10% FBS, 100U/ml penicillin, 100U/ml streptomycin in the presence of murine cytokines 20ng/ml M-CSF and 100ng/ml SCF on non-adherent petri dish. After overnight incubation, cells were counted using trypan blue and resuspended at 2mln/ml concentration. Desired viruses were added at MOI50 and incubated overnight at a 6-well non-adherent plate. Subsequently, cells were harvested and washed by adding a large amount of PBS 2% FBS to remove virus particles. After centrifugation, cells were resuspended in PBS 2% FBS, counted, washed again in ~40ml of PBS, and filtered through a 70µm cell mesh. The cell pellet was resuspended in PBS at concentration 100µl per $5x10^6$ cells.

Immunohistochemistry and immunofluorescence analysis

Semi-3D sections of 15µm were cut using a Leica AM1950 automated cryostat and slides were stored long term at -20°C. For immunostaining, slides were washed in PBS for 5 min and permeabilized for 10min in 0.1% Triton in PBS at RT. Blocking in 10% BSA, 0.1% Triton in PBS was performed for 1h in a wet chamber at RT. Primary antibodies were incubated in blocking buffer overnight in a wet chamber at 4°C. After triple 10min washing with 0.1 Trition PBS, slides were incubated with primary antibodies for 1.5h in a wet chamber protected from light at RT. Subsequently, slides were washed twice in 0.1% Triton PBS and once in PBS for 10min and mounted with Fluoromont G (Southern Biotech).

For microvasculature staining, the primary antibodies hamster α-CD31 (1:150), rat α-PDGFRβ (1:150) and α-SMA-Cy3 (1:400), the secondary antibodies goat α-hamster Alexa Fluor-647, chicken α-rat Alexa Fluor-488 (1:500), and Hoechst (1:10.000) were used. Images were acquired with a Leica SP5 confocal microscope using 40x objective (NA 1.25) with oil immersion. Z-stacks were acquired every 1µm.

To quantify cardiomyocyte size and macrophage content, the primary antibodies rabbit anti-Laminin (1:50) and rat anti-CD68 (1:200), the secondary antibodies chicken a-rb-488 and goat a-rat 568 (1:500), and Hoechst (1:10.000) were used.

Additionally, macrophage content was determined by immunohistochemistry staining to avoid autofluorescence in the infarct zone using anti-F4/80 antibody. CNIC's Histology Unit performed immunochemistry staining and tissue was visualized using NanoZoomer-2.ORS®, Hamamatsu.

Fibrosis was assessed based on Masson-Tichrome staining and tissue was visualized using NanoZoomer-2.ORS® (Hamamatsu).

In the homing experiment, tissue slices were stained with anti-RFP-594 antibody and Hoechst with 1:300 and 1:10 000 dilutions respectively.

For 3D pig vasculature analysis, thick slices of approximately 100µm were cut using Leica AM1950 automated cryostat. Immunostaining was performed in flotation using the following procedure: 2h permeabilization in 0.3% Triton, 0.1% Tween in PBS at RT; 1h blocking with 0:3% Triton, 4% FBS in PBS at 4°C. For the staining of the microvasculature, slices were incubated with primary antibodies goat VE-Cadherin and mouse SMA with dilution 1:100 and 1:200 respectively in blocking buffer overnight at 4°C. After washing with 0.3% Triton in PBS, incubation with secondary donkey anti-goat Alexa Fluor-568, chicken anti-mouse Alexa Fluor-647 at 1:500 and Hoechst 33342, 1:10.000 (Life Technologies) was performed for 2h in blocking buffer at RT. After washing, slices were mounted on the glass using FluoromountG. All incubations were performed on the nutator. Antibodies used are summarized in Table 4.

Table 4. List of antibodies/reagents used for immunostaining

Name	Species	Clone, company
anti-goat-568	donkey	Molecular Probes (A-11057)
anti-hamster-647	goat	Jackson ImmunoResearch (127-605-160)
anti-mouse-647	chicken	Molecular Probes (A-21463)
anti-rabbit-488	chicken	Molecular Probes (A-21441)
anti-rat-488	chicken	Molecular Probes (A-21472)
anti-rat-568	goat	Molecular Probes (A-11077)
anti-RFP-594	rabbit	polyclonal, Biotium (#20422)
CD31	hamster	2H8, Merck
CD68	rat	FA-11, Serotec
F4/80	rat	CI:A3-1, Abcam (Ab6640)

Hoechst 33342	-	Invitrogen (H1399)
IB4-biotynylated	-	Vector Laboratories (B-1205)
Laminin	rabbit	Sigma (L9393)
PDGFRβ	rat	APB5, eBioscience
SMA unconjugated	mouse	1A4, Sigma
SMA-Cy3	mouse	1A4, Sigma
streptavidin-488	-	Invitrogen (S32354)
Ve-Cadherin	goat	polyclonal, Santa Cruz (sc-6458)

Image analysis

Analysis of heart roundness was performed on images of the hearts after dissection using ImageJ software. Roundness was calculated as: $4 * \frac{area}{\pi * major\ axis x^2}$.

To quantify cardiomyocyte size, ImageJ based semi-automated macro was designed. Cardiomyocytes recognized by surrounding laminin staining were quantified by area and perimeter. Subsequently, all images were revised by eye and incorrectly recognized ones were removed and/or labelled manually.

Macrophage number based on CD68 immunofluorescence staining was analyzed using semi-automated ImageJ macro. At first, nuclei were recognized based on Hoechst staining and subsequently presence of $CD68^+$ signal within a band surrounding nuclei was analyzed. Macrophages were defined as $CD68^+$ cells and represented as a percentage of the total number of cells.

Macrophage number based on F4/80 immunochemistry staining was analyzed using semi-automated ImageJ macro. Channels were separated using the color deconvolution plugin and similarly to the macro for CD68 immunostaining, macrophages were defined as a nuclei surrounded with F4/80 staining and represented as a percentage of total number of nuclei.

All ImageJ-based macros were designed by Veronica Labrador Cantarero from CNIC's Microscopy Unit.

Quantification of fibrosis was performed using ImageJ software on seven sequential 15µm-thick cuts from the apex to the base of the heart. Results are represented as a percentage of fibrotic tissue area to the left ventricle area.

Analysis of the vasculature was performed using MATLAB-based 3D analysis method designed in our lab and described in detail in[70]. Capillaries were defined as $CD31^+$ vessels of diameter < 5µm, estimated from previously made measurements in various species and tissues[71-74]. Medium-size vessels were defined as $CD31^+$ vessels of diameter between 5.1 and 8.7 µm. This category may constitute post-capillary venules as well as dilated capillaries compensating vasculature loss in response to injury. Large vessels (venules) were defined as $CD31^+$ vessels of diameter > 8.7 µm based on literature[74-77]. Arterioles were defined as $CD31^+$ SMA^+ vessels independently of their size.

Echocardiography

Echocardiography was performed by an operator blinded to the study using a high-frequency ultrasound system (Vevo 2100, Visualsonics Inc., Canada) with a 30-MHz linear probe. Mice were lightly anesthetized with 0.5-2% isoflurane in oxygen, administrated through a nose cone. Echocardiography was acquired in supine position using a heating platform and warmed ultrasound gel to maintain body temperature. Standard two-dimensional echocardiography (2D) and M-mode was performed in parasternal long axis view and parasternal short axis view. Images were acquired and analyzed later by a blinded expert using Vevo 2100 software. Cardiac parameters such as end-diastolic and end-systolic volumes, stroke volume and left ventricular ejection fraction were quantified using area length.

Statistics

Statistical analysis was performed using GraphPad Prism 6/7 software. Dependently of data being normally or not-normally distributed (defined using D'Agostino-Pearson and Shapiro–Wilk normality tests), parametric or non-parametric tests were performed. To compare two datasets, an unpaired t-test was used. A paired t-test was performed only to

analyze echocardiography-based progress of heart function of individual mice over time. To compare more than two datasets, one way ANOVA with Turkey's test was used. *P-values* were defined as follows: *<0.05; **<0.005; ***< 0.0005, ****< 0.0001. Sample size (n) is indicated next to the each figure.

RESULTS

1. *Ex vivo* evaluation of combined angiotherapies. Aortic ring assay

To analyze the effect of single or combined proangiogenic factors on its capability to induce sprouting, we decided to use the aortic ring assay, a model used to analyze angiogenic processes *ex vivo*[78].

1.1 Soluble factor approach

At first, we sought to check the ability of single factors to induce angiogenesis; therefore, we cultured aortic rings in the presence of rhVEGF165, rhAng1 and S1P for 7 days **(Figure 8**). VEGF is a strong inductor of angiogenesis, however it was shown that VEGF-induced vessels regress[79] and leak[80]. Therefore, the use of a combination of angiogenic factors could be essential to establish a stable and mature vascular network. The use of VEGF, Ang1, and S1P in inducing angiogenesis was already described[60,81-83], but to our knowledge they were not compared in simultaneous experiments to select for the best combination. Thus, our experimental setup consisted of two approaches. The first being sequential delivery of factors where we use VEGF at day 1 of aortic ring assay and then after 4 days, an addition of either Ang1 or S1P. The second approach was prolonged delivery of VEGF and again addition of either Ang1 or S1P up until day 7 of assay whereby rings were fixed and stained. We then analyzed sprouting, using IB4 to stain ECs, and mural cell coverage, stained with αSMA.

Among groups exposed to single factors, only treatment with S1P showed significant improvement in inducing sprouting (represented as volume occupied by endothelial cells stained with IB4) (**Figure 9A**) compared to non-treated rings and those treated with hVEGF. Within groups exposed to combined therapies, those with media containing S1P together with both sequential (3d) and prolonged (7d) hVEGF treatment, have significant improvement in sprouting compared control. Furthermore, treatment with hVEGF 7d + S1P 4d significantly increased ECs volume density 6-fold compared to both groups with hVEGF +Ang1 treatment. Interestingly, any treatment including S1P improved aortic ring sprouting 9-fold compared to non-treated groups and 5-fold when compared to VEGF alone.

Additionally, morphology of the sprouts differed. All aortic rings with S1P-induced sprouts created more complex vessel networks compared to the other groups (**Figure 8**).

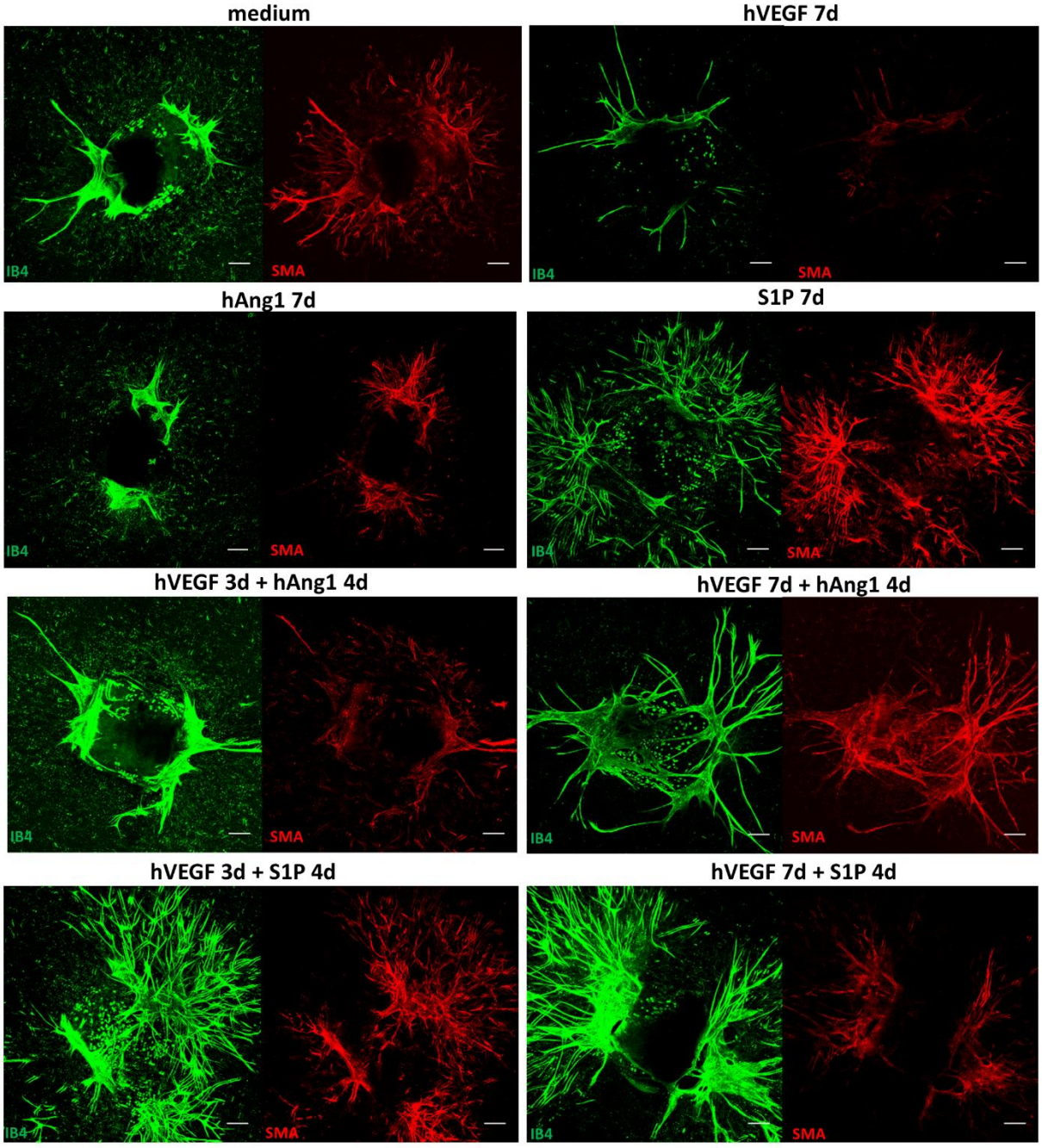

Figure 8. Proangiogenic efficacy of soluble factor combinations in aortic ring assay. Representative images of rings from each group. Collagen embedded rings were treated with single factors (hVEGF, hAng1 or S1P) for 7 days. In the combined approach, rings were exposed to prolonged (7d) or sequential (3d) presence of hVEGF in combination with either hAng1 or S1P for 4 days. At day 7 rings were fixed and stained with IB4 and SMA antibodies. Maximal intensity projection, scale bar 200µm.

IB4$^+$ endothelial volume parameter gives information about vascular volume, but not about their stability and maturation. Therefore, rings were co-stained with αSMA to determine mural cell coverage of vessels (**Figure 9B**). In our setting, we observed in all but one group, no significant differences in the percentage of SMA covered sprouts. The hVEGF 7d + S1P 4d combination group showed decreased mural coverage compared to both hAng1-combined treatments.

When summarizing both sprout abundance and their SMC coverage (**Figure 9C**), the two groups that show the best improvement in both categories are S1P alone and that with hVEGF 7d + S1P 4d combination, having no significant differences between them.

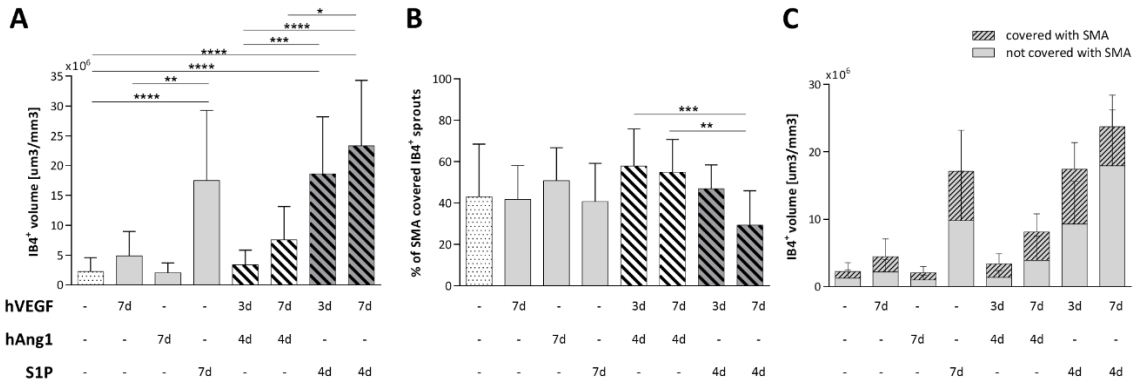

Figure 9. Proangiogenic effects of various combinations of soluble factors on aortic rings assay. A. Quantification of IB4$^+$ volume density. Rings were exposed for 7 days to either medium only or medium supplemented with indicated factors. Proangiogenic factors were added either alone or in combinations. **B.** Percentage of IB4$^+$ sprouts covered with SMA served as a mural cell marker. **C.** Summarized representation of IB4$^+$ volume covered and not covered with SMA. *Kruskal-Wallis test. n=18±2 rings per group in two independent experiments.*

1.2 Effects of lentiviral-infected bone marrow cells overexpressing proangiogenic factors.

After a broad screening process to select for the best combination of proangiogenic factors using commercially available hVEGF, hAng1, and S1P, we investigated whether bone marrow cells overexpressing chosen proangiogenic factors are capable of reproducing the same or similar phenotypes to those that we observed in the previous experiment.

1.2.1 Evaluation of lentivirus in HEK and mouse bone marrow cells

We first checked the ability of cloned lentiviruses to transduce cells to overexpress and secrete desired factors. In the first approach, we used a HEK cell line because of its ability to be easily transduced.

By real-time quantitative PCR, we observed a 100-fold change in expression of *hVEGF*, 500-fold of *hAng1* and over 300-fold of *hSphK1* mRNA compared to untransduced cells (**Figure 10B**). Next, we wanted to check the ability of these cells to produce desired factors and to secrete them. For that reason, we collected supernatants from above transduced cells, and tested the concentration of either hVEGF or hAng1 by ELISA (**Figure 10C, D**). In both cases, we observed increased amounts of protein compared to control, especially in the case of VEGF. A possible reason could be due to the fact that Ang1 protein is triple the size of VEGF and therefore, more difficult to secrete. In the qPCR experiment, we observed an increase in the mRNA levels of *hSphK1* but as overexpression of the kinase does not necessary mean higher amounts of phosphorylated sphingosine, we checked the abundance of S1P in transduced and untransduced cells by mass spectrometry. The results indicated an increase in LV_hSphK1 transduced cells (**Figure 10E**).

Once we confirmed that the lentiviruses were inducing overexpression and secreting desired factors in HEK cells, we tested their efficiency in primary mouse bone marrow cells (msBM).

As primary cells are notably more difficult to transduce[84], therefore, we began by establishing the best Multiplicity Of Infection (MOI) to infect msBM using a LV_GFP lentiviral vector (**Figure 10F**). The highest percentage of GFP^+ cells was observed with a MOI of 100, but it also resulted in a high mortality ratio; 47% of dead cells 6 days after transduction versus 26% with MOI50. Therefore, MOI50 was selected for further experiments. Similarly to HEK cells, we observed a higher secretion of hVEGF and hAng1 by transduced msBM cells (**Figure 10G and H**) as well as an abundance of S1P (**Figure 10I**).

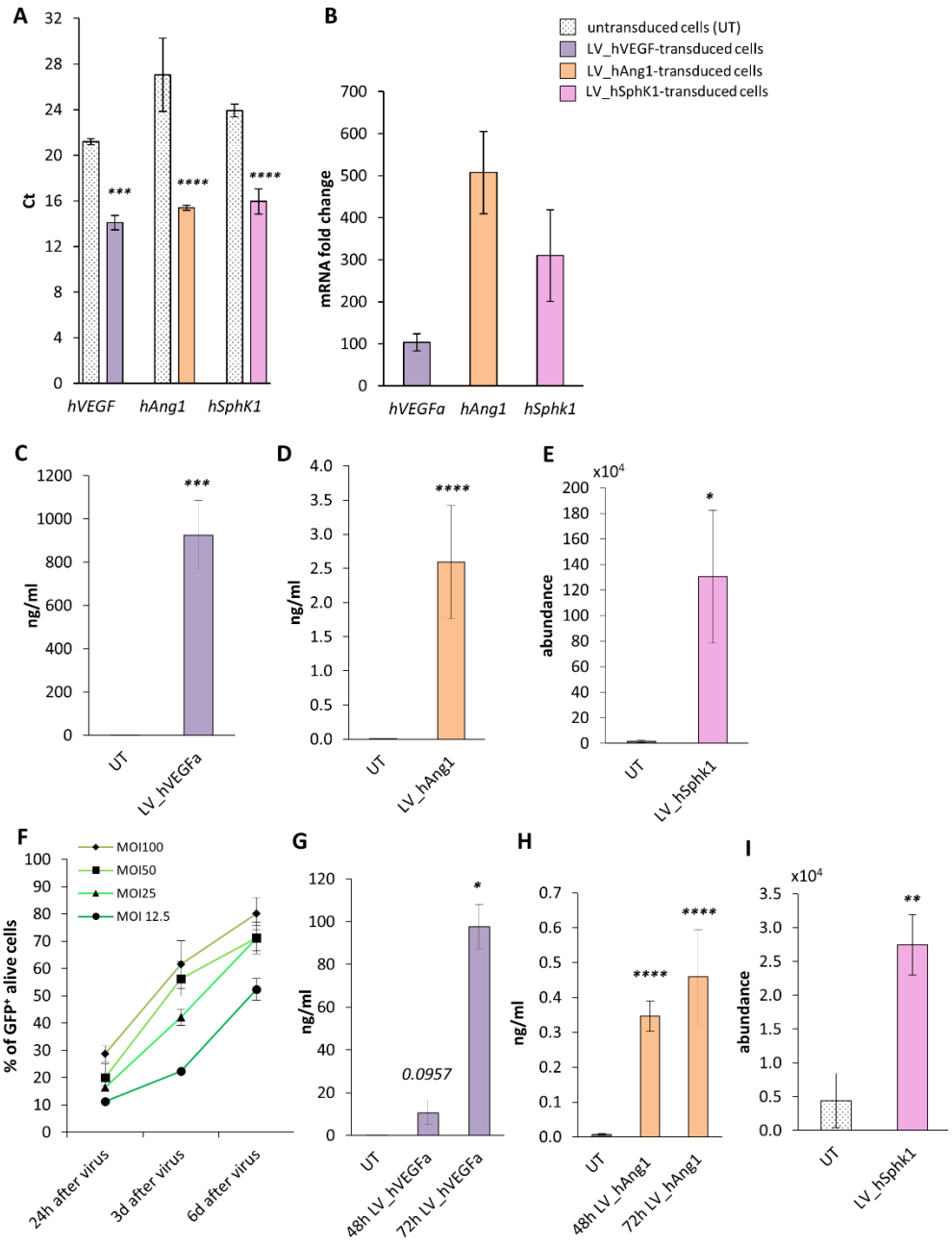

Figure 10. Evaluation of lentiviral vectors in HEK and msBM cells. A. Real-time quantitative PCR of *hVEGFa*, *hAng1* and *hSphK1* genes overexpressed in LV infected HEK cells compared to untransduced cells. **B.** mRNA fold change of gene expression. **C.-D.** ELISA of hVEGFa **(C)** and hAng1 **(D)** secretion in supernatants of LV-transduced HEK cells. **E.** Abundance of S1P in LV_hSphK1-transduced and untransduced HEK cells. **F.** Percentage of GFP^+ mouse bone marrow (msBM) infected with different MOI of LV_GFP lentivirus at different time points after LV-transduction. **G.-H.** ELISA of hVEGFa **(G)** and hAng1 **(H)** secretion by LV-infected msBM cells 48h and 72h post infection. **I.** Abundance of S1P in LV_hSphK1-transduced and control msBM. qPCR: *n=3 with 3 technical replicates each, in tree independent experiments. ELISA: n=6-7 in four experiments for HEK cells and n=4-5 in two experiments for msBM cells. S1P measurement: n=3 for HEK and n=2 for msBM cells with 3 technical replicates in one experiment. MOI test: n= 4 in two experiments. t-test (two samples)/one-way ANOVA (three samples).*

1.2.2 Effect of BM cells overexpressing proangiogenic factors in the aortic ring assay

Once we confirmed that msBM infected with the lentiviruses were capable of secreting soluble proangiogenic factors, we tested if they could induce sprouting *in vitro*.

In this approach, aortic rings were cultured with hVEGF_BM for 3 days followed by hAng1_BM or hSphK1_BM for 4 days (**Figure 11**). Control groups were cultured only with medium or with WT_BM. At day 7, rings were fixed and stained with CD31 for endothelial cells, and αSMA for mural cells.

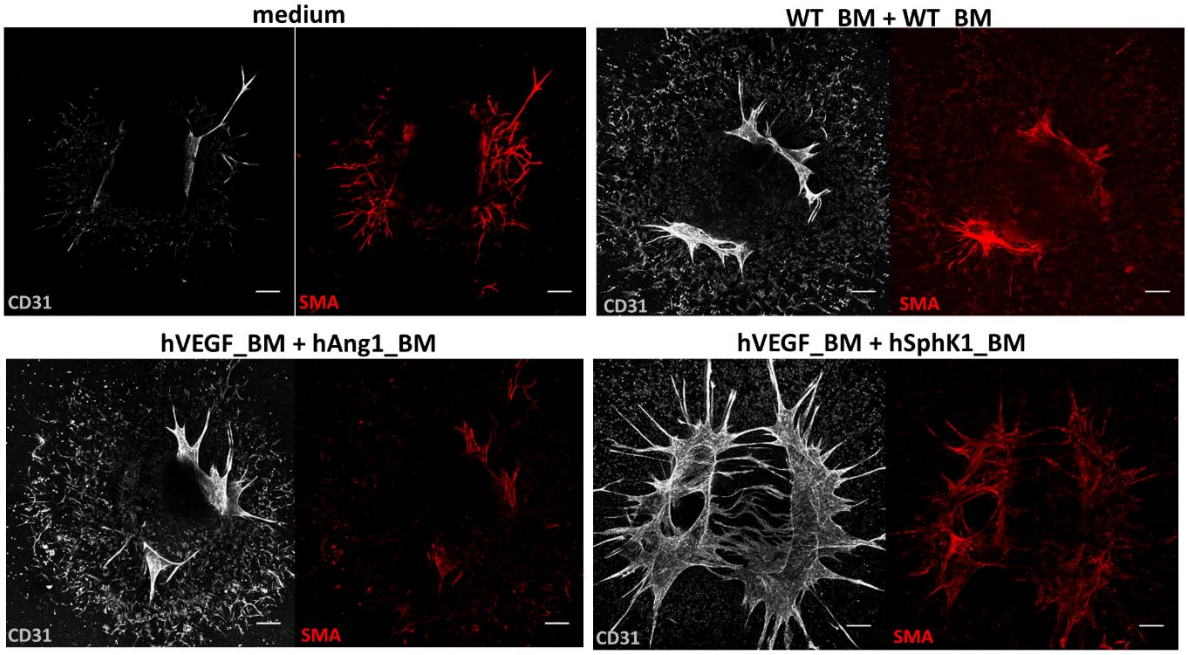

Figure 11. Aortic rings experiment using lentiviral-transduced bone marrow cells. Representative images of rings from each group. Collagen embedded rings were cultured in the presence of wild type BM cells or BM cells overexpressing hVEGF (BM_hVEGF) in combination with either BM_hAng or BM_hSphK1. Maximal intensity projection, scale bar 200µm.

Similarly to results seen in experiments with soluble factors, a combination of msBM overexpressing VEGF with SphK1 increased $CD31^+$ volume density (**Figure 12A**). We also observed a significant decrease in SMC coverage in hVEGF_BM + hSphK1_BM group (**Figure 12B**). This result is similar to that observed in the soluble factor approach where the

group of S1P with prolonged (7-day) exposure of VEGF, but not 3 days, showed impaired mural cell coverage. Here, even though we were delivering cells sequentially, BM cells overexpressing VEGF could have migrated into the collagen matrix and kept secreting VEGF. Nevertheless, combined hVEGF_BM + hSphK1_BM treatment yielded overall higher number of sprouts covered by SMA compared to the other groups (**Figure 12C**).

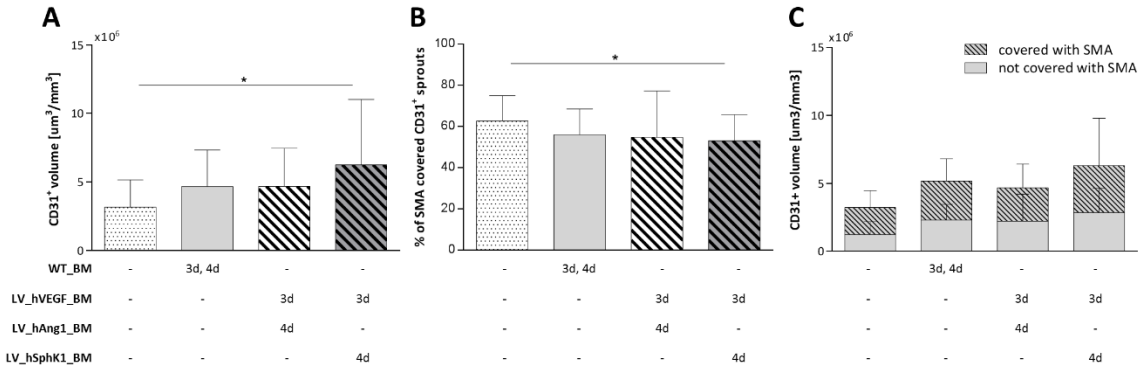

Figure 12. Proangiogenic effect of lentivirally infected bone marrow cells secreting soluble factors. A. Quantification of volume occupied by $CD31^+$ cells in aortic rings cultured for 7 days in the presence of medium, wild type bone marrow cells or bone marrow cells infected with LV_hVEGF in combination with either LV_hAng or LV_SphK1. **B**. Percentage of $CD31^+$ sprouts covered with SMA (mural cell marker). **C.** Representation of $CD31^+$ volume covered and not covered with SMA in each group. *Kruskal-Wallis test. n=25±2 rings per group in three independent experiments.*

2. Proangiogenic gene-cell therapy in ischemia/ reperfusion murine model of myocardial infarction

Experimental design

In light of *in vitro* results, we implemented a therapy to improve angiogenesis after myocardial infarction in a mouse model of 45-minute occlusion of the left anterior descending artery followed by reperfusion (**Figure 13**).

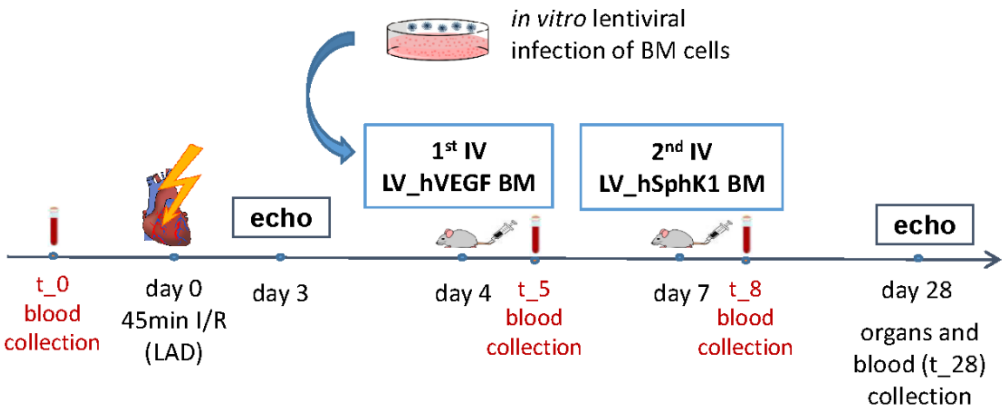

Figure 13. In vivo experimental design.

In the *ex vivo* approach, treatment of aortic rings with the combination of BM_hVEGF followed by BM_hS1P resulted in the highest amount of sprouts. Although the same combination showed decreased mural cell coverage, it remained close to 60%. Based on these results and taking into account the cardioprotective activity of S1P, we decided to use BM_hVEGF + BM_SphK1 combination in the *in vivo* setting. For that, bone marrow cells were isolated and infected with lentiviruses to overexpress hVEGF or hSphK1. Three days after I/R, echocardiography was performed to confirm myocardial infarction. At day 4 mice were randomly divided into control and treated groups, and injected intravenously with either PBS or $5x10^6$ of LV_hVEGF BM cells respectively. At day 7 post-I/R, mice from treated group were injected with $5x10^6$ of LV_hSphK1 BM cells and controls with PBS. At 28 days after myocardial infarction, endpoint echocardiography was performed, mice were sacrificed and organs collected for histological analysis. Blood samples were collected at

basal condition (~1 week before I/R), 24h after first and second i.v. injection, 14 days post-I/R and at the experimental end point.

2.1 Phenotype of lentivirally-infected bone marrow cells

In our experimental setting, bone marrow cells were lentivirally infected to secrete therapeutic proangiogenic factors: hVEGF and S1P (by overexpression of hSphK1).

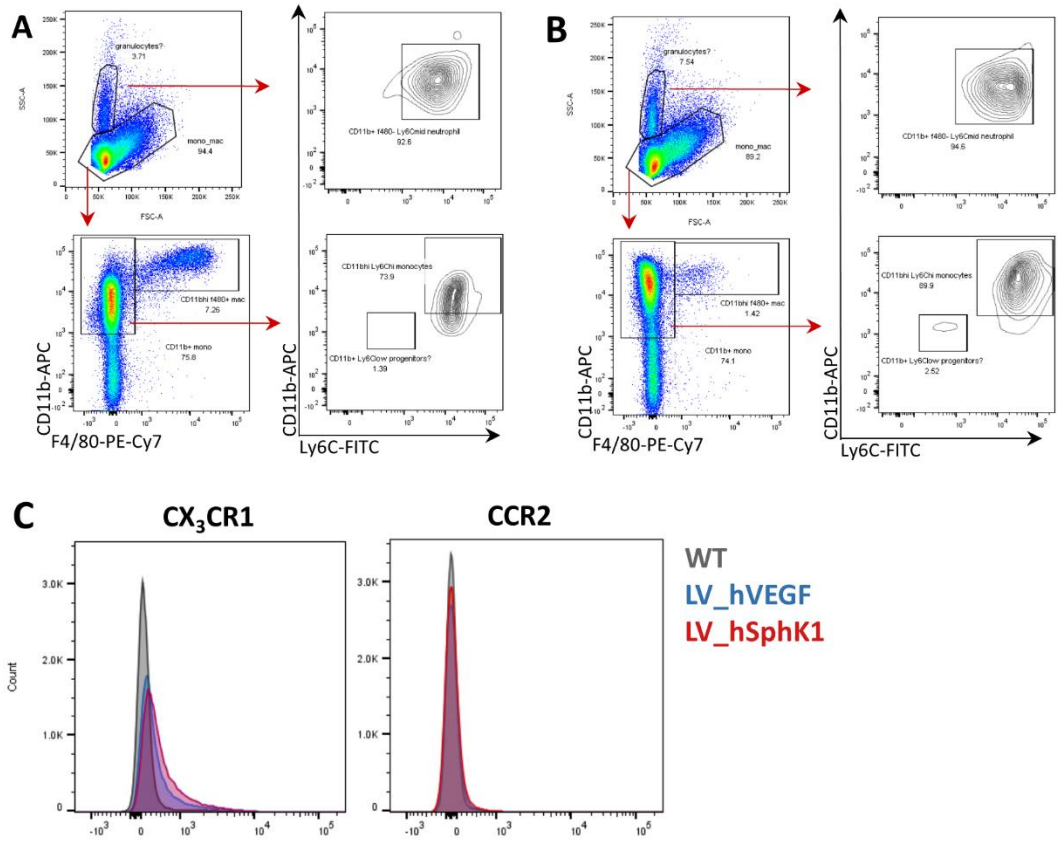

Figure 14. Characterization of lentivirally transduced bone marrow cells used for intravenous injection. A.-B. Gating strategy and representative plots of basal (**A**) and lentivirally infected bone marrow cells (**B**). **C.** Changes in CX_3CR1 and CCR2 receptors expression on monocyte subpopulation between wild type and lentivirally infected cells with both LV_hVEGF and LV_SphK1.

After infection, cells were harvested and intravenously injected into mice which had undergone a myocardial infarction.

To characterize whether lentiviral infection of msBM change their phenotype before injection, we analyzed them using flow cytometry. Prior to lentiviral infection, cells were cultured in the presence of M-CSF and SCF, which tends to shift their phenotype towards myeloid lineage[85]. This lineage includes, among other, the monocyte/macrophage and neutrophil populations. Therefore, at first, these populations were discriminated based on SSC/FSC plot (**Figure 14A, B**). Neutrophils were defined as $CD11b^{+}$ $F4/80^{-}$ $Ly6C^{mid}$ SSC^{hi}. Monocyte/macrophage subpopulation was further divided into macrophages ($CD11b^{hi}$ $F4/80^{+}$), monocytes ($CD11b^{hi}$ $F4/80^{-}Ly6C^{hi}$) and myeloid progenitors ($CD11b^{+}$ $F4/80^{-}$ $Ly6C^{low}$). Because of the role of chemokine receptors in monocyte homing, expression of CX_3CR1 and CCR2 receptors on the monocyte subpopulation was also determined in wild type (WT) and lentivirally-transduced bone marrow cells using median fluorescence intensity (**Figure 14C**).

As expected, monocytes constituted a majority of live cells (nearly 60%) (**Figure 15D**). Approximately 1% of live cells were myeloid progenitors (**Figure 15C**). Even though we did not observe differences in the size of monocyte population between infected and non-infected cells, we observed an increase of CX_3CR1 expression after LV infection. Furthermore, cells infected with LV_hSphK1 expressed more CX_3CR1 than the ones infected with LV_hVEGF (**Figure 15D**). In the case of CCR2 expression, we did not see any changes between groups (**Figure 15C**).

Both LV_hVEGF and LV_hSphK1 infection significantly decreased the amount of macrophages present in the bone marrow cell culture from 6% of live cells to less than 1.5% (**Figure 15A**). Conversely, there was an increase in the neutrophil population, from 3% in wild type cells to 6% in cells infected with LV_hVEGF and a slightly higher percentage (7%) after LV_hSphK1 infection (**Figure 15B**).

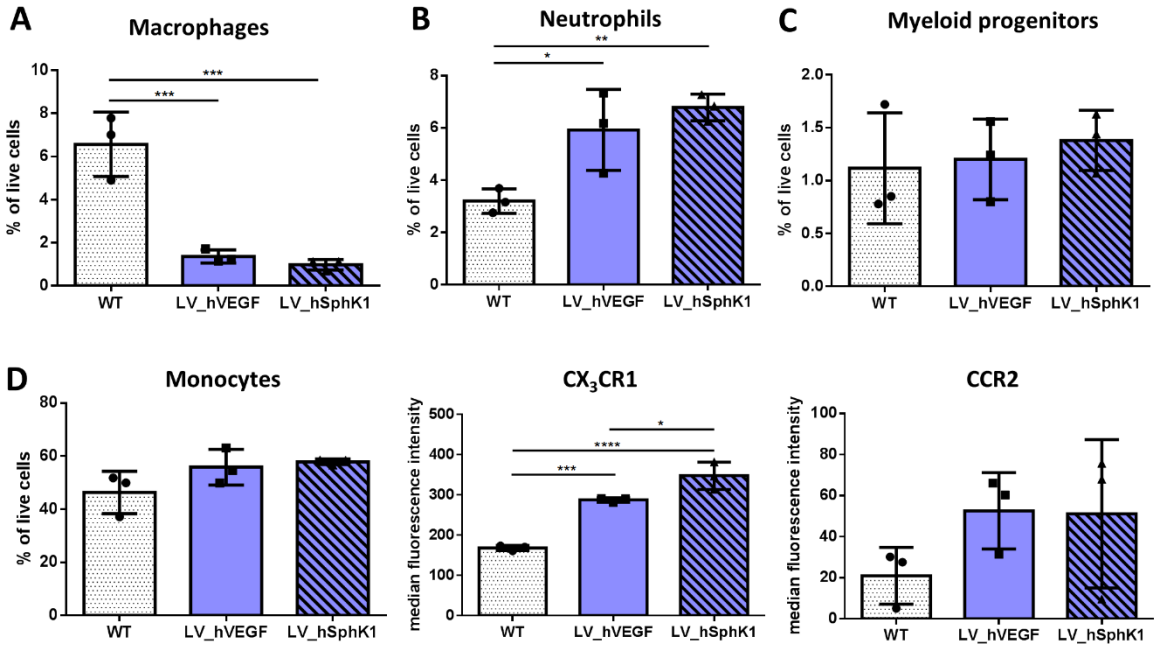

Figure 15. Quantitative representation of bone marrow subpopulations infected with lentivirus. Bone marrow cells were cultured in the presence of M-SCF and SCF which shifted their differentiation into the myeloid lineage. **A.** Percentage of the macrophage population defined as $CD11b^{hi}$ $F4/80^{+}$. Neutrophils were defined as $CD11b^{+}$ $F4/80^{-}$ $Ly6C^{mid}$ SSC^{hi} (**B**). **C.** Percentage of myeloid progenitors defined as $CD11b^{+}$ $F4/80^{-}$ $Ly6C^{low}$. **D.** Percentage of monocytes defined as $CD11b^{hi}$ $F4/80^{-}Ly6C^{hi}$ and their expression of CX_3CR1 and CCR2 receptors represented as median fluorescence intensity.

2.2 Analysis of therapeutic soluble factors in the plasma

To check whether intravenous delivery of infected bone marrow cells elevated the amount of therapeutic factors in the plasma, we collected blood samples 24 hours after each injection, as well ~1 week before surgery (baseline) and at 28 days post-I/R (experimental endpoint).

Analysis of the presence of S1P in the plasma was performed 24h after injection of LV_SphK1 BM (day 8 post-MI), at the baseline and endpoint. We observed an increased amount of S1P in the treated group at day 8 post-MI (24h after BM_hSphK1 injection) although not significant (**Figure 16**). Interestingly, at 28 hours after myocardial infarction, the amount of S1P in treated group returns to baseline levels, whereas in the control group, it is noticeably increased.

The hVEGF was not detectable in the plasma of the tested mice (data not shown).

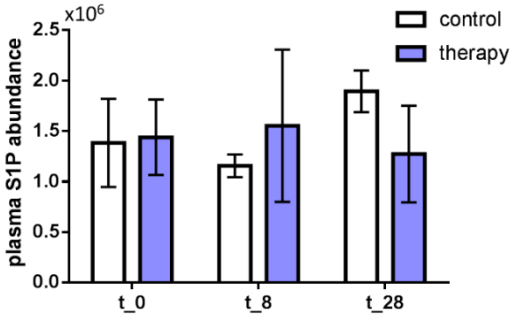

Figure 16. S1P levels in the plasma of mice injected with bone marrow cells overexpressing hSphK1 and controls. S1P presence was measured before I/R (t_0), 24h post LV_SphK1_BM injection (t_8) and at endpoint (t_28). *One-way ANOVA, n=3, 4 mice in control and therapeutic groups respectively in one experiment.*

2.3 Visualization of intravenously injected bone marrow cells homing to the damaged heart

To confirm the ability of intravenously injected bone marrow cells to migrate to the infarcted myocardium, we used bone marrow cells from Gt(ROSA)26Sor$^{tm4(ACTB-tdTomato,-EGFP)Luo}$ mice, which express dtTomato red fluorescence protein (RFP) on the membrane of all cells/tissues. 5x10^6 red bone marrow cells or PBS were intravenously injected at day 4 after ischemia-reperfusion and hearts were analyzed 24h after injection.

Histological analysis of the infarct zone of the hearts stained with anti-RFP antibody, confirmed the presence of cells with membrane dtTomato in the granulated tissue of the hearts of mice injected with red bone marrow cells (**Figure 17A,** lower panel) and also in the epicardium (**Figure 17A,** upper panel), although less. In contrast, in PBS injected mice, red fluorescence signal was not detected at the cell membrane. We observed unspecific red signal which followed the pattern of autofluorescence-control green channel. Infarct zone of the heart, similarly to other injured tissues, is characterized by a high level of autofluorescence in green but also in red channel of confocal microscopy, coming from infiltrating phagocytic cells (**Figure 17B**).

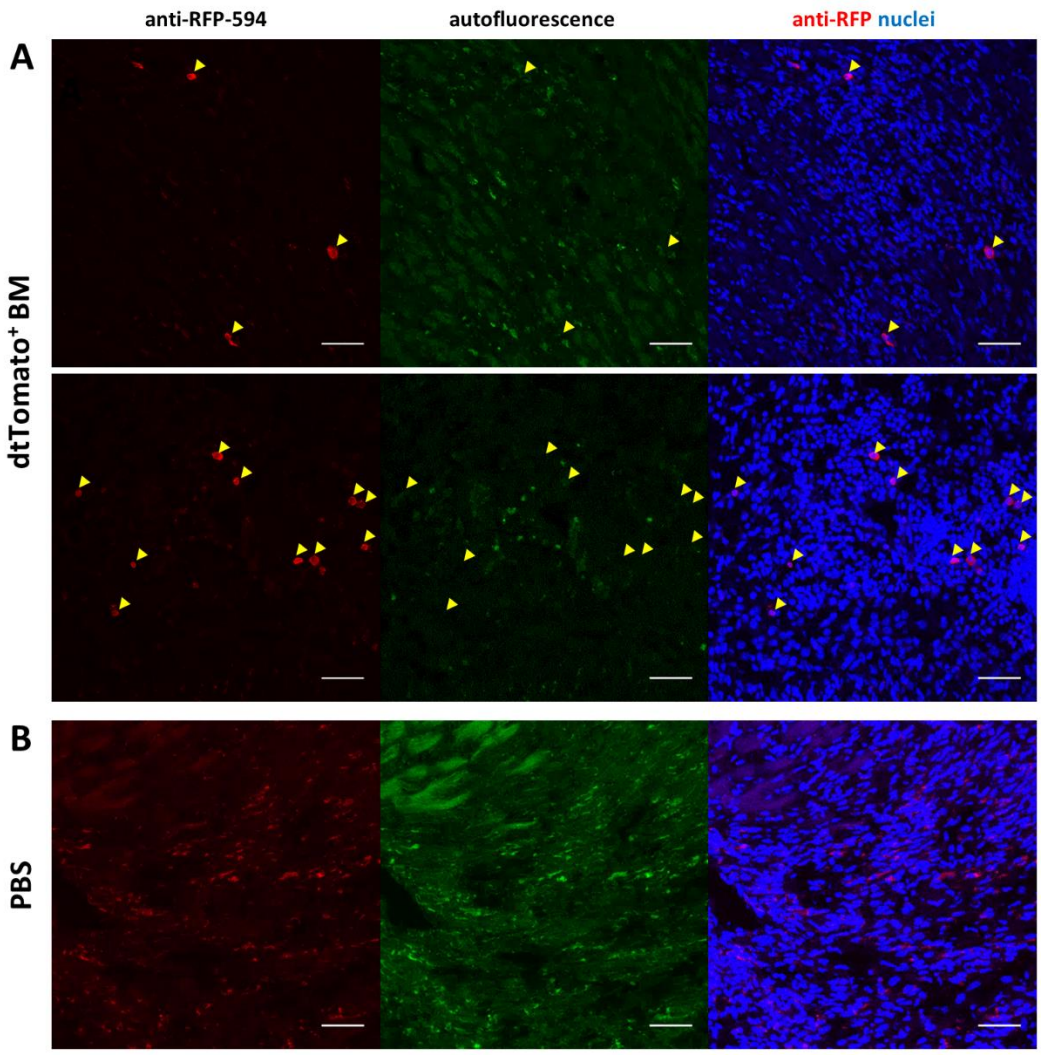

Figure 17. Intravenously injected bone marrow cells home to the infarcted myocardium. At day 4 after myocardial infarction, mice were intravenously injected with $5x10^6$ dtTomato bone marrow cells or PBS. 24h after injection mice were sacrificed and stained with anti-RFP-594 antibody**. A.** In the infarct zone of mice injected with dtTomato_BM, we observed dtTomato$^+$ cells (arrowheads), which were not present in the green channel (autofluorescence control). Upper panel shows cells infiltrating into epicardium. Lower panel shows cells infiltrating the granulated tissue. **B.** Unspecific red fluorescence signal in the heart of PBS-injected mice present the same pattern as green autofluorescence channel. Scale bar 50µm.

2.4 Analysis of the combined VEGF/S1P therapy on the left ventricle contractile function

To assess the systolic function of the left ventricle, echocardiographs were performed 3 days after surgery (one day before beginning the treatment) and at the endpoint, 28 days post-I/R. The LVEF and stroke volume (SV) were measured to assess contractile function

of the hearts. The LVEF describes the percentage of blood volume pumped and the SV is the actual volume of blood pumped by the heart during each contraction.

As expected, LVEF and SV decreased 3 days post-I/R compared to healthy mice (**Figure 18A, C**). At 28 days post-I/R, LVEF remained low, with no differences between groups (**Figure 18A**). In the analysis of individual mice, the treated group showed a slight increase in LVEF, although not significant (**Figure 18B**). At 28 days post-I/R, SV recovered in both groups, although to a higher extent in the mice treated with the combined angiotherapy (**Figure 18C, D**).

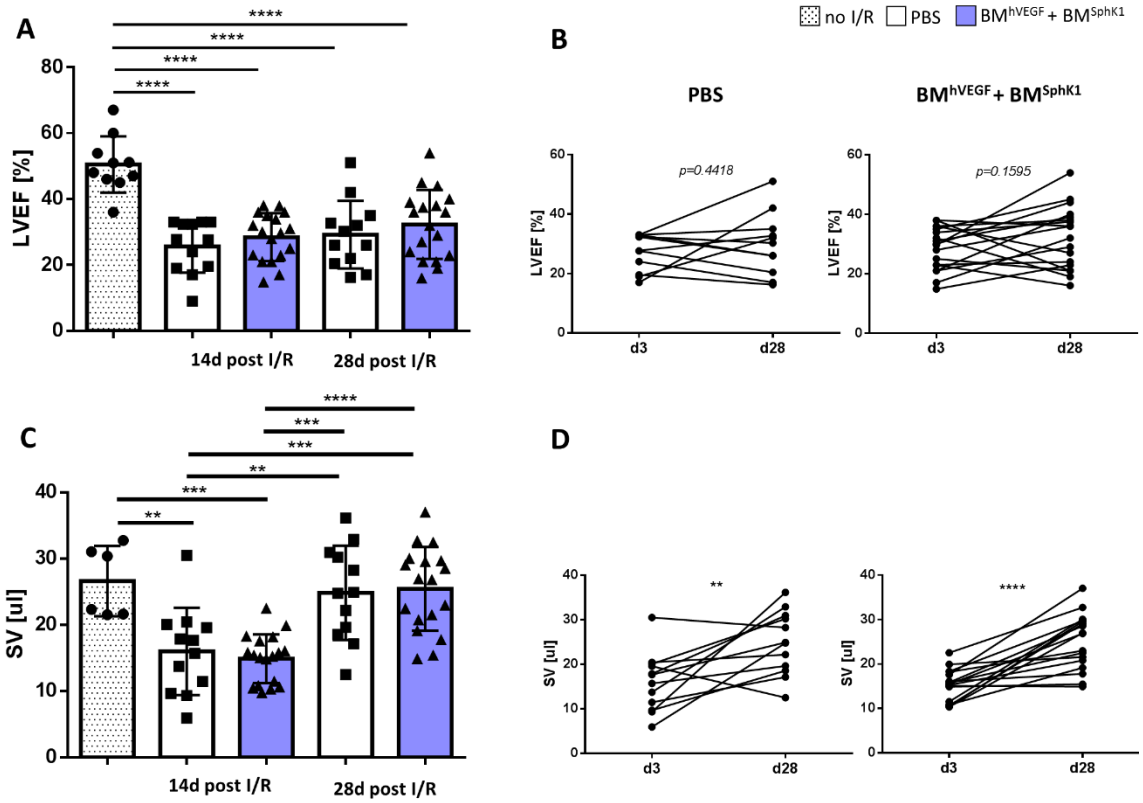

Figure 18. Systolic function of hearts from control and VEGF/S1P treated mice. Echocardiography was performed at day 3 post-I/R and mice were divided into control and treated groups. End-point echocardiography was performed at day 28 post-I/R. **A.** Left ventricle ejection fraction (LVEF) of treated, control and healthy mice. **B.** LVEF of individual mice from control and treated group. **C.** Stroke volume (SV) of treated, control and healthy mice. **B.** SV of individual mice from control and treated group. *One way ANOVA(a, c) and paired t-test (b, d), n=12 control, 18 therapy, 3 independent experiments.*

2.5 Impact of VEGF/S1P gene-cell therapy on cardiac remodeling

As described in the Introduction, a consequence of insufficient repair after myocardial infarction is adverse cardiac remodeling, which eventually leads to heart failure. One of the symptoms of heart failure is dilation of the heart muscle, manifested by an increase of left ventricle volume, especially in diastole, a change in the heart geometry towards a more circular shape, and at a cellular level by cardiomyocyte hypertrophy. Therefore, we examined whether combined BM_hVEGF + BM_SphK1 angiotherapy had an impact on heart remodeling.

2.5.1 Analysis of cardiac dilatation

Over time after MI the heart dilates as a result of pathological remodeling. Therefore, left ventricle end systolic and diastolic volumes (LVESV, LVEDV) were measured in control and treated hearts. As expected, at day 3 post-I/R, we observed no changes in both parameters between healthy and infarcted mice (**Figure 19, C**).

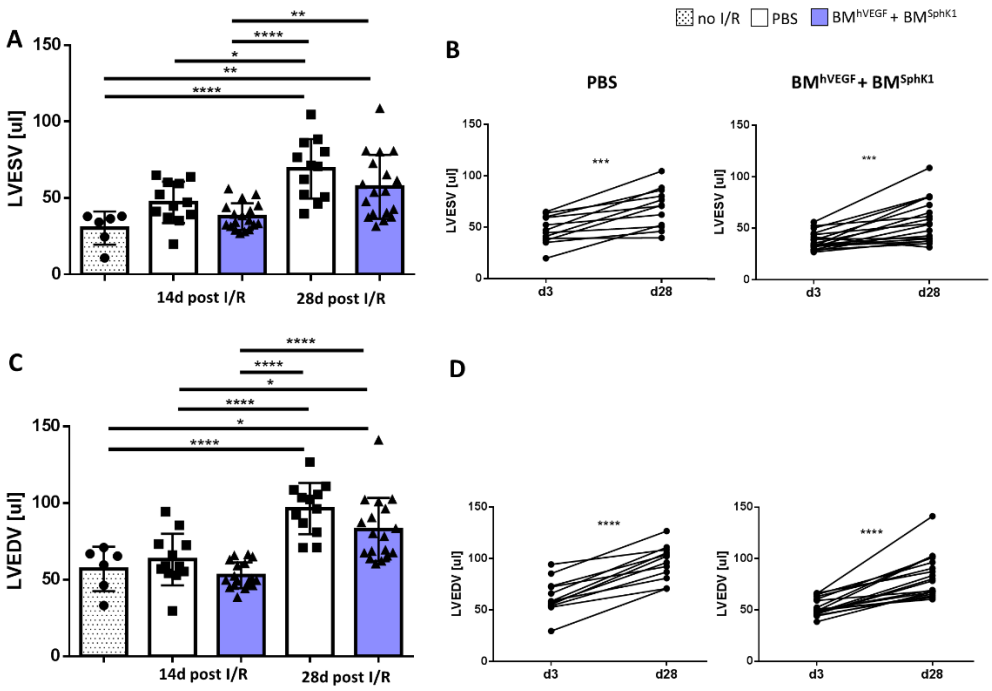

Figure 19. Analysis of left ventricle dilatation using echocardiography. Echocardiography was performed at day 3 (before the therapy started) and 28 (at the endpoint) post I/R. Left ventricle

end systolic volume (LVESV) and left ventricle diastolic volume (LVEDV) were measured in hearts from VEGF/S1P treated and control mice after MI and in healthy mice (**A,C** respectively). LVESV and LVEDV of individual mice of PBS and BM_hVEGF/BM_hSphK1 treated mice (**B,D** respectively). *One way ANOVA(a, c) and paired t-test (b, d), n=12 control, 18 therapy, 3 independent experiments.*

At day 28 post-I/R, LVESV and LVEDV increased significantly when compared to healthy hearts, although to a lower extent in the mice treated with BM_hVEGF + BM_SphK1. Analysis of left ventricle volumes in individual mice after MI, showed no differences between groups (**Figure 19B, D**).

The observed changes in left ventricle systolic and diastolic volumes, although mild, suggested ameliorated remodeling of the hearts in the treated group. Therefore, we decided to check global geometry of the hearts from VEGF/S1P-treated and control mice. Despite no changes in the heart weight (**Figure 20A**), we observed that hearts from the treated group kept their ellipsoid-like shape, whereas controls became rounder (**Figure 20C**).

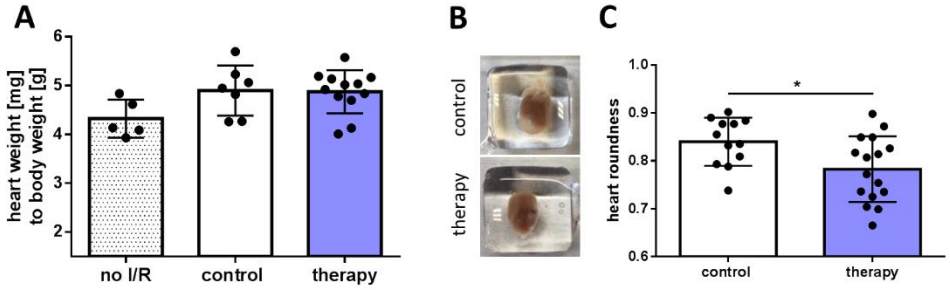

Figure 20. BM_hVEGF/BM_hSphK1 combined therapy prevented changes in the geometry of the heart after MI. A. Heart to body weight ratio. **B.** Representative images of dissected hearts from control and treated mice. **C.** Roundness of the heart was measured using ImageJ software. *A. One way ANOVA, n=5,7,12 (no I/R, control and therapy accordingly). C. Unpaired t-test, n=11,16 (control, treated). Two independent experiments.*

2.5.2 Cardiomyocyte hypertrophy

In order to determine changes in cardiomyocyte size, which is an important indicator of cardiac remodeling, we performed histological analysis of the heart tissue using anti-laminin antibody (**Figure 21A**). Analysis was performed in the remote zone of the heart due to the

fact that most of the dead cardiomyocytes in the infarct zone at this point are replaced by scar tissue.

Quantification of cardiomyocyte morphology, showed a decreased area and perimeter of cardiomyocytes in hearts from BM_hVEGF/BM_hSphK1-treated compared to control mice (**Figure 21B, C**). This suggests that PBS-treated mice developed cardiomyocyte hypertrophy whereas combined proangiogenic treatment had better preservation of cardiomyocyte size.

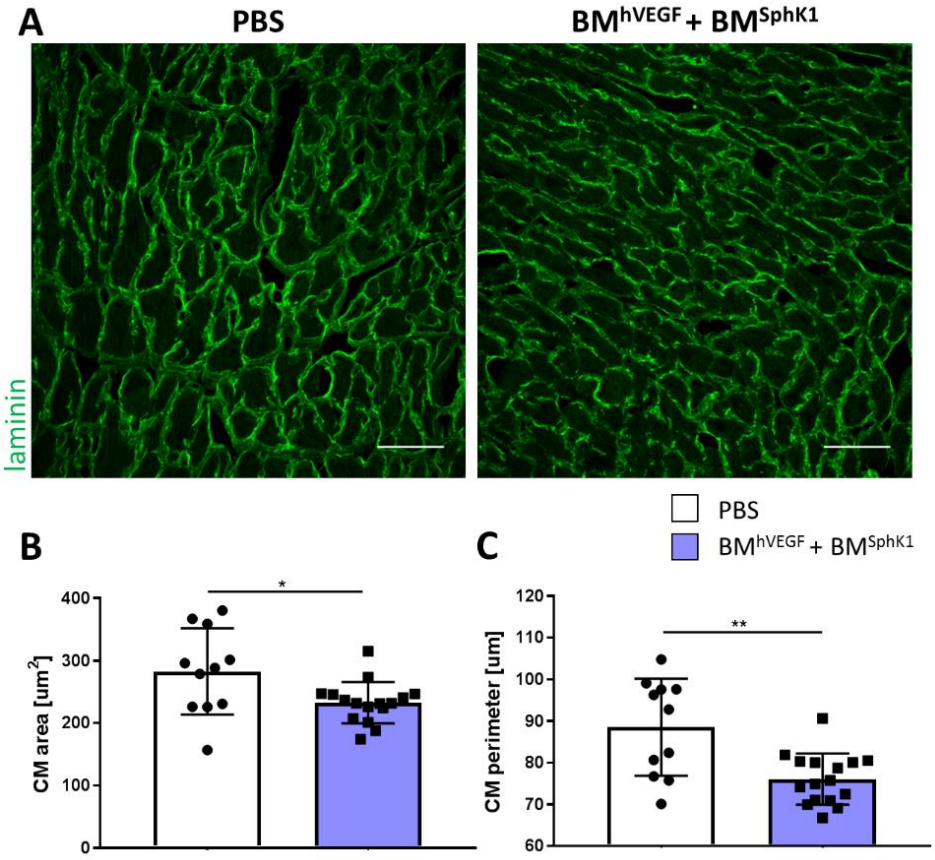

Figure 21. Gene-cell BM_hVEGF/BM_hSphK1 therapy prevents cardiomyocyte hypertrophy after MI. Hearts from PBS and BM_hVEGF/BM_hSphK1-treated mice were stained using anti-laminin antibody. **A.** Representative images of cardiomyocytes from remote zone of control and treated hearts. Maximal projection, scale bar 50µm. Cardiomyocyte area (**B**) and perimeter (**C**) was measured using ImageJ software. *Unpaired t-test, n=11,16 (control, therapy) in two independent experiments.*

2.6 Analysis of myocardial infarct size

Initial infarct size caused by the loss of viable myocardium, as well as its later expansion, plays an important role in cardiac remodeling and prognosis[86]. To quantify the infarct size, series of seven cuts from the apex to the base of hearts were stained using Masson-Trichrome (**Figure 22A**). Area occupied by scar was selected using ImageJ software and compared with total left ventricle area.

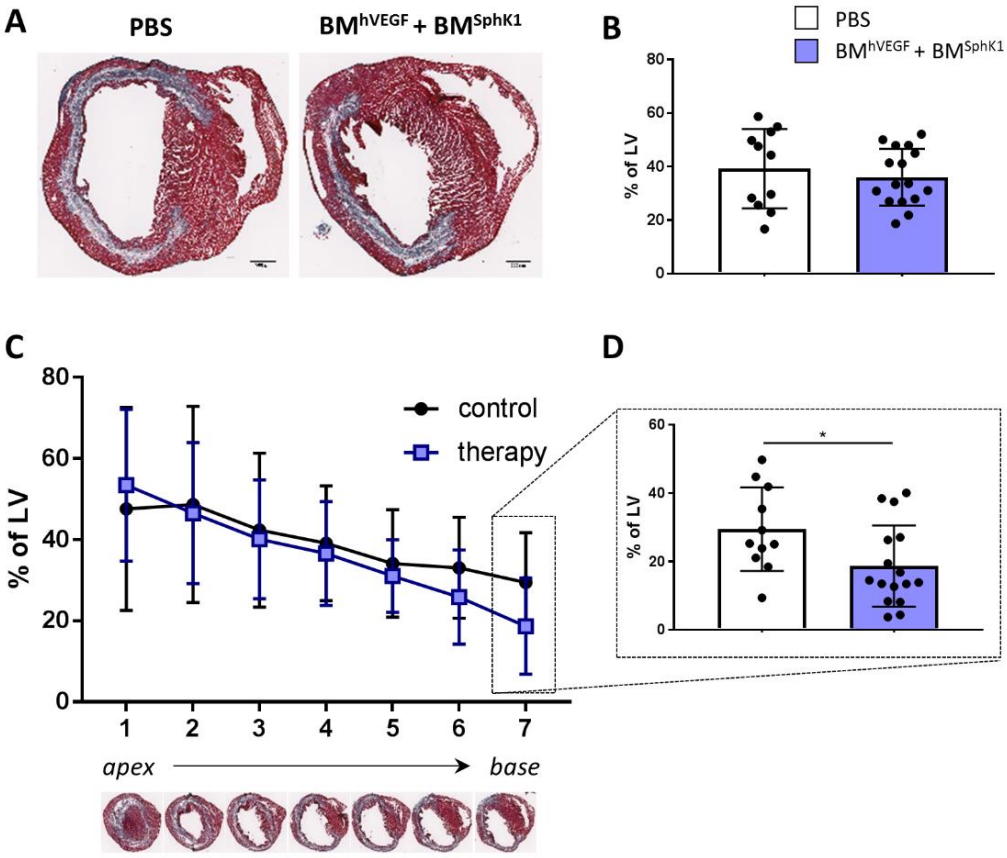

Figure 22. Infarct size and extension in hearts from VEGF/S1P- and PBS-treated mice. 45min ischemia/reperfusion model of myocardial infarction was performed and infarct size was analyzed 28 days after, in serial heart cuts stained with Masson-Trichrome. Infarct size is represented as % of left ventricle area occupied by scar tissue. **A.** Representative image of the staining and quantification of each heart as an average of serial cuts (**B**). **C.** Analysis of serial cuts from apex to the base of the heart and comparison of infarct size on each level. **D.** Infarct size of the cuts closest to the base of the heart. *Unpaired t-test, two-way ANOVA (levels comparison), n=11 control, n=16 therapy in two independent experiments.*

When we looked at the average of all cuts, the percentage of area occupied by the scar between groups show no differences (**Figure 22B**). Then, we analyzed whether there were differences in the scar expansion/extension when compared to correlative cuts (from apex to the base). Indeed, except in the section closest to the cardiac apex (cut 1), we observed a slight but consistent decrease in the area occupied by fibrotic tissue in the treated group, that reached significance in the section closest to the base of the heart (cut 7) (**Figures 22C and 22I**). Taking into account the fact that in the permanent LAD coronary artery occlusion model, MI appears largely in the area of the heart closest to the apex[87]. These results suggest that expansion of the fibrosis is diminished in the treated group.

2.7 Influence of VEGF/S1P gene-cell therapy on the inflammatory response after MI

As mentioned in the introduction, prolonged inflammatory response is one of the main players in the pathology of myocardial infarction. Therefore, we decided to analyze the monocyte subsets in the blood and the cardiac macrophage content of BM-hVEGF/BM-SphK1 and PBS-treated mice.

2.7.1 Analysis of peripheral blood monocytes

We sought to compare the phenotype of peripheral blood monocytes at three time points: before I/R (healthy mice), 14 days post I/R (one week after last injection), and 28 days post-surgery (at the experimental endpoint).

Circulating monocytes are usually defined by the expression of the following cell surface markers: $CD45^+$ $CD115^+$ $CD11b^+$ and are then divided into $Ly6C^{hi}$ and $Ly6C^{low}$ subpopulations. However, we were interested in analyzing two monocyte subsets which take part in the immune response upon myocardial infarction: proinflammatory $Ly6C^{hi}$ CX_3CR^{low} $CCR2^+$ and patrolling $Ly6C^{low}$ CX_3CR^{hi} $CCR2^-$ with inflammatory-attenuating properties[14,88,89]. As CX_3CR1 receptor is expressed on monocytes but not on neutrophils, we were able to distinguish the monocyte subset despite not using a CD115 marker[90]. We defined monocytes as $CD11b^+$ CX_3CR1^+ population and furthermore, $Ly6C^{hi}$ and $Ly6C^{low}$

subpopulations (**Figure 23A**). Consistently with the definition of proinflammatory monocytes, the Ly6C^{hi} subset expressed lower levels of CX_3CR1 and higher CCR2 than Ly6C^{low} patrolling monocytes which express CX3CR1^{hi} and CCR2^{low} (**Figure 23B**).

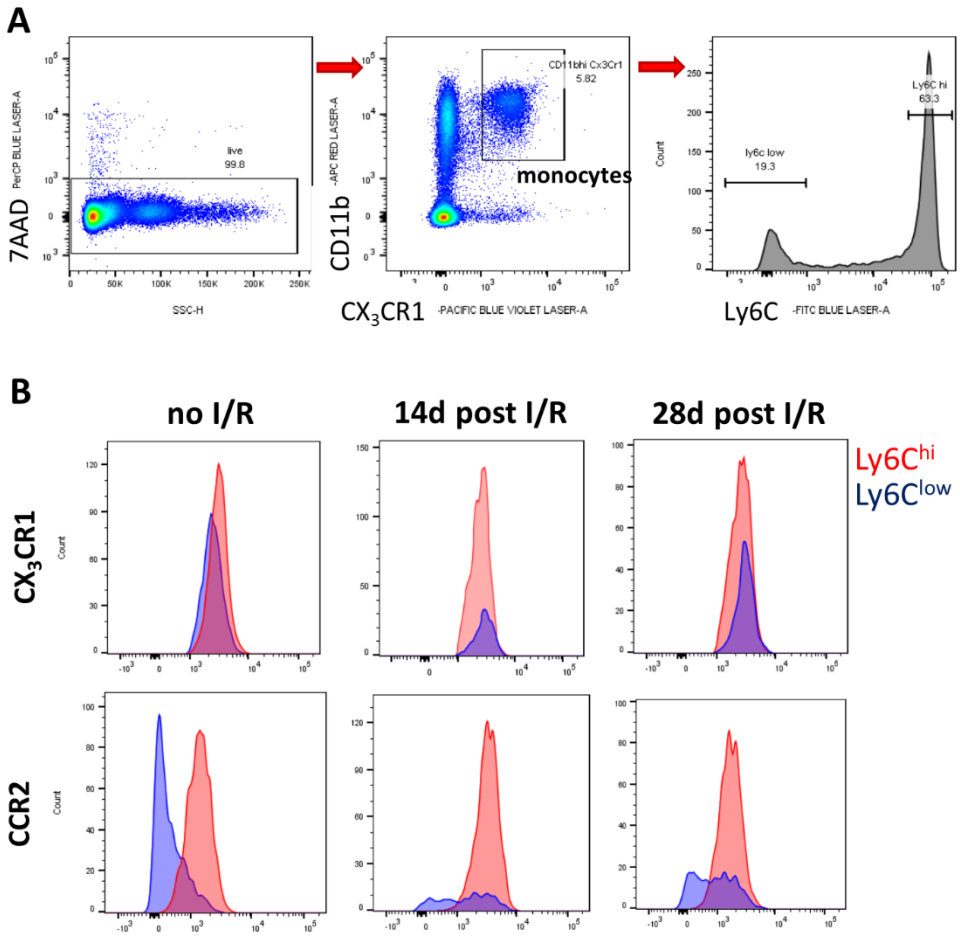

Figure 23. Monocyte gating strategy. Peripheral blood samples were harvested before I/R, at day 14 and 28 post I/R, and analyzed using flow cytometry. **A.** Monocytes were defined as CD11b^{+} CX_3CR1^{+} population and further defined as Ly6C^{hi} and Ly6C^{low}. **B.** Expression of CX_3CR1 and CCR2 receptors on Ly6C^{hi} and Ly6C^{low} monocyte subpopulations at the middle and end-point after myocardial infarction.

Analysis of total peripheral blood monocytes, showed a decrease in control group 28 days post-I/R comparing to the healthy animals (**Figure 24A**). More detailed analysis revealed significantly lower amount of Ly6C^{low} monocytes in PBS-treated group at 14 days post-I/R when compared to healthy animals (**Figure 24C**). Ly6C^{low} monocytes also

decreased in the BM_hVEGF/BM_SphK1 group, but to a lower extent. However, over time, the amount of Ly6C^{low} monocytes increased in the post-I/R mice and at 28 days there were no differences compared to the healthy animals. Notably, in addition to the significantly lower percentage of the Ly6C^{low} population found in the blood of PBS-treated group 14 days post-I/R, the expression of CX_3CR1 was significantly lower and of CCR2 higher compared to the healthy animals. Therefore, not only this population was lowered in number, but also lost its typical phenotype described as inflammation-attenuating: LyC6^{low} CX_3CR1^{hi} CCR2^{low} (**Figure 24E**).

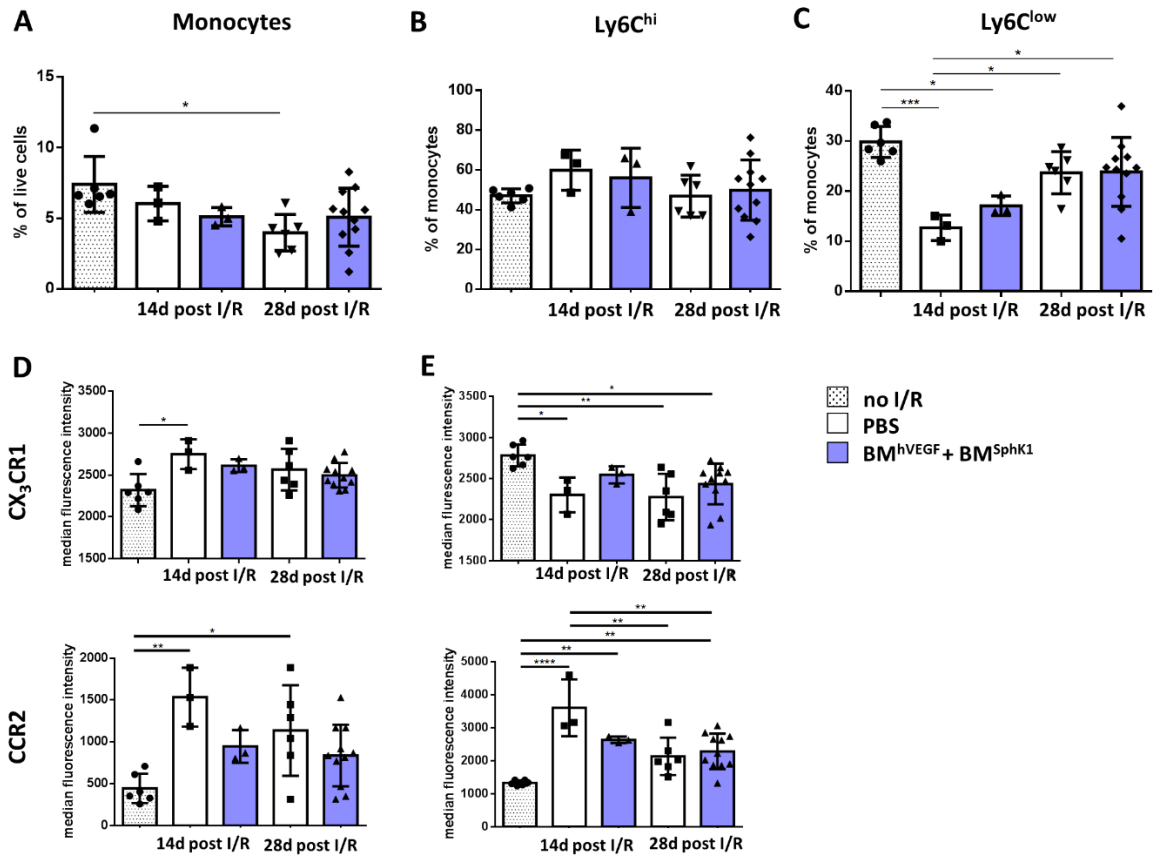

Figure 24. Distinct impact on blood monocytes in response to cardiac damage over time between PBS and BM_hVEGF/BM_hSphK1-treted mice. Blood samples were harvested before I/R, at day 14 and 28 post-I/R, and analyzed using flow cytometry. **A.** Monocytes defined as CD11b^{+} CX_3CR1^{+} and represented as % of live cells. **B.** Ly6C^{hi} and **C.** Ly6C^{low} monocyte subpopulations represented as % of monocyte population. Expression of CX_3CR1 and CCR2 receptors on **D.** Ly6C^{hi} and **E.** Ly6C^{low} monocyte subpopulations represented as median fluorescence intensity. *One way ANOVA, n=6 in no I/R control, n=3 mice (14d, both control and therapy), n=6 (d28 control), n=11 (d28 therapy) in one experiment.*

Despite no changes in the percentage of the Ly6C^{hi} subpopulation between groups and time-points, we observed increased expression of CX_3CR1 receptor in control group 14 days post-I/R. Additionally, CCR2 expression increased in the control group at both 14 and 28 days after I/R compared to the healthy animals (**Figure 24D,E**).

Based on the fact that some of the peripheral blood monocytes mobilized in response to MI come from the splenic reservoir[15], we decided to analyze monocyte and macrophage content in the spleen at the experimental endpoint (28 days post-I/R). To analyze splenic monocyte subsets we used the same gating strategy as for the peripheral blood (**Figure 23**). We did not observe differences in total monocyte amount, but a decreased amount of the Ly6C^{low} subset in control and treated animals when compared to the no-I/R group (**Figure 25B, C**). Among the Ly6C^{hi} monocyte subset, there were no differences between analyzed groups, but there was a trend towards an increase within infarcted versus healthy animals.

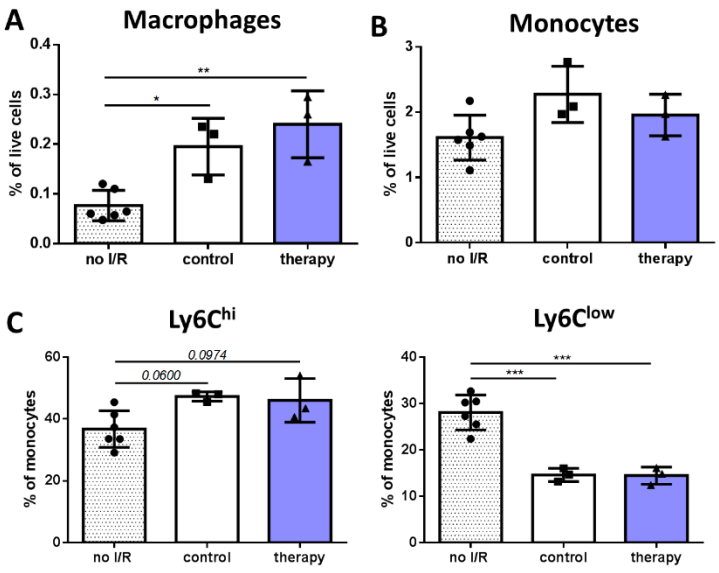

Figure 25. Characterization of splenic monocyte/macrophage population at 28 days post-I/R in VEGF/S1P- and -PBS treated mice. Spleens of control, treated and healthy mice were harvested and analyzed using flow cytometry. **A.** Macrophages were defined as CD11b^{hi} F4/80^{+}, Monocytes as CD11b^{+} CX_3CR1 (**B**), and represented as % of live cells. **C.** Monocyte Ly6C^{hi} and Ly6C^{low} subpopulations. *One way ANOVA, n=6 no I/R, n=3 (control and therapy) in one experiment.*

Despite a very low percentage of macrophages, we observed an increase in mice which have undergone a myocardial infarction, to a higher extent in the VEGF/S1P-treated group (**Figure 25A**).

2.7.2 Impact of VEGF/S1P gene-cell therapy on cardiac macrophages after I/R

In addition to analyzing changes in the inflammatory response on the systemic level, we next checked whether there were differences in the macrophage content in the hearts of control and treated mice at the experimental end point.

The hearts were stained with an anti-F4/80 antibody using the immunohistochemistry method and the percentage of F4/80$^+$ nuclei in the infarcted and remote zone of the hearts was quantified (**Figure 26**).

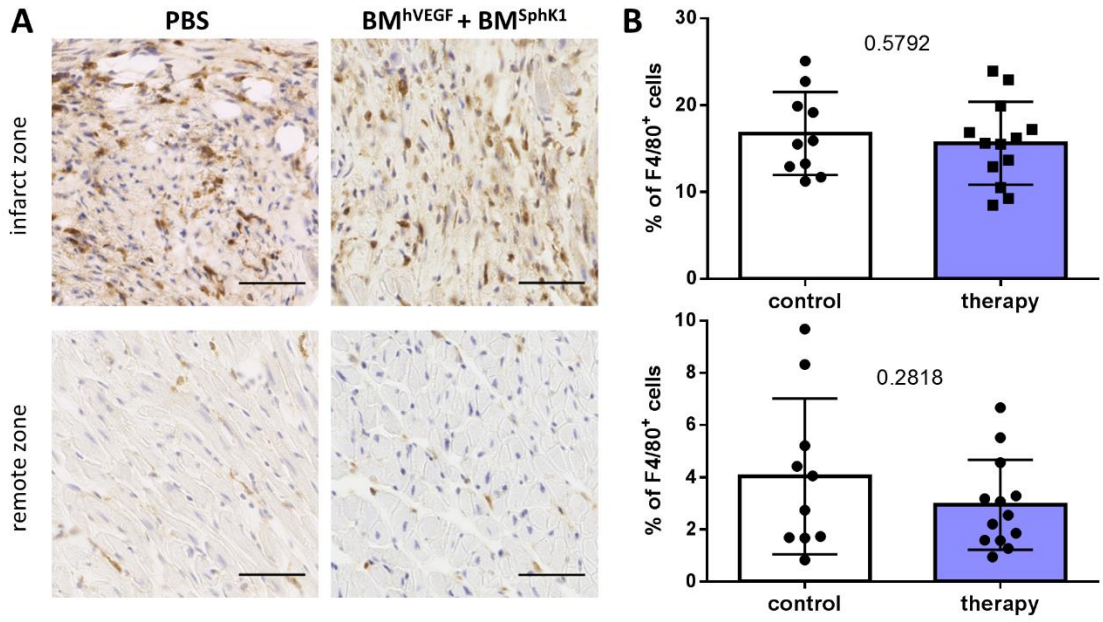

Figure 26. Immunohistochemical analysis of macrophage content in hVEGF/S1P-treated and control hearts. At 28 days post I/R hearts were stained using F4/80 pan-macrophage marker and analysis of remote and infarct zone was performed. **A.** Representative images of macrophages in the infarct and remote zone **B.** Macrophages were defined as F4/80$^+$ cells and represented as % of total number of cells. Scale bar 50µm. *Unpaired t-test, n=13 therapy and n=10 control, in two independent experiments.*

As shown in **Figure 26B**, F4/80^{+} macrophages in the infarct zone were representing over 15% of the cells in both groups and about 4% in the remote zone. In the infarct zone, we observed no significant differences in macrophage content between control and treated group. However, in the remote zone of hVEGF/S1P-treated group, the percentage of cardiac macrophages was slightly lower compared to the control group. Additionally, the distribution between subjects within treated group was more consistent than in control.

In addition to immunohistochemistry, we performed immunofluorescence staining using an anti-CD68 antibody to validate the data from F4/80 staining (**Figure 27**). We observed that the percentage of CD68^{+} macrophages in the remote zone was slightly higher compared to F4/80 staining (~6% and ~4% respectively). Similarly to F4/80^{+}, the percentage of CD68^{+} macrophages in the remote zone of hVEGF/S1P-treated group was lower, yet still not significant (**Figure 27**). Moreover, the distribution of subjects within the BM^{hVEGF}/BM^{hSphK1}-treated group was more consistent, and resembled the one observed in the F4/80 staining.

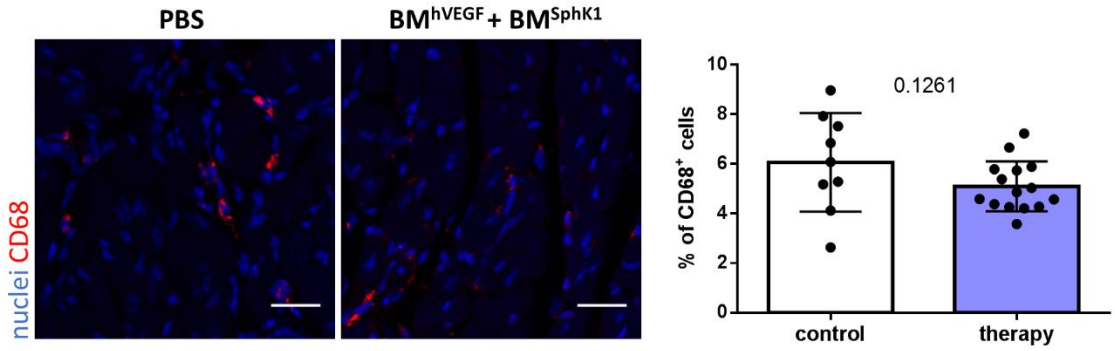

Figure 27. Immunofluorescence analysis of macrophage content in the remote zone of hearts from PBS and VEGF/S1P-treated mice. Staining with anti CD68 macrophage marker was performed in the remote zone of hearts 28 post-I/R. Representative images of CD68^{+} cells (left) and quantification of percentage of macrophages within total number of cells. Scale bar 25µm. *Unpaired t-test, n=15 therapy, n=9 control, in two independent experiments.*

2.8 Effects of VEGF/S1P gene-cell therapy on cardiac microvasculature after I/R

The primary goal of our designed angiotherapy was to increase and modulate endogenous angiogenesis after I/R, by sequential delivery of VEGF and S1P using lentiviral-infected bone marrow cells as a vehicle.

Histological analysis of 15um-thick heart sections was performed to observe changes in the microvascular response to the applied therapy after I/R. We decided to perform immunostaining on thicker than standard sections to achieve semi-3D images of the vasculature network. Heart sections of control and treated hearts were stained with anti-CD31 antibody for endothelial cells, anti-SMA for smooth muscle cells covering arterioles, and anti-PDGFRβ for mural cells and myofibroblasts (**Figure 28**). Confocal images were analyzed by a MATLAB-based automated method developed in our lab[70]. This image analysis method allowed us to compare the microvasculature of the PBS and VEGF/S1P-treated hearts at the structural and segment levels.

Structural analysis using Minkowski functionals and fractal-based analysis allowed us to observe the vasculature as a whole network. Minkowski functionals describe the morphology of a given structure, in this case, vascular volume densities of a distinct microvascular network category (**Figure 29A**). In the case of the infarct zone vasculature, we observed increased capillary volume density in hearts from VEGF/S1P-treated mice with no differences in total vascular volume density. At the same time, the vascular volume density of large vessels increased in hearts of PBS-treated mice. This observation indicates an angioadaptation mechanism is occurring in response to capillary loss, impaired oxygenation, and flow redistribution in the remaining vessels[70,91]. In the remote zone, total vascular volume density also remained unchanged between groups. Moreover, similarly to the infarct zone, we observed a trend towards an increase in capillary volume density in hearts from treated mice, and an increase in volume density of large and medium-size vessels in hearts from the PBS-treated group. An analysis of fractal parameters allowed us to observe differences in the complexity of the network structure (fractal dimension), heterogeneity in the distribution of gap sizes (lacunarity), and capacity of the blood to flow through the structure (succolarity) (**Figure 29B).**

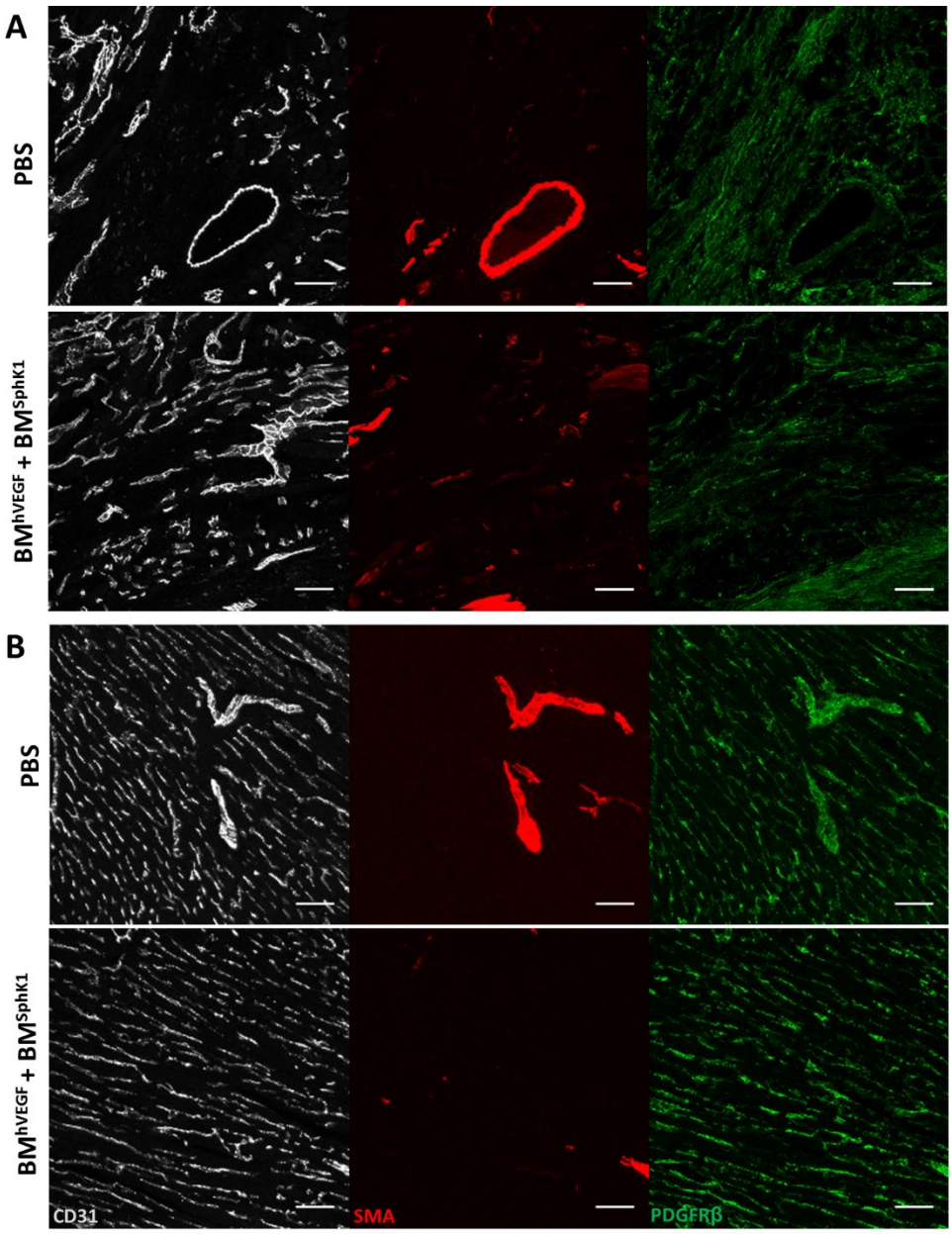

Figure 28. Representative images of the myocardial vasculature from infarct and remote zones of hearts from VEGF/S1P-treated and control mice. Transverse sections of mouse hearts (approximately 15µm-thick to obtain semi-3D vasculature network) were stained for **e**ndothelial cells with anti-CD31 antibody, smooth muscle cells with anti-SMA, and mural cells and myofibroblasts with anti-PDGFRβ. Images of the vasculature in infarct (**A**) and remote (**B**) zone of treated and control hearts. Scale bar: 50µm.

In addition, we observed a more homogenous distribution of non-vascularized areas in the hearts from treated animals, which is represented as a strong trend towards lower lacunarity in both remote and infarct zone.

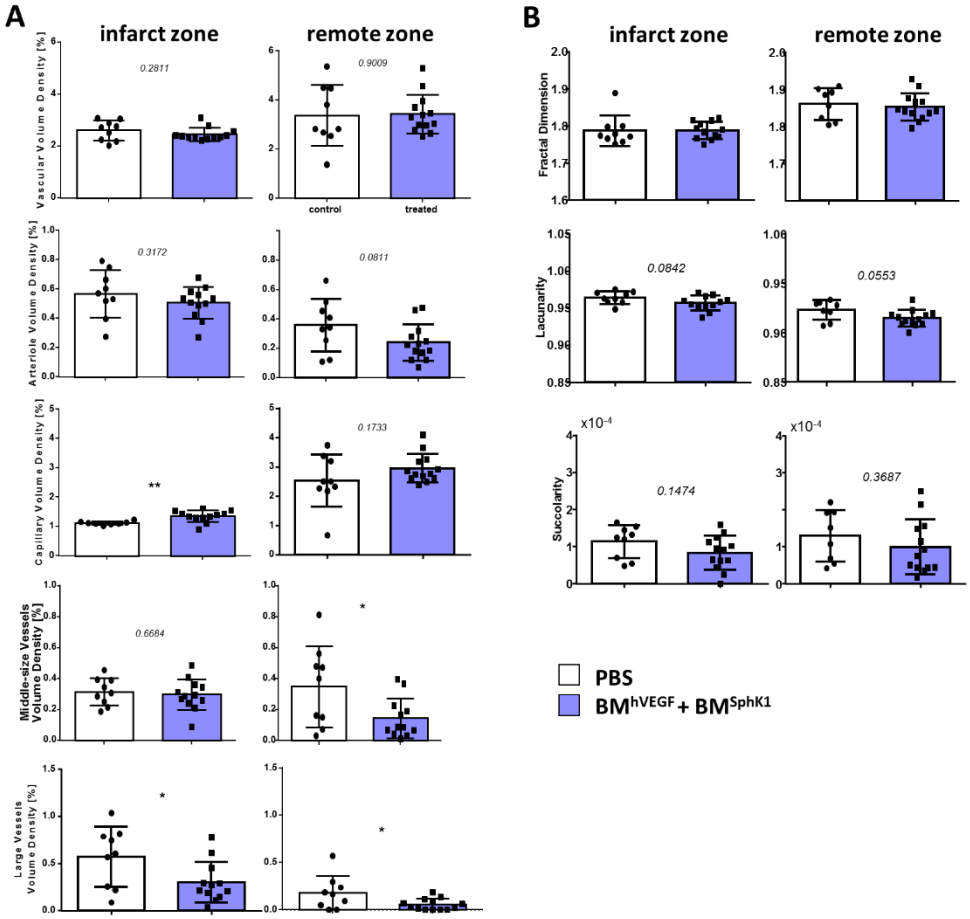

Figure 29. Structural analysis of the whole vasculature shows increased capillary content in the infarct zone of hearts from hVEGF/S1P-treated mice. A. Morphology of the vasculature assessed using Minkowski functionals. Vascular Volume Density consist; Arteriole Volume Density (defined as density of $CD31^+$ vessels covered with smooth muscle cells), Capillary Volume Density (defined as density of $CD31^+$ vessels of diameter <5µm), Medium-size Vessels Volume Density (defined as density of $CD31^+$ vessels of diameter 5.1 to 8.7µm) and Large Vessels Voluvme Density (defined as density of $CD31^+$ vessels of diameter >8.7µm). **B. Fractal-based analysis of vasculature network**. Fractal Dimension metrics describe morphological complexity of the network, Lacunarity describe heterogeneity of gap sizes and Succolarity shows capacity of a fluid to flow through the network. *n= in two independent experiments, non-parametric t-test.*

Detailed comparison of individual vessels in hearts from treated and control mice was possible using 3D graph-based segment level analysis. Consistent with the analysis of capillary volume, we observed a higher percentage of capillary content in the hearts from

VEGF/S1P-treated mice, although not significant in the case of the infarct zone. Additionally, in the remote zone of control hearts, the percentage of medium-sized and larger vessels was higher (**Figure 30D**).

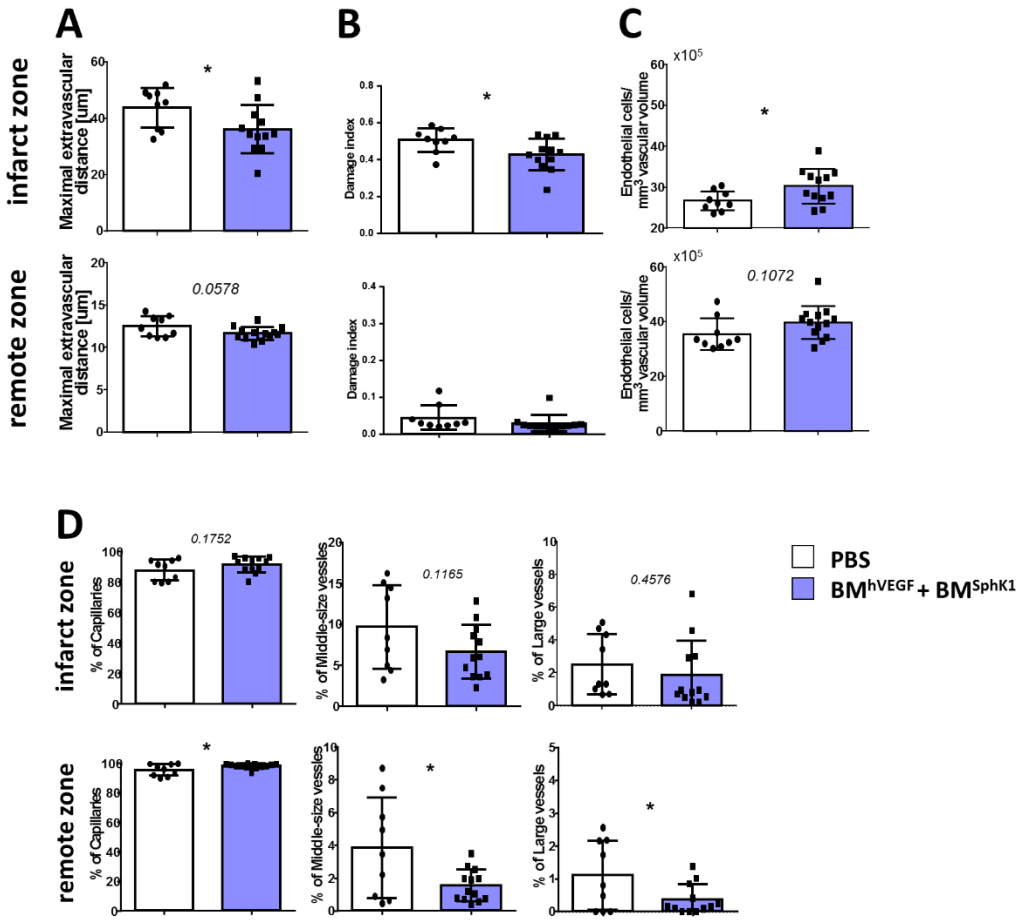

Figure 30. Applied proangiogenic therapy increases capillary content in remote zone and improves oxygenation of treated hearts. Analysis of the vasculature performed using graph-based method. **A.** Maximal extravascular distance measured in µm. **B.** Damage index defined as percentage of PDGFRβ^{+} volume not associated with vessels (*i.e.* myofibroblasts). **C.** Number of endothelial cells per mm^3 of vascular volume. **D.** Percentage of capillaries (left), medium-sized vessels (middle) and large vessels (right) in infarct and remote zone vasculature of treated and control hearts. *n= 9 in control, n=12 treated in two independent experiments (total 192 images analyzed), non-parametric t-test.*

Moreover, oxygen diffusion defined as smaller maximal extravascular distance, was improved in the VEGF/S1P-treated mice compared to the controls in both the infarct and remote zones (**Figure 30A**). This result was expected in light of the observed increase in

capillary volume and a higher percentage representation in the hearts from treated mice. Additionally, the amount of endothelial cells per vascular volume was also higher in the infarct zone of the hearts from the treated group, as well as in the remote zone although not significantly (**Figure 30C**). It might be a consequence of delivering hVEGF, which enhanced endothelial cell proliferation.

Notably, this 3D image analysis allowed for the quantification of myofibroblasts, defined as PDGFRβ^{+} cells distant from the vessels, as it was described that myofibroblasts from various tissues express PDGFRβ[92,93]. Damage index showed an increased amount of myofibroblasts in the infarct zone of the control hearts compared to the treated hearts (**Figure 30B**). In the case of remote zones, as expected, the damage index was close to zero, indicating the absence of myofibroblasts in this area of the hearts.

3. Analysis of angiogenesis-related events in porcine myocardium after ischemia-reperfusion injury

As a member of the CardioNext ITN network, I was involved in performing experiments on pigs to evaluate changes in the heart microvasculature after ischemia-reperfusion injury using confocal-based imaging method.

To analyze cardiac microvasculature after myocardial infarction, we used hearts of pigs which had undergone 30-minute occlusion of LAD artery followed by 1, 3 and 7 days of reperfusion. Basal hearts of the same age pigs served as controls.

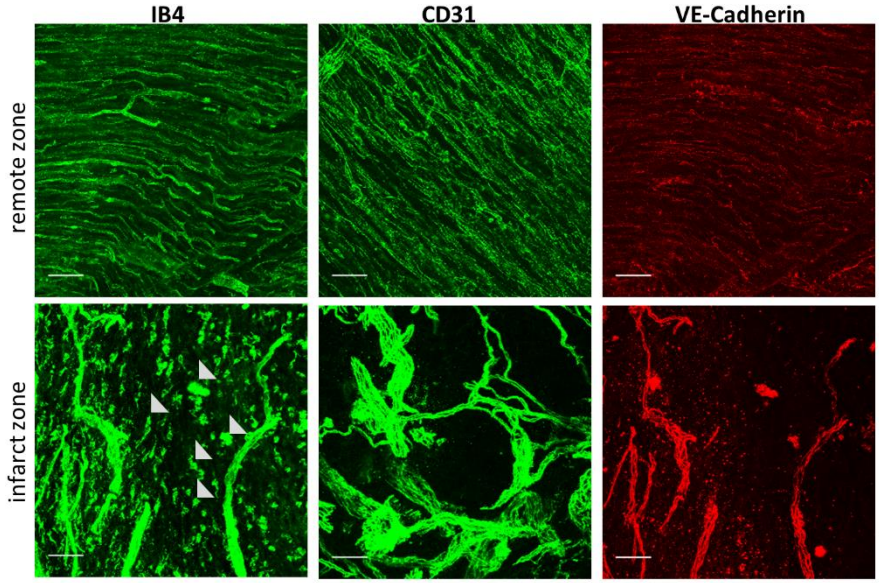

Figure 31. Representative images of the pig heart vasculature stained with various vascular markers. An IB4, CD31 and Ve-Cadhering staining of the infarct and remote zones of pig hearts at 45 days post I/R. In addition to EC, IB4 stains infiltrating cells in the remote zone (indicated by arrowheads). CD31 and VE-Cadherin specific vascular junction pattern in both remote and infarct zones. Maximal projection of 100µm-thick porcine heart tissue fixed with 0.4% PFA. Scale bar 50um.

To stain the microvasculature, we started by testing the reactivity of available antibodies in the pig tissue. We tested Isolectin B4, CD31 and VE-Cadherin. Isolectin B4 staining was vessel specific in the remote zone; however, in the infarct zone where the inflammation process occurs we observed a large contamination of the macrophage staining. Therefore, an IB4 staining was excluded from the study (**Figure 31**, arrowheads). We also tested a CD31

marker, which is present in endothelial cell junctions as well as in other cell types such as platelets, monocytes and macrophages[94]. In our settings, the CD31 staining was EC specific, even in the infarcted zone, and we could observe $CD31^+$ infiltrating cells only when 4%PFA fixation was used (personal observation).

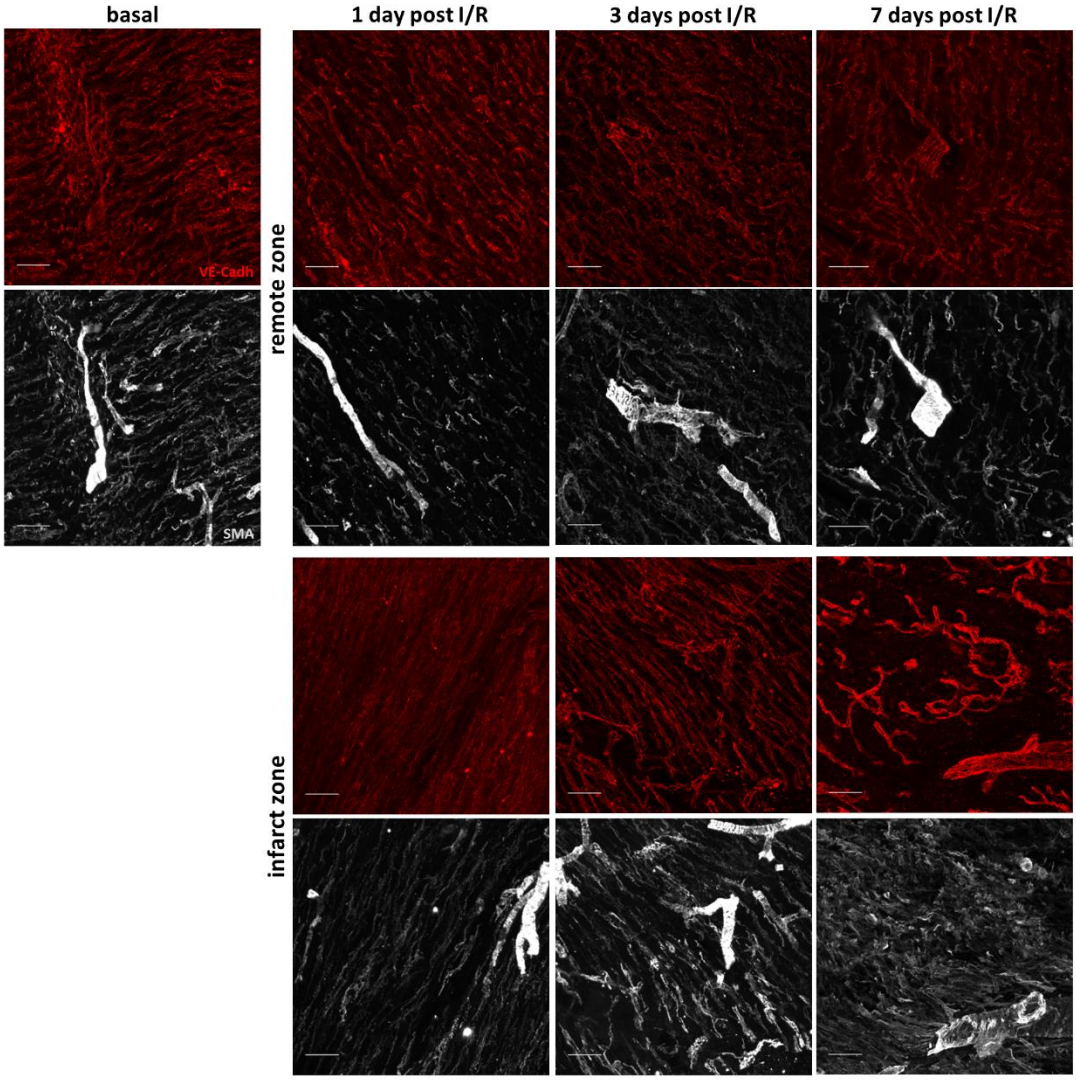

Figure 32. Representative images of microvasculature staining of porcine myocardium at 1, 3 and 7 days post I/R and basal. Immunostaining of VE-Cadherin for endothelial cells and SMA for smooth muscle cells/pericytes in the remote and the infarct zone. Maximal projection of approximately 70µm-thick sections, scale bar 50µm.

Furthermore, we tested the VE-Cadherin antibody, which is an exclusive endothelial cell junction marker[95], and as expected, it showed a similar staining pattern as CD31. Ultimately, we decided to use VE-Cadherin due to host species compatibly with other markers used for immunostaining.

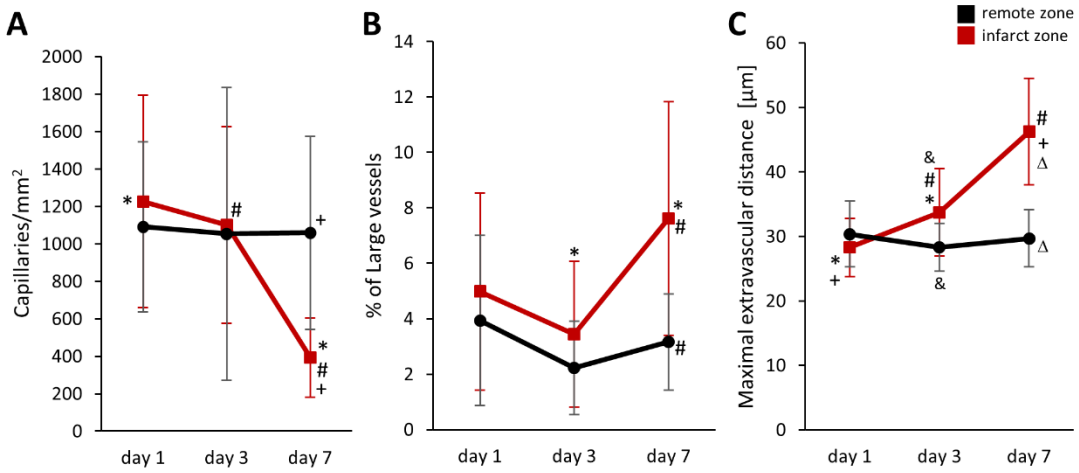

Figure 33. Quantification of vasculature changes in infarct and remote zones of porcine heart over time after I/R. Pig hearts after 30min of ischemia followed by 1, 3 and 7 days of reperfusion were analyzed. Tissue from remote and infarct zone was cut with ~100µm thickness, stained with VE-Cadherin and SMA, and 3D confocal images of were analyzed using automated method. **A.** Capillary density calculated as a number of capillaries per mm^2 in remote and infarct zone overtime post-I/R. **B.** Percentage of large vessels (defined as vessels with diameter >8.2µm). **C.** Maximal extravascular distance at different time-points after I/R. Our data published in[70].

To address changes in the microvasculature network and its functionality, hearts were stained with VE-Caherin and α-SMA (**Figure 32**). To perform detailed analysis of the vasculature, a 3D-automated image analysis pipeline was developed in our lab for confocal images[70]. The obtained results showed that in the infarct zone, capillary density decreased gradually from over 1200 capillaries per mm^2 at 1 day after I/R to around 400 capillaries/mm^2 at day 7, whereas in the remote zone it remained stable (**Figure 33A**). At the same time, a percentage of large vessels in the infarct zone (with diameter bigger than 8.2µm, e.g. venues and arterioles) increased from 5% at day 1 to 7.6% at day 7 post-I/R (**Figure 33B**). This data indicate loss of capillaries most probably due to the impaired oxygen and nutrient supply caused by ischemia, and also an adaptation mechanism through vasodilation to compensate for an impaired microvascular network. This is supported by the

increasing maximal extravascular distance within infarct zone vasculature overtime (**Figure 33C**).

Data obtained from infarct zone vasculature analysis indicate gradual regression of vascular network in the ischemic heart with significant differences between capillary density and SMA coverage as early as between day 3 and 7 post MI. Thus, our results obtained in pig tissue suggest that the time window for the therapies impairing vasculature loss – that is, pro-angiogenic – should be considered to be started around day 3 post-I/R

DISCUSSION

Over the past decades, the need for an effective therapy to improve or rather to prevent adverse remodeling and as a consequence a failure of the heart after myocardial infarction remains unmet. Since introduction of angioplasty in the late '70s, acute treatment of myocardial infarction has improved dramatically, although the mortality rate caused by CVD remains high[96]. Trying to overcome the inability of adult cardiac muscle to regenerate, many therapies have been implemented, including cell therapies, gene therapies (also with the use of viral vectors), the delivery of numerous cytokines, and soluble factors. These therapies aimed at various goals, including the prevention of cardiomyocyte death, the reprograming of cardiac fibroblasts into cardiomyocytes or cardiac progenitors, and modulating angiogenesis[52-55,60,97,98]. In recent years, more importance has been given to modulating immune response after myocardial infarction and its beneficial effects on heart regeneration[14,16,99,100].

After many years of research, including clinical trials, there is still room for improvement. In the field of proangiogenic therapies, use of a strong proangiogenic factor, VEGF, has brought a modest improvement. One of the main limitations of these studies seems to be a delivery route of healing factors, from delivery of the recombinant protein[101,102] and gene delivery using plasmids[52,53] or modified RNA[103] to virus-based approaches, mostly using AAV[57,59,60]. On the other hand, cell therapies whose main effect is believed to be based on secreting factors show some improvement in vascularization, but it is not sufficient[104,105].

Therefore, our hypothesis was that combining these two approaches (delivering beneficial cells but additionally transducing them to overexpress proangiogenic factors) might bring an improvement in heart performance after myocardial infarction. To modify the cells, we used lentiviral vectors because of their ability to transduce all cell types with high effectiveness. Because we used a general SFFV promoter, we decided to infect the cells *ex vivo* and inject them into the recipient mice afterwards. By using this approach, we were able to overcome safety concerns related to the lentivirus's potential to cause insertional oncogenesis.

After myocardial infarction, angiogenesis is one of the endogenous healing processes taking part after the acute inflammation response. We believed that sequential delivery of bone marrow cells, lentivirally-transduced to overexpress VEGF and other proangiogenic

factor, would help to mimic and boost endogenous angiogenesis, and to overcome the limitations appearing while using only gene/cell therapy and single angiogenic-related factors.

Prior to the mouse study, *in vitro* screenings of various combinations of proangiogenic factors were performed using an aortic ring assay. A broader screening was performed using commercially available hVEGF, hAng1 and S1P. Combinations of these factors have been used before to promote angiogenesis[81,82,106,107], although to the best of our knowledge they have not been compared simultaneously. To determine if a single or sequential approach is more effective at inducing sprouting, we treated rings with single factors as well as with hVEGF followed by hAng1 or S1P. We also tested how prolonged exposure to hVEGF influences the sprouts, because it has been observed before that long-term exposure to VEGF is deleterious to newly-formed vessels[61]. To check this, after adding hAng or S1P, we continued introducing hVEGF until the end of the experiment. We found that S1P alone is able to increase sprouting significantly. Additionally, we observed that combinations of either sequential or prolonged treatment with VEGF and S1P is more effective at inducing sprouting than any combination of VEGF and Ang1. Sequential delivery of VEGF followed by S1P in matrigel assays has shown greater EC recruitment and a higher maturation index (the percentage of vessels co-localized with αSMA^+ cells) compared to single or reverse order delivery of these factors[82]. In our experimental setting, VEGF/S1P sequential delivery also remarkably induced sprouting, although contrary to the matrigel study, we observed similar improvement in sprouting when using S1P alone. In the matrigel study, plugs were implanted *in vivo* into the dorsal skin; therefore, the angiogenic response was exposed to an environment with more complex variables than in an aortic ring setting. These factors might have limited the effect of single S1P exposure that we observed in aortic rings.

An analysis of smooth muscle cell coverage of new sprouts showed no differences between groups, except a decrease in the group with prolonged delivery of hVEGF in combination with S1P. It has been described that stimulation of endothelial cells with VEGF causes overexpression of S1P1 receptors on these cells; and in isolated arteries, enhances S1P-mediated vasorelaxation and eNOS phosphorylation[33]. This effect, at first favorable and contributing to prosurvival and a proangiogenic program of capillary endothelium, might

cause disruption in mural cell coverage when excessive due to the continuous presence of VEGF.

In the next step, aortic rings were cultured in the presence of msBM cells overexpressing selected factors, to check whether exposure to cell-derived factors would be able to reproduce the phenotype observed before. This step was crucial since we planned to use bone marrow cells as a vehicle to deliver proangiogenic factors after myocardial infarction. We observed the highest abundance of sprouts in rings treated with a combination of BM^{hVEGF} followed by BM^{hSphK1}. On the other hand, SMA coverage in this group was decreased, although it remained higher than 50%. Despite washing away BM^{hVEGF} while adding BM^{hSphK1}, some of the cells could have migrated into the collagen matrix and kept secreting hVEGF in addition to S1P from BM^{hSphK1}. This was similar to the lowest SMC coverage in the group with prolonged hVEGF exposure in combination with S1P observed in the first *in vitro* approach. Treatment with wild type bone marrow cells did not increase sprouting of aortic rings, and therefore they were not used in further studies.

We concluded that the combination of BM^{hVEGF} followed by BM^{hSphK1} induced sprouting most efficiently; therefore, despite lowered SMC coverage, this approach was used to treat mice with the I/R model of MI. We decided to use a combination of factors, even though in the soluble factor approach, the use of S1P alone significantly induced sprouting as well. We hypothesized that the cross-talk between VEGF and S1P discussed above may have a favorable effect *in vitro* as observed in the aforementioned matrigel study.

The best time window during which to start the treatment after MI remained an open question. A 3D analysis of changes in porcine heart microvasculature performed in our lab revealed a possible time window for therapeutic intervention to be the 3rd day after MI. At this time, the structure of the vasculature is mostly preserved, but its function becomes impaired, manifested in larger extravascular distances causing disturbed oxygen diffusion[70]. Additionally, the endogenous angiogenesis after the acute inflammatory phase of MI is believed to appear from 3 to 14 days after the ischemic event[3,89,108].

We decided to use the 45-minute ischemia/reperfusion model of MI rather than permanent LAD ligation to mimic the clinically-common model of MI, which includes PCI intervention. Following the aortic rings experimental set-up, BM^{hVEGF} were intravenously

injected (4 days post I/R), followed by BM^{hSphK1} at day 7. Experiment with dtTomato bone marrow cells, intravenously injected 4 days post-I/R, confirmed that these cells are capable of homing in on ischemic myocardium and are present there 24 hours after injection. On the other hand, human VEGF in the mice plasma 24 hours after cell injection was not detectable using ELISA. That might have been due to the very short half-life of this protein in the plasma, which is only a few minutes[109]. The presence of S1P in the plasma 24 hours after BM^{SphK1} injection was increased, although not significantly. The limitation here was the small number of animals tested (n=3).

An analysis of bone marrow cells before injection into infarcted mice showed that over 50% of them were monocytes. These cells were cultured and transduced in the presence of SCF and M-CSF; therefore, we expected a shift towards a myeloid lineage. We observed a higher monocyte expression of CX_3CR1 receptors on cells infected with the lentivirus compared to the wild-type bone marrow. Interestingly, bone marrow cells infected with LV_hSphK1 expressed a higher amount of this receptor than ones infected with LV_hVEGF. A higher expression of this receptor may facilitate the homing of these cells on to infarcted myocardium, especially in the case of BM^{hSphK1} which were injected at the later time point. Time-lapse imaging of immune cells homing on to infarcted myocardium has demonstrated increasing infiltration of CX_3CR1^+ monocytes into the injury site up to day 6 post-MI, which was the experimental endpoint[110]. Furthermore, the role of CX_3CR1 in the process of cell homing into the injury site was described in a rat model of cerebral artery occlusion, where silencing of CX_3CR1 expression in MSC notably decreased their homing into injured brain after intravenous injection[111]. Moreover, we observed lower amounts of macrophages in cells infected with lentivirus, which may have a beneficial effect since already differentiated macrophages are not capable of extravasating into the damaged tissue.

In terms of the global heart function, VEGF/S1P therapy resulted in better recovery of the stroke volume 28 days after I/R despite no differences in ejection fraction between groups. Additionally, adverse cardiac remodeling seemed to be ameliorated in the treated animals as seen in the reduced increase of LVESV and LVEDV compared to controls at 28 days post I/R. This finding was supported by an analysis of the whole organ shape and the observation that treated hearts kept their ellipsoid-like shape, whereas controls become more

round, suggesting heart dilation. Furthermore, when we analyzed cardiomyocytes in the remote zone, we observed cardiomyocyte hypertrophy in the hearts of the control animals. It has been shown that in a permanent LAD ligation model of MI, cardiomyocyte hypertrophy starts at 1 week post-MI, and continues to increase concurrently with the left ventricle dimension starting at 2 weeks post-MI[112]. In the I/R model used in our study, which is less severe than LAD ligation, it seemed that the development of pathological changes may have started later. Furthermore, although at 4 weeks after MI we clearly saw cardiomyocyte hypertrophy in the non-treated group and a change in the whole heart shape, we did not observe dilation of the left ventricle in echocardiography.

BM^{hVEGF}/BM^{hSphK1} angiotherapy had no influence on overall cardiac fibrosis, although it seemed to prevent scar extension. When we analyzed the part of the heart most distant from the injury site, we observed significantly less fibrosis in the treated group. This might have been due to the fact that the control hearts, which showed signs of cardiac dilation, started developing secondary fibrosis. The damage index, defined as the amount of myofibroblasts present in the tissue, was significantly lower in the infarct zone of treated hearts. This observation correlates with a constant, although not significant, decrease in fibrotic content measured using Masson-Trichrome staining on various levels of the left ventricle.

As mentioned before, more attention has been given to the analysis of the immune response after MI because of its importance in the recovery process and prognosis[113-115]. In addition to its role in angiogenesis, S1P is also involved in immune response, especially immune cell trafficking[116]. Therefore, we decided to analyze the immune response of treated and control animals. In the blood of control mice, 14 days after I/R we observed a larger decrease in $Ly6C^{low}$ monocytes compared to the healthy mice. This fact might have had an influence on the healing process, especially since this monocyte subset plays an important role in healing after MI[14,89]. Additionally, the chemokine receptor profile of these cells was altered. We observed a lower expression of CX_3CR1 and a higher expression of CCR2 in this subpopulation, which may suggest a loss of the 'reparative' phenotype of these monocytes. It has been demonstrated that depletion of the CCR2 receptor is beneficial for preventing cardiac remodeling in a mouse model of MI[117,118]. Moreover, better preserved expression of the CX_3CR1 receptor on circulating $Ly6C^{low}$ monocytes in mice treated with

BM^{hVEGF}/BM^{hSphK1} could have a positive effect on their recruitment and the promotion of angiogenesis in the injury site as has been described in hind limb ischemia[119] and carotid injury[120] models.

In addition to analyzing the systemic inflammatory response, we examined cardiac macrophage content, as it is related to the healing of infarcted myocardium[16]. We observed a higher amount of macrophages in the remote zone of control hearts confirmed by two experimental methods, yet it was not significant. This increase might have been a result of greater infiltration or proliferation. It has been described that cardiac macrophages proliferate in response to mechanical stretching caused by stiffer failing myocardium[16]. On the other hand, although we did not observe differences in abundance of circulating $Ly6C^{hi}$ between groups, the chemokine receptor profile on these cells differed. In control animals, $Ly6C^{hi}$ monocytes shown increased expression of CX_3CR1 and CCR2 receptors at 14 days, and of CCR2 up to day 28 post-I/R. This phenotype could have facilitated their extravasation and differentiation into macrophages in the ischemic hearts[121]. It has been proposed that the presence of macrophages in the remote zone of infarcted myocardium correlates with adverse heart remodeling via ECM turnover and fibroblast proliferation[122]. Therefore, a lower amount of cardiac macrophages in the remote zone of VEGF/S1P-treated hearts might be both a cause and a result of better-preserved heart outcome.

Finally, we wanted to know if the BM^{hVEGF}/BM^{hSphK1} therapy caused changes in the heart vasculature. Thanks to the automated analysis method developed in our lab, we were able to have a deeper look at the alterations in post-ischemic myocardium. Structural analysis of the infarct zone vasculature revealed that even though overall vascular density was the same in control and treated hearts, in the former large vessel volume density was higher while in the latter capillary volume density was higher. Moreover, in the remote zone, we observed a similar trend, although the difference in capillary volume density was not significant. Observed changes suggest that the vascular network in the treated hearts was better preserved, which could be further confirmed by a strong trend towards a lower degree of heterogeneity in the gap sizes described as lacunarity. It has been demonstrated that in response to shear and/or metabolic stress, blood vessels increase their diameter[123]. In our experimental setting, we observed higher amounts of large vessels in the infarct and remote

zones of untreated animals, which might suggest angioadaptation in response to insufficient blood supply. On the other hand, the increased amount of capillaries in treated hearts suggests better preservation of the vascular network and, therefore, no need for vasodilation in these hearts. Equal distribution of non-vascularized areas ensures proper oxygenation of the surrounding tissue; and, in addition to lacunarity, maximal extravascular distance can be used to describe the oxygenation potential of tissue. This distance was shorter in both the infarct and remote zones of treated hearts, suggesting better oxygenation. Furthermore, in the infarct zone of treated hearts, we observed a higher amount of endothelial cells per vascular volume although still lower than in the remote zone. In various previously-tested proangiogenic therapies, including AAV-mediated overexpression of VEGF and Ang1 in a pig model of MI [60], plasmid-mediated overexpression of bFBF and PDGF in a rat model of MI[125], and microcapsule release of FGF2 and HGF in a rat model of HF[126], improvement in cardiac vasculature was observed. In these trials, both capillary and arteriole/large vessel content was increased, the latter of which we believe is an angioadaptative response to impaired capillarization of the tissue. This assumption is supported by the fact that in our VEGF/S1P-treated hearts, higher capillary content was associated with a smaller maximal intravascular distance and lower lacunarity.

Despite the fact that the adult mammalian heart has a limited ability to regenerate, it has been shown that there is very restricted, but constant, cardiomyocyte proliferation over the lifespan of the organism (approximately 1% of cardiomyocytes annually)[127,128]. It was also demonstrated that this ability increases to over 3% in the border zone over 8 weeks after MI[127]. Therefore, a stable and functional vasculature is of great importance to keep these cardiomyocytes alive and to preserve cardiac function. In addition, despite the proangiogenic effect of BM^{hVEGF}/BM^{hSphK1} therapy, S1P may play an important role in the overall improvement observed in this study. Expression of both sphingosine kinase isoforms (SphK1 and SphK2) was described in cardiac fibroblasts and cardiomyocytes which are an important source of endogenous S1P in the heart[129]. It has been shown that S1P generation in the heart increases in response to transient ischemia, suggesting its beneficial role in pre- and post-conditioning phenomena[130]. Cardiomyocytes predominantly express the S1P1[131], which is involved in hypertrophic response and cardiac protection, because cardiomyocyte-restricted depletion of S1P1 caused progressive cardiomyopathy and premature death of

mutant mice[29]. In the same study, the ischemic preconditioning effect was abolished in S1P1$^{\alpha MHCCre}$ mice, suggesting that S1P1 plays a role in this mechanism. Furthermore, S1P signaling seems to be involved in pathological remodeling of the remote zone of the heart post-MI. In a porcine model of MI, delivery of fingolimod, a functional agonist of S1P receptors, reduced infarct size, improved cardiac function, and ameliorated pathological cardiac remodeling[132]. These beneficial effects were explained by the activation of protective pathways against ischemia-reperfusion injury, the RISK (Reperfusion Injury Salvage Kinase) and SAFE (Survivor Activating Factor Enhancement) pathways. The beneficial role of S1P in reducing infarct size via these pathways was also demonstrated in a *ex vivo* isolated Langendorff heart model of myocardial infarction[133].

In this study, we performed an I/R model of MI and our final time-point was 4 weeks after MI. However, to access global changes in the heart geometry (e.g. left ventricle remodeling) 4 weeks might not have been enough. In a permanent LAD ligation model of MI, the main changes in cardiac parameters occur within the first month post-MI[112]. On the other hand, in a 30-minute I/R model in mice, it was shown that between 2 and 8 weeks after MI, end diastolic and systolic volumes kept increasing, while the ejection fraction remained unchanged[134]. Therefore, we propose that in future experiments the timeline be expanded to at least 8 weeks to allow for further development of the HF phenotype and to observe the beneficial effects of the therapy.

We believe there are a few questions in this study requiring further elucidation. One of them is the abovementioned prolongation of the study to see an impact of the therapy on preventing remodeling and subsequent heart failure. We observed favorable features in treated hearts (i.e., prevented cardiomyocyte hypertrophy, preserved heart shape, a trend towards preservation of left ventricle volumes), but we cannot come to definitive conclusions, since we are not sure if the final phenotype was achieved in the control hearts. To confirm or exclude developing of HF in these mice, lung analysis for the presence of edema and/or pulmonary hypertension might be useful.

In our study, gene-cell therapy was compared to a placebo (PBS) to acquire a clear determination of its efficacy. However, a comparison with wild type BM or mock-infected BM could have helped to establish the precise contribution of paracrine signaling by the BM

cells and of the VEGF/S1P proangiogenic factors delivered. In terms of global left ventricle function, clinical trials using intracoronary injection of whole BM showed no long-term improvement in LVEF after MI[38,40], despite promising short-term effects[37,135]. However, these trials did not assess the pro-angiogenic effect of the cells. Yoon et al, demonstrated that selective elimination of endothelium-committed BM cells previously transplanted into ischemic myocardium decreased LVEF and reduced capillary and arteriole density at 4 weeks post-MI compared to whole GFP-BM. In this experimental setting, although it showed a trend, treatment with GFP-BM did not significantly increase capillary or SMA^+ density compared to PBS treated mice[136]. This result resembles our *in vitro* study, where treatment with wild type BM cells only slightly increased aortic ring sprouting. Therefore, since the effect of whole BM remains undetermined and there are studies showing an improvement in vascularization after whole BM cell treatment of MI[137,138], it would have been informative to have included this control group in our study.

It would also be interesting to perform a more robust study of the homing of intravenously-injected cells by injecting BM cells with lentivirally-induced overexpression of luciferase together with GFP. This would allow for *in vivo* tracking of cell distribution after intravenous injection in infarcted mice using the IVIS system. This way, we could examine if cells home on to organs other than the heart, and the duration of their presence *in vivo*. It would also allow for the determination of whether lentivirally-infected BM cells home only to the ischemic tissue or if they enter the remote zone of the heart as well.

CONCLUSIONS

1. Lentiviral (LV) infection of mouse bone marrow cells is an efficient system for inducing their secretion of the human proangiogenic factors VEGF-A (VEGF), angiopoietin-1 (Ang1), and sphingosine-1-phosphate (S1P).
2. The most efficient combination of proangiogenic factors *in vitro* is the sequential delivery of VEGF and S1P or S1P alone, compared with VEGF plus Ang1 or these factors separately.
3. Sequential delivery of VEGF and S1P by mouse bone marrow cells is also the optimal combination to induce angiogenesis *in vitro*.
4. Lentiviral infection of bone marrow cells shifts their phenotype increasing neutrophil abundance and inducing higher monocytes expression of the chemokine receptor CX_3CR1.
5. Sequential VEGF/S1P gene-cell therapy by intravenous injection on LV-infected bone marrow cells positively impacts cardiac performance by inducing mild improvement of pump function and ameliorating adverse remodeling after ischemia/reperfusion in mice compared with control.
6. Sequential VEGF/S1P gene-cell therapy also ameliorates the inflammatory monocyte response observed in control mice, favoring healing and decreasing macrophage abundance in the remote zone.
7. As primarily aimed, sequential VEGF/S1P gene-cell therapy enhances capillary density, decreases adverse angioadaptation and reduces extravascular distances in the infarcted zone, resulting in overall better oxygenation of the heart.
8. Despite no major reduction in scar size, sequential VEGF/S1P gene-cell therapy leads to a lower damage index (myofibroblast density) in the infarcted area, indicating milder fibrosis.

BIBLIOGRAPHY

1 Benjamin, E. J. *et al.* Heart Disease and Stroke Statistics-2017 Update: A Report From the American Heart Association. *Circulation* **135**, e146-e603, doi:10.1161/CIR.0000000000000485 (2017).

2 Frangogiannis, N. G. Pathophysiology of Myocardial Infarction. *Compr Physiol* **5**, 1841-1875, doi:10.1002/cphy.c150006 (2015).

3 Matsui, Y., Morimoto, J. & Uede, T. Role of matricellular proteins in cardiac tissue remodeling after myocardial infarction. *World J Biol Chem* **1**, 69-80, doi:10.4331/wjbc.v1.i5.69 (2010).

4 Schirone, L. *et al.* A Review of the Molecular Mechanisms Underlying the Development and Progression of Cardiac Remodeling. *Oxid Med Cell Longev* **2017**, 3920195, doi:10.1155/2017/3920195 (2017).

5 Bhatt, A. S., Ambrosy, A. P. & Velazquez, E. J. Adverse Remodeling and Reverse Remodeling After Myocardial Infarction. *Curr Cardiol Rep* **19**, 71, doi:10.1007/s11886-017-0876-4 (2017).

6 Jessup, M. & Brozena, S. Heart failure. *N Engl J Med* **348**, 2007-2018, doi:10.1056/NEJMra021498 (2003).

7 Kemp, C. D. & Conte, J. V. The pathophysiology of heart failure. *Cardiovasc Pathol* **21**, 365-371, doi:10.1016/j.carpath.2011.11.007 (2012).

8 Taimeh, Z., Loughran, J., Birks, E. J. & Bolli, R. Vascular endothelial growth factor in heart failure. *Nat Rev Cardiol* **10**, 519-530, doi:10.1038/nrcardio.2013.94 (2013).

9 Torabi, A., Cleland, J. G., Rigby, A. S. & Sherwi, N. Development and course of heart failure after a myocardial infarction in younger and older people. *J Geriatr Cardiol* **11**, 1-12, doi:10.3969/j.issn.1671-5411.2014.01.002 (2014).

10 Epelman, S., Liu, P. P. & Mann, D. L. Role of innate and adaptive immune mechanisms in cardiac injury and repair. *Nat Rev Immunol* **15**, 117-129, doi:10.1038/nri3800 (2015).

11 Frangogiannis, N. G. *et al.* Resident cardiac mast cells degranulate and release preformed TNF-alpha, initiating the cytokine cascade in experimental canine myocardial ischemia/reperfusion. *Circulation* **98**, 699-710 (1998).

12 Sangiuliano, B., Perez, N. M., Moreira, D. F. & Belizario, J. E. Cell death-associated molecular-pattern molecules: inflammatory signaling and control. *Mediators Inflamm* **2014**, 821043, doi:10.1155/2014/821043 (2014).

13 Frangogiannis, N. G. & Entman, M. L. Chemokines in myocardial ischemia. *Trends Cardiovasc Med* **15**, 163-169, doi:10.1016/j.tcm.2005.06.005 (2005).

14 Nahrendorf, M. *et al.* The healing myocardium sequentially mobilizes two monocyte subsets with divergent and complementary functions. *J Exp Med* **204**, 3037-3047, doi:10.1084/jem.20070885 (2007).

15 Swirski, F. K. & Nahrendorf, M. Leukocyte behavior in atherosclerosis, myocardial infarction, and heart failure. *Science* **339**, 161-166, doi:10.1126/science.1230719 (2013).

16 Sager, H. B. *et al.* Proliferation and Recruitment Contribute to Myocardial Macrophage Expansion in Chronic Heart Failure. *Circ Res* **119**, 853-864, doi:10.1161/CIRCRESAHA.116.309001 (2016).

17 Pugin, J. *et al.* Activation of human macrophages by mechanical ventilation in vitro. *Am J Physiol* **275**, L1040-1050 (1998).

18 Ismahil, M. A. *et al.* Remodeling of the mononuclear phagocyte network underlies chronic inflammation and disease progression in heart failure: critical importance of the cardiosplenic axis. *Circ Res* **114**, 266-282, doi:10.1161/CIRCRESAHA.113.301720 (2014).

19 Cochain, C., Channon, K. M. & Silvestre, J. S. Angiogenesis in the infarcted myocardium. *Antioxid Redox Signal* **18**, 1100-1113, doi:10.1089/ars.2012.4849 (2013).

20 David, L., Feige, J. J. & Bailly, S. Emerging role of bone morphogenetic proteins in angiogenesis. *Cytokine Growth Factor Rev* **20**, 203-212, doi:10.1016/j.cytogfr.2009.05.001 (2009).

21 Carmeliet, P. Angiogenesis in health and disease. *Nat Med* **9**, 653-660, doi:10.1038/nm0603-653 (2003).

22 Adams, R. H. & Alitalo, K. Molecular regulation of angiogenesis and lymphangiogenesis. *Nat Rev Mol Cell Biol* **8**, 464-478, doi:10.1038/nrm2183 (2007).

23 Takuwa, Y. *et al.* Roles of sphingosine-1-phosphate signaling in angiogenesis. *World J Biol Chem* **1**, 298-306, doi:10.4331/wjbc.v1.i10.298 (2010).

24 Brindle, N. P., Saharinen, P. & Alitalo, K. Signaling and functions of angiopoietin-1 in vascular protection. *Circ Res* **98**, 1014-1023, doi:10.1161/01.RES.0000218275.54089.12 (2006).

25 De Palma, M. *et al.* Tie2 identifies a hematopoietic lineage of proangiogenic monocytes required for tumor vessel formation and a mesenchymal population of pericyte progenitors. *Cancer Cell* **8**, 211-226, doi:10.1016/j.ccr.2005.08.002 (2005).

26 De Palma, M., Venneri, M. A., Roca, C. & Naldini, L. Targeting exogenous genes to tumor angiogenesis by transplantation of genetically modified hematopoietic stem cells. *Nat Med* **9**, 789-795, doi:10.1038/nm871 (2003).

27 Suri, C. *et al.* Requisite role of angiopoietin-1, a ligand for the TIE2 receptor, during embryonic angiogenesis. *Cell* **87**, 1171-1180 (1996).

28 Venkataraman, K. *et al.* Extracellular export of sphingosine kinase-1a contributes to the vascular S1P gradient. *Biochem J* **397**, 461-471, doi:10.1042/BJ20060251 (2006).

29 Keul, P. *et al.* Sphingosine-1-Phosphate Receptor 1 Regulates Cardiac Function by Modulating Ca2+ Sensitivity and Na+/H+ Exchange and Mediates Protection by Ischemic Preconditioning. *J Am Heart Assoc* **5**, doi:10.1161/JAHA.116.003393 (2016).

30 Argraves, K. M., Wilkerson, B. A. & Argraves, W. S. Sphingosine-1-phosphate signaling in vasculogenesis and angiogenesis. *World J Biol Chem* **1**, 291-297, doi:10.4331/wjbc.v1.i10.291 (2010).

31 Liu, Y. *et al.* Edg-1, the G protein-coupled receptor for sphingosine-1-phosphate, is essential for vascular maturation. *J Clin Invest* **106**, 951-961, doi:10.1172/JCI10905 (2000).

32 Paik, J. H. *et al.* Sphingosine 1-phosphate receptor regulation of N-cadherin mediates vascular stabilization. *Genes Dev* **18**, 2392-2403, doi:10.1101/gad.1227804 (2004).

33 Igarashi, J., Erwin, P. A., Dantas, A. P., Chen, H. & Michel, T. VEGF induces S1P1 receptors in endothelial cells: Implications for cross-talk between sphingolipid and growth factor receptors. *Proc Natl Acad Sci U S A* **100**, 10664-10669, doi:10.1073/pnas.1934494100 (2003).

34 in *Myocardial Infarction with ST-Segment Elevation: The Acute Management of Myocardial Infarction with ST-Segment Elevation National Institute for Health and Clinical Excellence: Guidance* (2013).

35 Khare, R. K., Courtney, D. M., Kang, R., Adams, J. G. & Feinglass, J. The relationship between the emergent primary percutaneous coronary intervention quality measure and inpatient myocardial infarction mortality. *Acad Emerg Med* **17**, 793-800, doi:10.1111/j.1553-2712.2010.00821.x (2010).

36 Orlic, D. *et al.* Bone marrow cells regenerate infarcted myocardium. *Nature* **410**, 701-705, doi:10.1038/35070587 (2001).

37 Schachinger, V. *et al.* Intracoronary bone marrow-derived progenitor cells in acute myocardial infarction. *N Engl J Med* **355**, 1210-1221, doi:10.1056/NEJMoa060186 (2006).

38 Assmus, B. *et al.* Clinical outcome 2 years after intracoronary administration of bone marrow-derived progenitor cells in acute myocardial infarction. *Circ Heart Fail* **3**, 89-96, doi:10.1161/CIRCHEARTFAILURE.108.843243 (2010).

39 Meyer, G. P. *et al.* Intracoronary bone marrow cell transfer after myocardial infarction: eighteen months' follow-up data from the randomized, controlled BOOST (BOne marrOw transfer to enhance ST-elevation infarct regeneration) trial. *Circulation* **113**, 1287-1294, doi:10.1161/CIRCULATIONAHA.105.575118 (2006).

40 Meyer, G. P. *et al.* Intracoronary bone marrow cell transfer after myocardial infarction: 5-year follow-up from the randomized-controlled BOOST trial. *Eur Heart J* **30**, 2978-2984, doi:10.1093/eurheartj/ehp374 (2009).

41 Lunde, K. *et al.* Intracoronary injection of mononuclear bone marrow cells in acute myocardial infarction. *N Engl J Med* **355**, 1199-1209, doi:10.1056/NEJMoa055706 (2006).

42 Jeevanantham, V. *et al.* Adult bone marrow cell therapy improves survival and induces long-term improvement in cardiac parameters: a systematic review and meta-analysis. *Circulation* **126**, 551-568, doi:10.1161/CIRCULATIONAHA.111.086074 (2012).

43 Zhang, H., van Olden, C., Sweeney, D. & Martin-Rendon, E. Blood vessel repair and regeneration in the ischaemic heart. *Open Heart* **1**, e000016, doi:10.1136/openhrt-2013-000016 (2014).

44 Hastings, C. L. *et al.* Drug and cell delivery for cardiac regeneration. *Adv Drug Deliv Rev* **84**, 85-106, doi:10.1016/j.addr.2014.08.006 (2015).

45 Urbich, C. & Dimmeler, S. Endothelial progenitor cells: characterization and role in vascular biology. *Circ Res* **95**, 343-353, doi:10.1161/01.RES.0000137877.89448.78 (2004).

46 Estefanía Nova-Lamperti, F. Z., Valeska Ormazábal, Carlos Escudero and Claudio Aguayo in *Microcirculation Revisited - From Molecules to Clinical Practice* (ed Helena Lenasi) Ch. 10, (2016).

47 Mackie, A. R. & Losordo, D. W. CD34-positive stem cells: in the treatment of heart and vascular disease in human beings. *Tex Heart Inst J* **38**, 474-485 (2011).

48 Povsic, T. J. *et al.* A phase 3, randomized, double-blinded, active-controlled, unblinded standard of care study assessing the efficacy and safety of intramyocardial autologous CD34+ cell administration in patients with refractory angina: design of

the RENEW study. *Am Heart J* **165**, 854-861 e852, doi:10.1016/j.ahj.2013.03.003 (2013).

49 Tendera, M. *et al.* Intracoronary infusion of bone marrow-derived selected CD34+CXCR4+ cells and non-selected mononuclear cells in patients with acute STEMI and reduced left ventricular ejection fraction: results of randomized, multicentre Myocardial Regeneration by Intracoronary Infusion of Selected Population of Stem Cells in Acute Myocardial Infarction (REGENT) Trial. *Eur Heart J* **30**, 1313-1321, doi:10.1093/eurheartj/ehp073 (2009).

50 Rincon, M. Y., VandenDriessche, T. & Chuah, M. K. Gene therapy for cardiovascular disease: advances in vector development, targeting, and delivery for clinical translation. *Cardiovasc Res* **108**, 4-20, doi:10.1093/cvr/cvv205 (2015).

51 Eibel, B. *et al.* Gene therapy for ischemic heart disease: review of clinical trials. *Rev Bras Cir Cardiovasc* **26**, 635-646 (2011).

52 Vera Janavel, G. L. *et al.* Effect of vascular endothelial growth factor gene transfer on infarct size, left ventricular function and myocardial perfusion in sheep after 2 months of coronary artery occlusion. *J Gene Med* **14**, 279-287, doi:10.1002/jgm.1608 (2012).

53 Kastrup, J. *et al.* Direct intramyocardial plasmid vascular endothelial growth factor-A165 gene therapy in patients with stable severe angina pectoris A randomized double-blind placebo-controlled study: the Euroinject One trial. *J Am Coll Cardiol* **45**, 982-988, doi:10.1016/j.jacc.2004.12.068 (2005).

54 Stewart, D. J. *et al.* VEGF gene therapy fails to improve perfusion of ischemic myocardium in patients with advanced coronary disease: results of the NORTHERN trial. *Mol Ther* **17**, 1109-1115, doi:10.1038/mt.2009.70 (2009).

55 Hedman, M. *et al.* Safety and feasibility of catheter-based local intracoronary vascular endothelial growth factor gene transfer in the prevention of postangioplasty and in-stent restenosis and in the treatment of chronic myocardial ischemia: phase II results of the Kuopio Angiogenesis Trial (KAT). *Circulation* **107**, 2677-2683, doi:10.1161/01.CIR.0000070540.80780.92 (2003).

56 Dakin, R. S., Parker, A. L., Delles, C., Nicklin, S. A. & Baker, A. H. Efficient transduction of primary vascular cells by the rare adenovirus serotype 49 vector. *Hum Gene Ther* **26**, 312-319, doi:10.1089/hum.2015.019 (2015).

57 Vassalli, G., Bueler, H., Dudler, J., von Segesser, L. K. & Kappenberger, L. Adeno-associated virus (AAV) vectors achieve prolonged transgene expression in mouse myocardium and arteries in vivo: a comparative study with adenovirus vectors. *Int J Cardiol* **90**, 229-238 (2003).

58 Zincarelli, C., Soltys, S., Rengo, G., Koch, W. J. & Rabinowitz, J. E. Comparative cardiac gene delivery of adeno-associated virus serotypes 1-9 reveals that AAV6 mediates the most efficient transduction in mouse heart. *Clin Transl Sci* **3**, 81-89, doi:10.1111/j.1752-8062.2010.00190.x (2010).

59 Pacak, C. A. *et al.* Recombinant adeno-associated virus serotype 9 leads to preferential cardiac transduction in vivo. *Circ Res* **99**, e3-9, doi:10.1161/01.RES.0000237661.18885.f6 (2006).

60 Tao, Z. *et al.* Coexpression of VEGF and angiopoietin-1 promotes angiogenesis and cardiomyocyte proliferation reduces apoptosis in porcine myocardial infarction (MI)

heart. *Proc Natl Acad Sci U S A* **108**, 2064-2069, doi:10.1073/pnas.1018925108 (2011).

61 Spilsbury, K., Garrett, K. L., Shen, W. Y., Constable, I. J. & Rakoczy, P. E. Overexpression of vascular endothelial growth factor (VEGF) in the retinal pigment epithelium leads to the development of choroidal neovascularization. *Am J Pathol* **157**, 135-144, doi:10.1016/S0002-9440(10)64525-7 (2000).

62 Larcher, F., Murillas, R., Bolontrade, M., Conti, C. J. & Jorcano, J. L. VEGF/VPF overexpression in skin of transgenic mice induces angiogenesis, vascular hyperpermeability and accelerated tumor development. *Oncogene* **17**, 303-311, doi:10.1038/sj.onc.1201928 (1998).

63 Papayannakos, C. & Daniel, R. Understanding lentiviral vector chromatin targeting: working to reduce insertional mutagenic potential for gene therapy. *Gene Ther* **20**, 581-588, doi:10.1038/gt.2012.88 (2013).

64 Mangi, A. A. *et al.* Mesenchymal stem cells modified with Akt prevent remodeling and restore performance of infarcted hearts. *Nat Med* **9**, 1195-1201, doi:10.1038/nm912 (2003).

65 Askari, A. *et al.* Cellular, but not direct, adenoviral delivery of vascular endothelial growth factor results in improved left ventricular function and neovascularization in dilated ischemic cardiomyopathy. *J Am Coll Cardiol* **43**, 1908-1914, doi:10.1016/j.jacc.2003.12.045 (2004).

66 Follenzi, A. & Naldini, L. Generation of HIV-1 derived lentiviral vectors. *Methods Enzymol* **346**, 454-465 (2002).

67 Dai, L. *et al.* Sphingosine kinase (SphK) 1 and SphK2 play equivalent roles in mediating insulin's mitogenic action. *Mol Endocrinol* **28**, 197-207, doi:10.1210/me.2013-1237 (2014).

68 Hyams, D. G. *CurveExpert software*, <http://www.curveexpert.net> (2010).

69 Baker, M. *et al.* Use of the mouse aortic ring assay to study angiogenesis. *Nat Protoc* **7**, 89-104, doi:10.1038/nprot.2011.435 (2011).

70 Gkontra, P. *et al.* Deciphering microvascular changes after myocardial infarction through 3D fully automated image analysis. *Sci Rep* **8**, 1854, doi:10.1038/s41598-018-19758-4 (2018).

71 Kassab, G. S. & Fung, Y. C. Topology and dimensions of pig coronary capillary network. *Am J Physiol* **267**, H319-325, doi:10.1152/ajpheart.1994.267.1.H319 (1994).

72 Kayar, S. R. *et al.* Estimating transit time for capillary blood in selected muscles of exercising animals. *Pflugers Arch* **421**, 578-584 (1992).

73 Mayrovitz, H. N. Skin capillary metrics and hemodynamics in the hairless mouse. *Microvasc Res* **43**, 46-59 (1992).

74 Asaishi, K., Endrich, B., Gotz, A. & Messmer, K. Quantitative analysis of microvascular structure and function in the amelanotic melanoma A-Mel-3. *Cancer Res* **41**, 1898-1904 (1981).

75 Rakusan, K. & Nagai, J. Morphometry of arterioles and capillaries in hearts of senescent mice. *Cardiovasc Res* **28**, 969-972 (1994).

76 Wiedeman, M. P. Dimensions of blood vessels from distributing artery to collecting vein. *Circ Res* **12**, 375-378 (1963).

77 Kisler, K. *et al.* Pericyte degeneration leads to neurovascular uncoupling and limits oxygen supply to brain. *Nat Neurosci* **20**, 406-416, doi:10.1038/nn.4489 (2017).
78 Nicosia, R. F. The aortic ring model of angiogenesis: a quarter century of search and discovery. *J Cell Mol Med* **13**, 4113-4136, doi:10.1111/j.1582-4934.2009.00891.x (2009).
79 Baluk, P. *et al.* Regulated angiogenesis and vascular regression in mice overexpressing vascular endothelial growth factor in airways. *Am J Pathol* **165**, 1071-1085, doi:10.1016/S0002-9440(10)63369-X (2004).
80 Sano, H., Hosokawa, K., Kidoya, H. & Takakura, N. Negative regulation of VEGF-induced vascular leakage by blockade of angiotensin II type 1 receptor. *Arterioscler Thromb Vasc Biol* **26**, 2673-2680, doi:10.1161/01.ATV.0000245821.77155.c3 (2006).
81 Samuel, S. M. *et al.* Coadministration of adenoviral vascular endothelial growth factor and angiopoietin-1 enhances vascularization and reduces ventricular remodeling in the infarcted myocardium of type 1 diabetic rats. *Diabetes* **59**, 51-60, doi:10.2337/db09-0336 (2010).
82 Tengood, J. E., Kovach, K. M., Vescovi, P. E., Russell, A. J. & Little, S. R. Sequential delivery of vascular endothelial growth factor and sphingosine 1-phosphate for angiogenesis. *Biomaterials* **31**, 7805-7812, doi:10.1016/j.biomaterials.2010.07.010 (2010).
83 Zhang, H. *et al.* Sequential, timely and controlled expression of hVEGF165 and Ang-1 effectively improves functional angiogenesis and cardiac function in vivo. *Gene Ther* **20**, 893-900, doi:10.1038/gt.2013.12 (2013).
84 Bai, Y. *et al.* Effective transduction and stable transgene expression in human blood cells by a third-generation lentiviral vector. *Gene Ther* **10**, 1446-1457, doi:10.1038/sj.gt.3302026 (2003).
85 Heyworth, C. M., Whetton, A. D., Nicholls, S., Zsebo, K. & Dexter, T. M. Stem cell factor directly stimulates the development of enriched granulocyte-macrophage colony-forming cells and promotes the effects of other colony-stimulating factors. *Blood* **80**, 2230-2236 (1992).
86 Ertl, G. & Frantz, S. Healing after myocardial infarction. *Cardiovasc Res* **66**, 22-32, doi:10.1016/j.cardiores.2005.01.011 (2005).
87 Bayes de Luna, A. *et al.* A new terminology for left ventricular walls and location of myocardial infarcts that present Q wave based on the standard of cardiac magnetic resonance imaging: a statement for healthcare professionals from a committee appointed by the International Society for Holter and Noninvasive Electrocardiography. *Circulation* **114**, 1755-1760, doi:10.1161/CIRCULATIONAHA.106.624924 (2006).
88 Gordon, S. & Taylor, P. R. Monocyte and macrophage heterogeneity. *Nat Rev Immunol* **5**, 953-964, doi:10.1038/nri1733 (2005).
89 Silvestre, J. S., Smadja, D. M. & Levy, B. I. Postischemic revascularization: from cellular and molecular mechanisms to clinical applications. *Physiol Rev* **93**, 1743-1802, doi:10.1152/physrev.00006.2013 (2013).
90 Jung, S. *et al.* Analysis of fractalkine receptor CX(3)CR1 function by targeted deletion and green fluorescent protein reporter gene insertion. *Mol Cell Biol* **20**, 4106-4114 (2000).

91 Zakrzewicz, A., Secomb, T. W. & Pries, A. R. Angioadaptation: keeping the vascular system in shape. *News Physiol Sci* **17**, 197-201 (2002).
92 Armulik, A., Genove, G. & Betsholtz, C. Pericytes: developmental, physiological, and pathological perspectives, problems, and promises. *Dev Cell* **21**, 193-215, doi:10.1016/j.devcel.2011.07.001 (2011).
93 Yazdani, S., Bansal, R. & Prakash, J. Drug targeting to myofibroblasts: Implications for fibrosis and cancer. *Adv Drug Deliv Rev* **121**, 101-116, doi:10.1016/j.addr.2017.07.010 (2017).
94 Pusztaszeri, M. P., Seelentag, W. & Bosman, F. T. Immunohistochemical expression of endothelial markers CD31, CD34, von Willebrand factor, and Fli-1 in normal human tissues. *J Histochem Cytochem* **54**, 385-395, doi:10.1369/jhc.4A6514.2005 (2006).
95 Vestweber, D. VE-cadherin: the major endothelial adhesion molecule controlling cellular junctions and blood vessel formation. *Arterioscler Thromb Vasc Biol* **28**, 223-232, doi:10.1161/ATVBAHA.107.158014 (2008).
96 Bennett, J. & Dubois, C. Percutaneous coronary intervention, a historical perspective looking to the future. *J Thorac Dis* **5**, 367-370, doi:10.3978/j.issn.2072-1439.2013.04.21 (2013).
97 Doppler, S. A., Deutsch, M. A., Lange, R. & Krane, M. Cardiac regeneration: current therapies-future concepts. *J Thorac Dis* **5**, 683-697, doi:10.3978/j.issn.2072-1439.2013.08.71 (2013).
98 Ieda, M. *et al.* Direct reprogramming of fibroblasts into functional cardiomyocytes by defined factors. *Cell* **142**, 375-386, doi:10.1016/j.cell.2010.07.002 (2010).
99 van den Akker, F., Deddens, J. C., Doevendans, P. A. & Sluijter, J. P. Cardiac stem cell therapy to modulate inflammation upon myocardial infarction. *Biochim Biophys Acta* **1830**, 2449-2458, doi:10.1016/j.bbagen.2012.08.026 (2013).
100 Hamid, T. & Prabhu, S. D. Immunomodulation Is the Key to Cardiac Repair. *Circ Res* **120**, 1530-1532, doi:10.1161/CIRCRESAHA.117.310954 (2017).
101 Lopez, J. J. *et al.* VEGF administration in chronic myocardial ischemia in pigs. *Cardiovasc Res* **40**, 272-281 (1998).
102 Henry, T. D. *et al.* The VIVA trial: Vascular endothelial growth factor in Ischemia for Vascular Angiogenesis. *Circulation* **107**, 1359-1365 (2003).
103 Zangi, L. *et al.* Modified mRNA directs the fate of heart progenitor cells and induces vascular regeneration after myocardial infarction. *Nat Biotechnol* **31**, 898-907, doi:10.1038/nbt.2682 (2013).
104 Kocher, A. A. *et al.* Neovascularization of ischemic myocardium by human bone-marrow-derived angioblasts prevents cardiomyocyte apoptosis, reduces remodeling and improves cardiac function. *Nat Med* **7**, 430-436, doi:10.1038/86498 (2001).
105 Bartunek, J. *et al.* Intracoronary injection of CD133-positive enriched bone marrow progenitor cells promotes cardiac recovery after recent myocardial infarction: feasibility and safety. *Circulation* **112**, I178-183, doi:10.1161/CIRCULATIONAHA.104.522292 (2005).
106 Su, H. *et al.* Additive effect of AAV-mediated angiopoietin-1 and VEGF expression on the therapy of infarcted heart. *Int J Cardiol* **133**, 191-197, doi:10.1016/j.ijcard.2007.12.034 (2009).

107 Smith, A. H. *et al.* Sustained improvement in perfusion and flow reserve after temporally separated delivery of vascular endothelial growth factor and angiopoietin-1 plasmid deoxyribonucleic acid. *J Am Coll Cardiol* **59**, 1320-1328, doi:10.1016/j.jacc.2011.12.025 (2012).

108 Prabhu, S. D. & Frangogiannis, N. G. The Biological Basis for Cardiac Repair After Myocardial Infarction: From Inflammation to Fibrosis. *Circ Res* **119**, 91-112, doi:10.1161/CIRCRESAHA.116.303577 (2016).

109 Rudge, J. S. *et al.* VEGF Trap complex formation measures production rates of VEGF, providing a biomarker for predicting efficacious angiogenic blockade. *Proc Natl Acad Sci U S A* **104**, 18363-18370, doi:10.1073/pnas.0708865104 (2007).

110 Jung, K. *et al.* Endoscopic time-lapse imaging of immune cells in infarcted mouse hearts. *Circ Res* **112**, 891-899, doi:10.1161/CIRCRESAHA.111.300484 (2013).

111 Zhu, J., Zhou, Z., Liu, Y. & Zheng, J. Fractalkine and CX3CR1 are involved in the migration of intravenously grafted human bone marrow stromal cells toward ischemic brain lesion in rats. *Brain Res* **1287**, 173-183, doi:10.1016/j.brainres.2009.06.068 (2009).

112 Yang, F. *et al.* Myocardial infarction and cardiac remodelling in mice. *Exp Physiol* **87**, 547-555 (2002).

113 de Lemos, J. A. *et al.* Serial measurement of monocyte chemoattractant protein-1 after acute coronary syndromes: results from the A to Z trial. *J Am Coll Cardiol* **50**, 2117-2124, doi:10.1016/j.jacc.2007.06.057 (2007).

114 Oyama, J. *et al.* Reduced myocardial ischemia-reperfusion injury in toll-like receptor 4-deficient mice. *Circulation* **109**, 784-789, doi:10.1161/01.CIR.0000112575.66565.84 (2004).

115 Seropian, I. M., Toldo, S., Van Tassell, B. W. & Abbate, A. Anti-inflammatory strategies for ventricular remodeling following ST-segment elevation acute myocardial infarction. *J Am Coll Cardiol* **63**, 1593-1603, doi:10.1016/j.jacc.2014.01.014 (2014).

116 Aoki, M., Aoki, H., Ramanathan, R., Hait, N. C. & Takabe, K. Sphingosine-1-Phosphate Signaling in Immune Cells and Inflammation: Roles and Therapeutic Potential. *Mediators Inflamm* **2016**, 8606878, doi:10.1155/2016/8606878 (2016).

117 Kaikita, K. *et al.* Targeted deletion of CC chemokine receptor 2 attenuates left ventricular remodeling after experimental myocardial infarction. *Am J Pathol* **165**, 439-447, doi:10.1016/S0002-9440(10)63309-3 (2004).

118 Lavine, K. J. *et al.* Distinct macrophage lineages contribute to disparate patterns of cardiac recovery and remodeling in the neonatal and adult heart. *Proc Natl Acad Sci U S A* **111**, 16029-16034, doi:10.1073/pnas.1406508111 (2014).

119 Park, Y. *et al.* Fractalkine induces angiogenic potential in CX3CR1-expressing monocytes. *J Leukoc Biol* **103**, 53-66, doi:10.1189/jlb.1A0117-002RR (2018).

120 Getzin, T. *et al.* The chemokine receptor CX3CR1 coordinates monocyte recruitment and endothelial regeneration after arterial injury. *EMBO Mol Med*, doi:10.15252/emmm.201707502 (2017).

121 Sager, H. B., Kessler, T. & Schunkert, H. Monocytes and macrophages in cardiac injury and repair. *J Thorac Dis* **9**, S30-S35, doi:10.21037/jtd.2016.11.17 (2017).

122 Lin, Y. H. *et al.* The relationship between serum galectin-3 and serum markers of cardiac extracellular matrix turnover in heart failure patients. *Clin Chim Acta* **409**, 96-99, doi:10.1016/j.cca.2009.09.001 (2009).
123 Pries, A. R., Reglin, B. & Secomb, T. W. Modeling of angioadaptation: insights for vascular development. *Int J Dev Biol* **55**, 399-405, doi:10.1387/ijdb.103218ap (2011).
124 Gerhardt, H. & Betsholtz, C. Endothelial-pericyte interactions in angiogenesis. *Cell Tissue Res* **314**, 15-23, doi:10.1007/s00441-003-0745-x (2003).
125 Hao, X. *et al.* Angiogenic effects of dual gene transfer of bFGF and PDGF-BB after myocardial infarction. *Biochem Biophys Res Commun* **315**, 1058-1063, doi:10.1016/j.bbrc.2004.01.165 (2004).
126 Banquet, S. *et al.* Arteriogenic therapy by intramyocardial sustained delivery of a novel growth factor combination prevents chronic heart failure. *Circulation* **124**, 1059-1069, doi:10.1161/CIRCULATIONAHA.110.010264 (2011).
127 Senyo, S. E. *et al.* Mammalian heart renewal by pre-existing cardiomyocytes. *Nature* **493**, 433-436, doi:10.1038/nature11682 (2013).
128 Bergmann, O. *et al.* Evidence for cardiomyocyte renewal in humans. *Science* **324**, 98-102, doi:10.1126/science.1164680 (2009).
129 Karliner, J. S. Sphingosine kinase and sphingosine 1-phosphate in the heart: a decade of progress. *Biochim Biophys Acta* **1831**, 203-212, doi:10.1016/j.bbalip.2012.06.006 (2013).
130 Vessey, D. A., Li, L., Honbo, N. & Karliner, J. S. Sphingosine 1-phosphate is an important endogenous cardioprotectant released by ischemic pre- and postconditioning. *Am J Physiol Heart Circ Physiol* **297**, H1429-1435, doi:10.1152/ajpheart.00358.2009 (2009).
131 Means, C. K. & Brown, J. H. Sphingosine-1-phosphate receptor signalling in the heart. *Cardiovasc Res* **82**, 193-200, doi:10.1093/cvr/cvp086 (2009).
132 Santos-Gallego, C. G. *et al.* Sphingosine-1-Phosphate Receptor Agonist Fingolimod Increases Myocardial Salvage and Decreases Adverse Postinfarction Left Ventricular Remodeling in a Porcine Model of Ischemia/Reperfusion. *Circulation* **133**, 954-966, doi:10.1161/CIRCULATIONAHA.115.012427 (2016).
133 Somers, S. J., Frias, M., Lacerda, L., Opie, L. H. & Lecour, S. Interplay between SAFE and RISK pathways in sphingosine-1-phosphate-induced cardioprotection. *Cardiovasc Drugs Ther* **26**, 227-237, doi:10.1007/s10557-012-6376-2 (2012).
134 De Celle, T. *et al.* Long-term structural and functional consequences of cardiac ischaemia-reperfusion injury in vivo in mice. *Exp Physiol* **89**, 605-615, doi:10.1113/expphysiol.2004.027649 (2004).
135 Wollert, K. C. *et al.* Intracoronary autologous bone-marrow cell transfer after myocardial infarction: the BOOST randomised controlled clinical trial. *Lancet* **364**, 141-148, doi:10.1016/S0140-6736(04)16626-9 (2004).
136 Yoon, C. H. *et al.* Mechanism of improved cardiac function after bone marrow mononuclear cell therapy: role of cardiovascular lineage commitment. *Circulation* **121**, 2001-2011, doi:10.1161/CIRCULATIONAHA.109.909291 (2010).
137 Fernandes, S. *et al.* Comparison of Human Embryonic Stem Cell-Derived Cardiomyocytes, Cardiovascular Progenitors, and Bone Marrow Mononuclear Cells

for Cardiac Repair. *Stem Cell Reports* **5**, 753-762, doi:10.1016/j.stemcr.2015.09.011 (2015).

138 Tao, B. *et al.* Percutaneous intramyocardial delivery of mesenchymal stem cells induces superior improvement in regional left ventricular function compared with bone marrow mononuclear cells in porcine myocardial infarcted heart. *Theranostics* **5**, 196-205, doi:10.7150/thno.7976 (2015).